The processing, microstructure, texture, and magnetic properties of electrical steels A review

He, Youliang; Kestens, Leo A.I.

DOI
10.1177/09506608251317143

Publication date
2025

Document Version
Final published version

Published in
International Materials Reviews

Full Critical Review

ASM INTERNATIONAL

I·M3 Institute of Materials, Minerals & Mining

International Materials Reviews
2025, Vol. 70(5) 353–393

DOI: 10.1177/09506608251317143
journals.sagepub.com/home/inr

Sage

The processing, microstructure, texture, and magnetic properties of electrical steels: A review

Youliang He[1] and Leo AI Kestens[2,3]

Abstract

Electrical steels, also known as silicon steels, play an essential role in the generation, transmission, and use of electricity. The magnetic quality of electrical steels and thus the energy efficiency of electromagnetic devices are highly dependent on the thermomechanical processing procedures employed to manufacture the electrical steel sheets. Every processing step, from casting, hot rolling, cold rolling to annealing, introduces a specific microstructure and texture, which influences the microstructure and texture of next processing steps as well as the final magnetic properties. In this paper, both types of electrical steel, i.e., grain-oriented electrical steel (GOES) and non-oriented electrical steel (NOES), are reviewed bearing in mind that NOES has perhaps received less attention till now. The magnetism of ferromagnetic materials and the metallurgical factors that affect the magnetic properties of electrical steels are first briefly discussed. The effect of each thermomechanical processing step on the formation of the microstructure and texture of the final electrical steel sheets is then scrutinised. The status and challenges in optimising the crystallographic texture of electrical steels are discussed. Future directions to the development of energy-efficient and cost-effective electrical steels are pointed out.

Keywords

grain-oriented electrical steel, non-oriented electrical steel, magnetic properties, microstructure, crystallographic texture, hot rolling, cold rolling, recrystallisation, abnormal grain growth, phase transformation, electric motors, electric vehicles, transformers, generators

Received: 21 August 2024; accepted: 14 January 2025

Introduction

To reduce greenhouse gas (GHG) emissions and mitigate global warming, fossil fuels are to be substituted by other clean and sustainable energies, e.g., hydro, solar, wind, geothermal, tide, hydrogen, etc. Almost all these renewable energies are utilised to produce electricity to power other machines.[1] The generation, transmission, and use of electricity all rely on the use of electrical steels to manufacture soft magnetic cores for the generators, transformers, electric motors, etc., to facilitate the conversion from other energies to electricity or *vice versa*. More recently, as vehicle electrification gains momentum in the transportation sector, it is projected that the demands for electrical steels will significantly increase, mostly driven by the demand in traction motors for electric vehicles (EV) and the need to build more power plants and charging stations.[2]

Electrical steels are used in electromagnetic devices to conduct and amplify magnetic flux to enable efficient energy conversion. The two most important magnetic properties of electrical steels are *core loss* (also called iron loss) and *magnetic flux density* (or magnetic permeability). For better electromagnetic performance, a lower core loss and a higher magnetic permeability are desired. Both the core loss and magnetic permeability are structure sensitive properties,[3] implying that in addition to the chemical composition, the microstructure, impurities, and crystallographic texture also significantly affect the magnetic properties. While the core loss can be considerably reduced by increasing the electrical resistivity (e.g., by adding silicon to the steel) and reducing the sheet thickness, once the chemical composition is fixed, the magnetic permeability can be

[1]CanmetMATERIALS, Natural Resources Canada, Hamilton, Ontario, Canada
[2]Department of Electromechanical, Systems and Metal Engineering, Ghent University, Ghent, Belgium
[3]Materials Science and Engineering Department, Delft University of Technology, Delft, Netherlands

Corresponding author:
Youliang He, CanmetMATERIALS, Natural Resources Canada, 183 Longwood Rd S, Hamilton, Ontario, L8P 0A5, Canada.
Email: youliang.he@nrcan-rncan.gc.ca

most effectively improved by generating specific textures in the steel.

There are two types of electrical steel: grain-oriented electrical steel (GOES), also known as grain-oriented (GO) silicon steel, and non-oriented electrical steel (NOES), also known as non-grain oriented (NGO) silicon steel. GOES has a unique Goss orientation ({011}<100>) in the final microstructure (with a grain size in centimetres), which is suitable for the manufacturing of transformer cores (static equipment). NOES does not have a unique grain orientation and the grain size is much smaller (up to a few hundred microns), which is widely used in generators and electric motors (rotating machines). In these devices, the magnetisation is required to be equally distributed in the plane of the sheet, which needs the steel to have uniform and superior magnetic properties in all directions in the final sheet. As a result, the processing procedures for GOES and NOES are different, although the chemistry of the two types of electrical steel may be very similar.

Although NOES has been in use since around 1850, much earlier than GOES (since around 1935), the research on GOES has a longer history and obtained much more attention than NOES. The research on GOES dated back to the 1930's when the well-known Goss method was developed and patented.[4] Since then, slightly different production methods have been developed by several companies based on the Goss concept to produce the {110}<100> (Goss) texture in GOES, and many scientific papers have also been published trying to understand the mechanisms governing the formation of the unique Goss texture, especially the abnormal grain growth (AGG) of the Goss grains during secondary recrystallisation.[5–7] NOES did not get as much scientific attention as GOES, mainly because the magnetisation of NOES is multidirectional (the anisotropy among various directions is not as large as in GOES) and there is not a strong demand to develop unidirectionally oriented grains in this steel. From a practical point of view, producing steel sheets having *uniform* and *optimum* magnetic properties in all directions in the steel sheets (as required in NOES) is more challenging than producing sheets having optimum properties in only one direction (as in GOES). This is because, during the production of electrical steels, almost all the processing steps tend to form preferred crystal orientations (textures) instead of random orientations in the material, and these textures are normally not the desired <001>//ND (normal direction) texture for NOES. How to obtain a final texture with the <100> easy axes uniformly distributed in all directions of the steel sheet has been the topic of numerous investigations. However, up to now, an industrially viable technique has not been developed, although many methods have been demonstrated on laboratory scale.

Although texture control is critical to both types of electrical steel, the focus is different between GOES and NOES. In GOES processing, producing a sharp Goss texture in the final sheet is the main goal to achieve excellent magnetic permeability, while in NOES, both the microstructure (grain size) and texture should be optimised to minimise the core loss. After the steel sheets are produced, the core manufacturing processes, e.g., stamping, interlocking, assembling, etc., can also affect the magnetic properties of the steel core; thus, they should also be carefully controlled to deliver the best performance to the final electromagnetic devices. This review will cover all the processing steps for both GOES and NOES and evaluate the evolution of microstructure and texture from casting, rolling, to final annealing. The status of current research and development in both GOES and NOES is discussed, and the future research directions are pointed out.

Magnetic properties and material structure

Magnetism in ferromagnetic materials

The magnetism of a crystalline solid originates from the rotation of electrons (both orbital and spin), which creates fundamental magnetic moments (magnetic dipoles) parallel to the rotation axes. The orbital moments are strongly coupled to the crystal lattice and cannot change direction[8–10]; thus, the magnetism of the material is essentially caused by spin only. These magnetic moments are normally randomly oriented in the material, leading to mutual cancellation on a microscopic scale.[8,11] As a result, the material usually does not show a macroscopically observable magnetic moment.

In ferromagnetic materials, the magnetic moments caused by spin tend to align parallel to each other and create a local permanent magnetisation.[8,11] The direction of alignment is along the magnetic easy axis, i.e., the direction that requires the least energy to magnetise. Ferritic iron in electrical steels (body centred cubic, BCC) has easy axes in the <100> lattice directions and hard axes in the <111> directions.[12,13] If a cuboid volume of a ferromagnetic single crystal is considered (Figure 1(a)), the alignment of magnetic moments would result in the generation of a magnetic field outside of the material, which costs magnetostatic energy. To minimise the energy, magnetic domains are created within the material in such a way that the magnetostatic energy is zero and no magnetisation is generated outside the material. The domains (normally 1–100 μm in size) are separated by domain walls (usually tens of nanometres in thickness) that accommodate the gradual rotation of the magnetic moment of one domain to the adjacent domain.[11]

In polycrystalline materials (Figure 1(b)), there are numerous grains separated by grain boundaries, and each grain has its own crystallographic orientation and corresponding axes of spontaneous magnetisation. Within each grain, there are magnetic domains with magnetic moments either anti-parallel or perpendicular to the easy axis (creating 180° and 90° domain walls). When the material is magnetised, the magnetic domains undergo a series of changes as shown in Figure 1(c): i) domain growth and shrinkage through domain wall movement (O→A), ii) increase of the favourably aligned domains and decrease/disappearance of unfavourably aligned domains (A→B), iii) domain rotation towards the external magnetic field

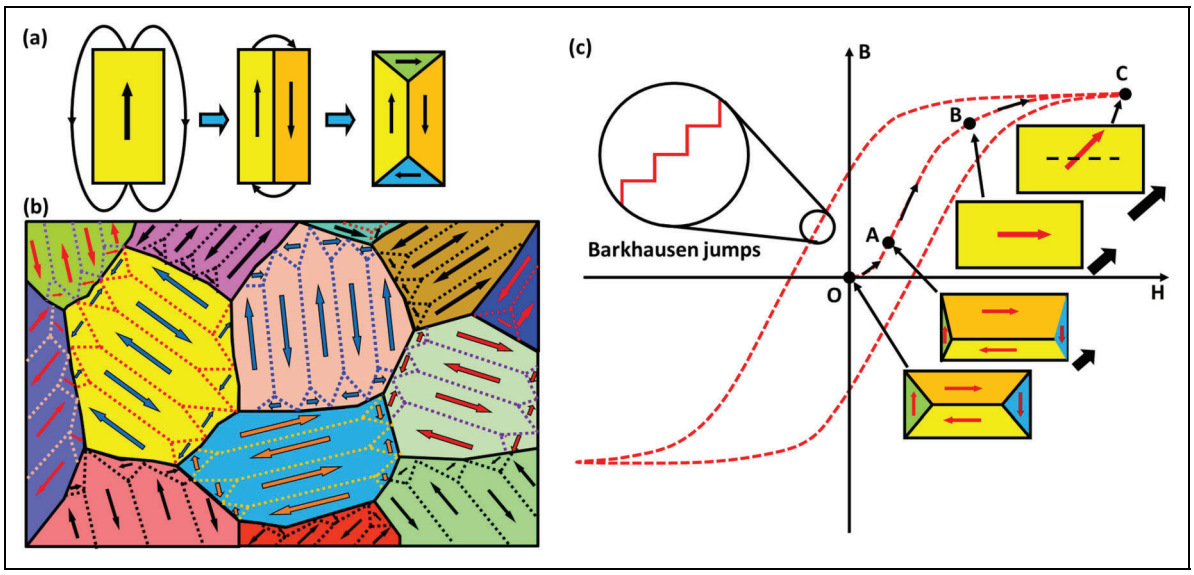

Figure 1. Schematic illustration of the magnetic domains in ferromagnetic materials and the change of the domains due to an external magnetic field: (a) the split of a magnetic domain in a rectangular material into subdomains to reduce the magnetostatic energy, (b) the magnetic domains within different grains in a polycrystalline material,[11] (c) hysteresis loop showing the change of the domains due to external field.[14]

(B→C). It should be noted that the growth of the domains is not continuous because the motion of the domain walls is hindered by pinning sites such as grain boundaries, dislocations, precipitates, stress fields, etc., which causes discontinuous magnetisation events known as Barkhausen jumps.[15] The rotation of domains is associated with the increase of the magnetocrystalline anisotropy energy (MAE) – the energy needed to deflect the magnetic moment from an easy direction to a hard direction.[12,14] This energy is related to the angles (α, β, γ) between the magnetisation direction (H) and each of the easy axes (Figure 2(a)), e.g., the [100], [010], [001] lattice directions of a BCC crystal. The MAE can be calculated as[12,13]:

$$E_{MAE} = k_0 + k_1 A(\vec{h}) + k_2(cos^2\alpha cos^2\beta cos^2\gamma) \quad (1)$$

where k_0 is a constant independent of the crystal orientations, k_1 and k_2 are the first- and second- order magnetocrystalline anisotropy constants, respectively. The term:

$$A(\vec{h}) = cos^2\alpha cos^2\beta + cos^2\beta cos^2\gamma + cos^2\gamma cos^2\alpha \quad (2)$$

is called the *anisotropy parameter*,[16,17] which directly correlates the crystallographic texture to the magnetocrystalline anisotropy energy. The value of $A(\vec{h})$ ranges from 0 to 0.333,[17] and the smaller this value, the smaller the energy needed to magnetise the material. Alternatively, the smallest angle between the magnetisation direction (H) and the three easy axes of a crystal can be utilised to quantify the magnetic quality of the crystal orientation[18]:

$$A_\theta(g) = min(\alpha, \beta, \gamma) \quad (3)$$

The orientation averaged value of $A_\theta(g)$ for an arbitrary magnetic field direction θ, considering the volume fraction of each texture component, is called the *texture parameter*. The smaller this parameter, the higher the magnetic quality of the texture. Therefore, the magnetisation of ferromagnetic materials is highly dependent on the crystal orientations (texture).

For transformers, the magnetisation is in one direction only (RD, see Figure 2(b)); thus, only the RD is required to have superior magnetic properties. This can be achieved by aligning the <100> lattice direction to the rolling direction (RD), i.e., forming a <100>//RD texture. Although any orientations with the <100> directions parallel to the RD can fulfil this requirement, e.g., {001}<100> (cube), {012}<100>, {011}<100> (Goss), etc., up to now, only the Goss texture (Figure 2(e)) has been successfully produced in mass production. For electric motors and generators, since the magnetisation direction rotates in the sheet plane (Figure 2(c)), a texture with the <100> directions parallel to the sheet plane is required, i.e., a <001>//ND fibre texture is ideal for NOES, Figure 2(f). It is desired that these orientations be uniformly distributed in the steel sheet so that the laminates have uniform magnetic properties along all the directions in the sheet plane (Figure 2(d)).

Energy losses in electrical steels

The motion of the domain walls, the passing of the domain walls over pinning sites (Barkhausen jumps), the rotation of the domains, etc., all cost energy. As a result, when using electrical steels in electromagnetic devices to amplify the magnetic flux, it will result in energy loss. The magnetisation process is complicated, and many intrinsic and structural parameters control this process; thus, although plenty of research has been carried out to predict the energy loss in magnetic materials, a comprehensive physical model that can accurately predict core losses has not been developed.[19] Nevertheless, the total loss is normally

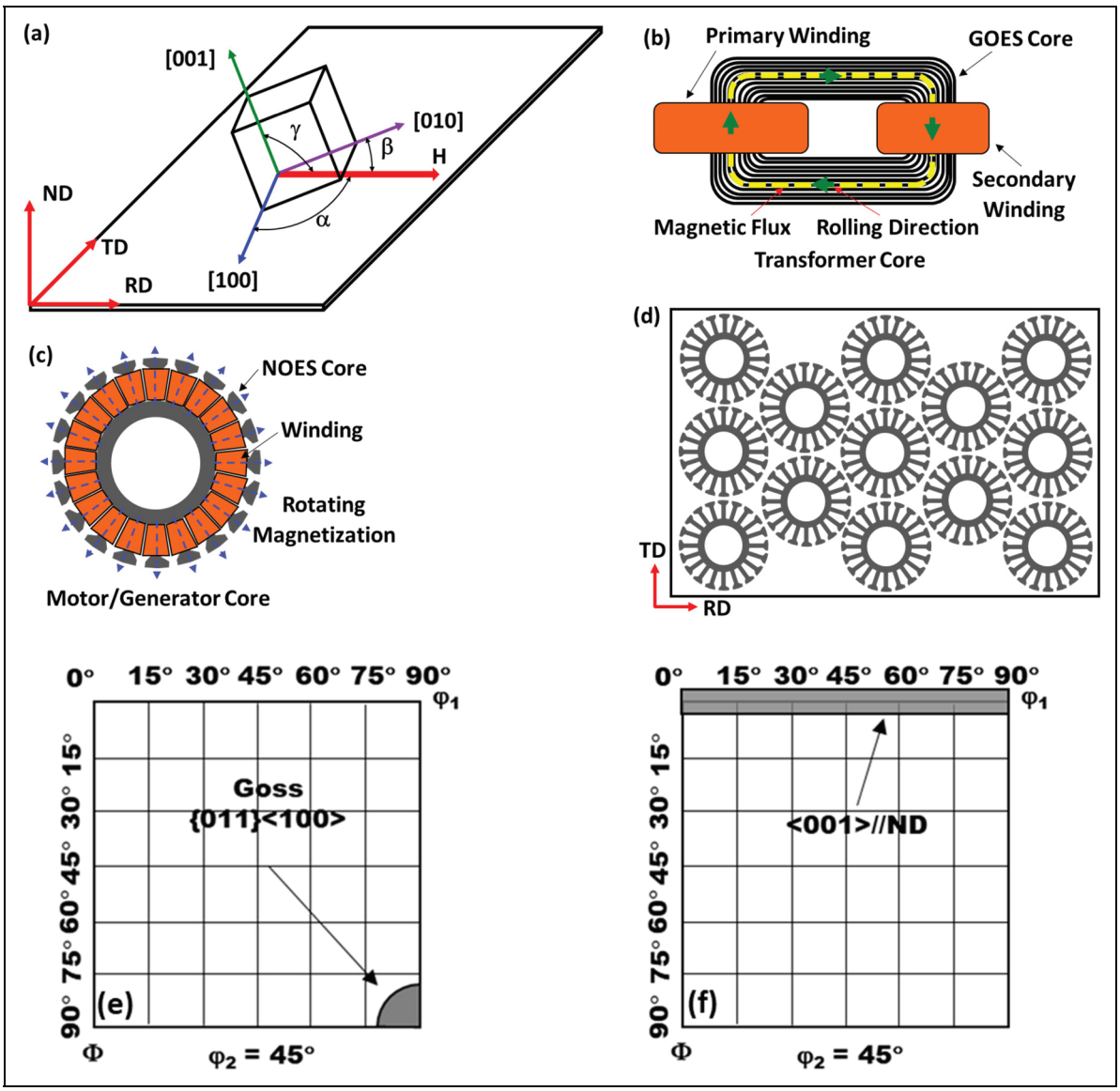

Figure 2. Schematic illustration of the relationship between the crystal orientation and the magnetisation direction (H) in electrical steels: (a) the angles between the magnetisation direction and the crystal easy axes, (b) the magnetisation direction in GOES core for transformers, (c) the rotating magnetisation directions in NOES core for electric motors and generators, (d) motor/generator laminates cut from NOES sheets, (e) desired texture for GOES, (f) desired texture for NOES. Texture is plotted in Bunge's Euler space.

divided into two parts: a static component, P_h, and a dynamic component, P_d. The static component is the total loss when the frequency, f, approaches zero, which is commonly called the *hysteresis loss*. The dynamic component (P_d) is the loss associated with the frequency of the excitation, which is the sum of two types of *eddy current loss*: one being the classical eddy current loss (P_{cl}), and the other the excess (anomalous) eddy current loss (P_e). Thus, the total loss is usually expressed as[19]:

$$P = P_h + P_d = P_h + P_{cl} + P_e \tag{4}$$

Of the three terms in the above equation, only P_{cl} can be accurately calculated on a macroscopic level when it is considered as the eddy current loss caused by an ideal material free of any domain structure under uniform magnetisation, while both P_h and P_e have to be determined experimentally due to the lack of a comprehensive physical model. For a homogenous material (a thin sheet) under uniform magnetic field (with a sinusoidal waveform) ignoring skin effect, the classical eddy current loss per unit volume (W/m^3) can be calculated as[14,20,21]:

$$P_{cl} = \frac{\sigma(\pi B_m f d)^2}{6} \tag{5}$$

where B_m is the peak magnetic field (T), d is the thickness of the sheet (m), σ is the electrical conductivity of the material (S/m), and f is the magnetisation frequency (Hz). Apparently, increasing the electrical resistivity and reducing the sheet thickness reduce P_{cl}. It should be noted that, at high frequencies, the classical eddy current loss is not only related to the thickness of the sheet and the material's electrical resistivity, but also to the magnetic

permeability, which in turn is dependent on the chemistry, microstructure, and crystallographic texture. Thus, the structural properties of the material also influence the classical eddy current loss.[14]

The hysteresis loss per cycle (P_h/f), i.e., the quasi-static part of eddy current loss, is the result of domain wall dynamics (Barkhausen effect), which is very difficult to model because it depends on the multitude of physical interaction phenomena of the domain walls with a variety of microstructural elements of the electrical steel sheet. This loss is conventionally approximated using statistical or empirical equations.[19] A classical model to evaluate the hysteresis loss was proposed by Steinmetz as[22]:

$$P_h = C_0 B_m^{\alpha} f \tag{6}$$

where C_0 is the coefficient of the hysteresis loss and α is the exponent of the flux density.

The excess loss, P_e, originates from the microscopic eddy currents induced by moving domain walls,[23] which was initially estimated as a function of the ratio of domain width to the lamination thickness. The mechanism governing the excess loss is the competition between the external magnetic field and the highly inhomogeneous local counterfields due to eddy currents and microstructural interactions. The excess loss can be calculated as[19]:

$$P_e = 8\sqrt{\sigma G S V_0} B_m^{3/2} f^{3/2} \tag{7}$$

where S is the cross section of the lamination, σ is the electrical conductivity, V_0 is a parameter related to the microstructural properties of the material, and G is a mobility coefficient.

Except for the classical eddy current loss (P_{cl}), which can be accurately calculated under idealised conditions at low frequencies (only related to the lamination's thickness and electrical conductivity, Eq. 5), the other two terms are all affected by the material's characteristics, e.g., crystal type, grain size, crystal orientations, impurities, dislocations, grain boundaries, etc. All of these are not only determined by the chemistry of the electrical steel, but also by the final microstructure and texture, which are highly affected by the thermomechanical processing procedures employed to produce the final steel sheets. In the following, the evolution of microstructure and texture during the processing of both GOES and NOES is reviewed.

Overview of GOES processing

Research on GOES started right after Goss filed the patent 'Grain oriented silicon steel' in 1934[4] and Bozorth[24] proved that the texture produced in Goss's silicon iron was {011}<100>. It was first pointed out by Dunn[25] that secondary recrystallisation was the metallurgical process responsible for the formation of the {011}<100> texture in GOES. Since then, a large volume of literature has appeared and several reviews have also been published dedicated to GOES, e.g.[5,7,26–29] Although numerous theories (and models) have been proposed in the literature, so far none of these theories has obtained a consensus level of agreement in the scientific community. Until now, GOES and the formation mechanism of the Goss texture are still very much under debate, and it remains as a very attractive research area.

GOES processing steps

GOES sheets are produced through a complicated procedure including casting, high temperature reheating, hot rolling, hot band annealing (normalisation), cold rolling, primary annealing (decarbonisation), and final annealing (secondary recrystallisation), see Figure 3. The largest difference between the production of GOES and other steels (including NOES) is that secondary recrystallisation is required to obtain the unique Goss texture in the final microstructure. To initiate the AGG of Goss during secondary recrystallisation, the Goss orientation must be present in the microstructure after primary recrystallisation, although only very few Goss grains (i.e., one out of a million)[7] can abnormally grow. The Goss grains after primary recrystallisation are believed to originate from the hot rolling process due to the friction between the rolls and the steel[30,31] and are retained after cold rolling.[32] The investigation on texture evolution in GOES is mainly focused on the final high-temperature annealing process, i.e., the AGG of Goss. One of the most important aspects of texture control in the production of GOES is the controlled precipitation of finely dispersed second-phase particles (size <100 nm)[33] in the steel, which serve as inhibitors to prevent the growth of recrystallised grains during primary recrystallisation. During secondary recrystallisation, the inhibitors initially prohibit the normal growth of the primary recrystallised grains (by pinning the grain boundaries) but selectively promote the AGG of Goss grains in later stages (after they are dissolved). The steel's chemistry plays an important role in determining the processing routes adopted for GOES production.

Chemistry of GOES

Silicon is the main alloying element added in GOES to reduce the core loss, since it is the most efficient element to increase the electrical resistivity of the steel which reduces the eddy current loss (Eq. 5). Silicon also increases the maximum permeability and decreases the hysteresis loss.[3] However, when the silicon content exceeds about 3.30% (weight percentage, the same for the rest of the paper), the ductility of the material is significantly reduced, and it is difficult to cold roll the steel, especially when very thin gauge (0.3–0.1 mm) is to be achieved. Therefore, the silicon content in GOES is normally below 3.30%, although 6.5% (the theoretical optimum due to a zero magnetostriction and a minimum loss)[3] or higher silicon steels have been investigated in laboratories.[34]

To form the desired final Goss texture in GOES, appropriate inhibitors need to be precipitated at the right stage, which must be strictly controlled to ensure fine particle size, enough density, proper morphology, and uniform distribution.[33] In traditional GOES processing, the inhibitor is

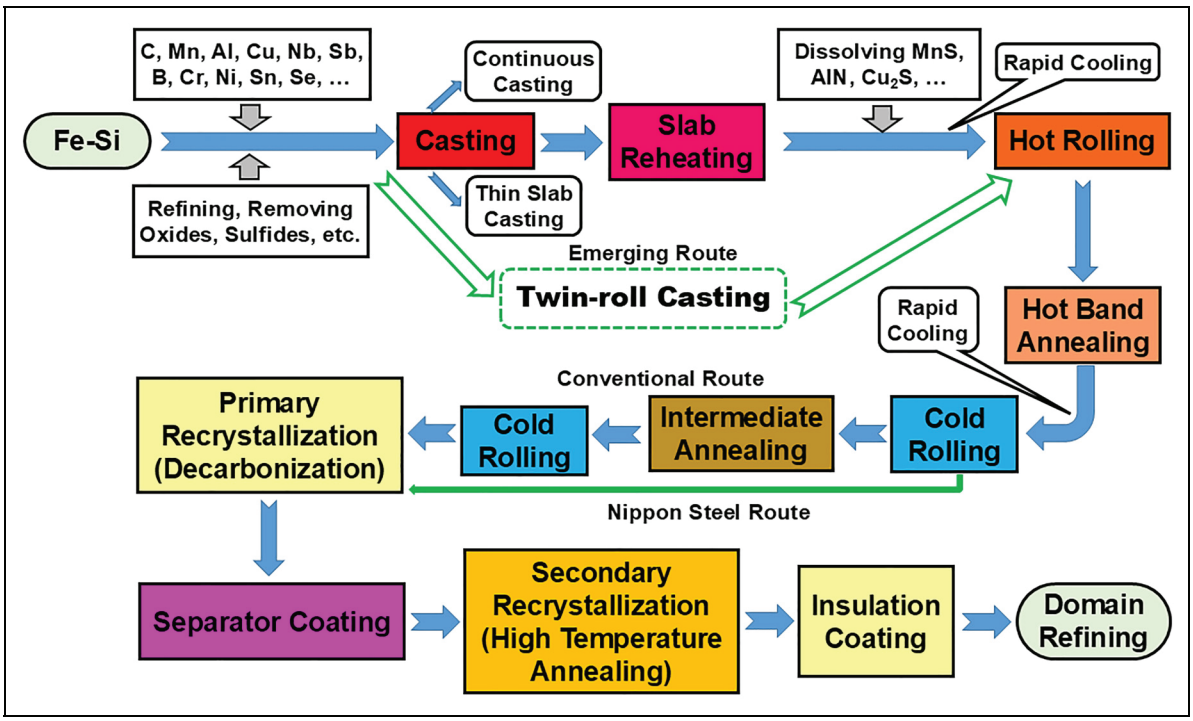

Figure 3. Schematic illustration of the GOES processing steps.

Table 1. List of common alloying (or residual) elements in GOES (wt%).

Element	Min	Max	Optimal Range	Reference
Si	1.0	7.0	2.90–3.30	[4,35–38]
C	0.0017	0.15	0.02–0.05	[35–37,39–41]
Mn	0.05	2.0	0.05–0.30	[35,36,39,42]
Al§	0.004	0.04	0.005–0.019	[33,35,36,39]
S+Se¶	0.003	0.04	<0.006	[35,38,42]
N	0.003	0.012	0.003–0.012	[35,36,43,44]
Cu	0	0.7	0.3–0.7	[36,42]
Nb	0	0.1	0.005–0.009	[33]
Cr	0	0.2	0.03–0.18	[35,36,45,46]
Sn	0	0.19	0.04–0.15	[33,42]
Ni	0	0.18	0.03–0.18	[35,36]
B	0	0.012	0.001–0.012	[33,36,43]
Bi	0	0.05	0.0005–0.05	[33,38]

§Soluble aluminum. ¶S, Se or S and Se together. The Min and Max are obtained from some published papers or patents and may not cover all the literature. The optimal ranges are also cited from some specific papers or patents which may not apply to all the cases. Not all the elements may be present in a steel; it depends on the specific processing.

MnS, which is the reaction product of Mn and S in the steel. Other alloying elements are also added to GOES to form different inhibitors. Table 1 lists common alloying (or residual) elements in GOES and the optimal amounts as given in the literature.

Carbon is not desired in the final GOES sheets since it will cause magnetic aging by forming carbide precipitation. However, it is traditionally added to GOES to prevent the excess growth of the grains during reheating, refine the hot-rolled microstructure by dynamic recrystallisation,[5] and enable an austenite phase in steel with high silicon content (> 2.5%) to control the microstructure during hot rolling through phase transformation since carbon can extend the austenite region of high-silicon steel,[3] which can have a significant effect on the AGG of Goss during secondary recrystallisation. Although carbides are not commonly used as inhibitors in GOES processing, NbC and Nb(C, N) have been reported to be suitable for use as inhibitors in GOES.[33] Thus, the initial carbon in GOES is usually much higher than in NOES. Most of the carbon, however, is removed (to below ~0.003%) during the decarbonisation process to reduce the carbide precipitation in the final sheet.

Manganese is an important alloying element for GOES because of its role in forming the MnS inhibitor during the steel processing. In addition, Mn enlarges the austenite region and increases the steel's ductility.[3] Although Mn also increases the resistivity of the steel, excessive Mn decreases the magnetic flux density[36] and deteriorates the adherence of the insulating coating.[35] Thus, Mn is usually kept below ~0.30% in GOES. Aluminium is another important element in GOES, which is added to the steel to remove oxygen[33] due to its superior deoxidising power. Soluble Al in the steel also plays a critical role in forming the inhibitor AlN in GOES. Al increases the resistivity of the steel, like Si; thus, adding Al to GOES is usually advantageous, but normally only up to 0.019% if AlN is not the inhibitor.[36] Excess amount of Al deteriorates the steel's hot rollability. However, for GOES with AlN as the inhibitor, Al can be added up to 0.05%.[36]

O, N, and S are impurity elements dissolved in the steel, which form oxides, nitrides, and sulfides (>1 μm inclusions), respectively, with Si, Mn, Al, etc., and deteriorate

the microstructure and mechanical properties of the steel.[33] However, nanosized (<100 nm) and well-dispersed precipitates such as MnS, AlN, and Cu_xS are required inhibitors for GOES processing. Therefore, these elements should be rationally controlled to reduce the formation of unwanted inclusions while obtaining the necessary precipitates. To form the desired inhibitors, e.g., MnS or AlN,[47] a certain amount of S or N (see Table 1) should be maintained in the steel, or a nitriding process must be added.[48] The oxygen content is normally controlled within 0.001–0.002% to reduce the harmful oxide inclusions.[33] Selenium is an alternative element to S, which forms MnSe in GOES as an inhibitor.[49] All the other elements such as Cu, Nb, Cr, Mo, Sb, Sn, Ni, B, and Bi, either added to the steel (to lower the reheating temperature and thus reducing the manufacturing costs) or as impurity elements in the steel, may form main inhibitors, auxiliary inhibitors, or promote grain boundary segregations,[33] which may benefit the steel processing to form the Goss texture.

Casting

Continuous casting is the main technology currently employed for GOES production. The typical casting structure, from the surface to the centre, consists of a fine equiaxed grain zone, a columnar crystal zone, and a coarse equiaxed grain zone. The texture in the columnar zone is mainly <100>//heat flow direction. Although these structures and textures will be destroyed in the subsequent processing steps, controlling the morphology, size, and the relative ratios of these structures can reduce segregation and improve the quality of the steel for further processing. A major advancement in the continuous casting technology is the employment of electromagnetic stirring to refine the casting microstructure and reduce segregation.[50,51] The benefits of electromagnetic stirring include the increase of the volume fraction of equiaxed grains in the slab, the decrease of segregation bands,[52,53] and the decrease of grain size, which lead to higher slab toughness and strength.[50] However, electromagnetic stirring cannot solve the shrinkage problem at solidification or eliminate the central porosity. In fact, it has been shown that[54] although electromagnetic stirring can increase the area ratio of the equiaxed grains while reducing that of the columnar crystals, centreline segregation of Si and C increases due to the increased segregation spots (as a result of the increased equiaxed grains).

Starting from the 1980's, Compact Strip Production (CSP) technology, also known as Thin Slab Casting and Rolling (TSCR),[27,55–57] has been developed to integrate casting and hot rolling into a compact line so that the slab reheating and roughing can be eliminated, which has been used to produce thin slabs (50–90 mm) with reduced energy consumption and fine and uniform primary recrystallisation microstructure.[58,59] This technology has been successfully employed to produce electrical steels, which showed improved efficiency and product quality.[27] Another casting technology that has been employed to produce GOES sheets is twin-roll casting (TRC),[39,60–62] also known as twin-roll strip casting (TRSC), which can significantly simplify the production procedures and shorten the production time by combining the casting and hot rolling into an integral process to produce very thin strips in the range of 1–10 mm. It should be noted that the CSP technology still needs separated casting and hot rolling facilities (an equalising heating furnace is also needed), while in TRC, the casting (solidification) and hot rolling are carried out in a single twin-roll caster.

Many papers have been published based on the results from pilot-scale TRC facilities, e.g.,.[63–68] A few phenomena that are different from the conventional GOES processing have been identified[63]: i) coarse MnS particles (~100 nm) are precipitated at the grain boundaries and subgrain boundaries during the strip casting process, ii) fine AlN particles (20–50 nm) are formed in the intermediately annealed sheet after first cold rolling, iii) Goss nuclei for secondary recrystallisation originate from the intermediate annealing process (instead of hot rolling as in conventional GOES processing), iv) the carbon content can be very low and phase transformation is not required, since the precipitation of the fine AlN particles is from the deformed ferrite grains with high dislocation density (not from the ferrite that is transformed from N-rich austenite). Due to the rapid solidification and fast cooling associated with the TRC process, fine inhibitors (AlN) can be readily formed in the primary recrystallisation microstructure, which then enable the formation of the final Goss texture in the steel after secondary recrystallisation.

Slab reheating

The inhibitors in GOES are the key to preventing regular grain growth during primary recrystallisation and selectively promoting AGG of the Goss grains while prohibiting the growth of primary recrystallised grains in the early stage of secondary recrystallisation. These inhibitors must be dissolved during the traditional slab reheating process, which requires very high reheating temperatures (up to ~1400°C) and a long holding time (several hours to tens of hours). In the original process developed by Goss, MnS was the inhibitor, and the cold rolling was performed in two stages with an intermediate annealing in between. Nippon Steel Corporation[47,69] developed a different process which used AlN as the inhibitor and the cold rolling was performed in one stage. In both cases, rapid cooling is needed to form the respective fine inhibitor particles: in Goss's process, rapid cooling is carried out before hot rolling, while in Nippon's process, it is applied after hot rolling (Figure 3). To achieve the final Goss texture by AGG, finely dispersed inhibitors should be reprecipitated at appropriate temperatures and with proper sizes and distributions. For example, for MnS to have an inhibition function, the contents of Mn and S should be controlled within 0.05–0.10% and 0.02–0.03%, respectively, and particle sizes should be 20–70 nm.[33] For AlN as an inhibitor, the contents of (soluble) Al and N are to be controlled to 0.02–0.03%

and 0.006–0.01%, respectively,[33] and the particle size should be within 20–50 nm.[70]

To reduce the energy consumption and manufacturing costs associated with the high-temperature slab reheating, lowering the slab reheating temperature has been an attractive research area for many GOES manufacturers.[27] The reheating temperature has been reduced to around 1250–1280°C (close to the reheating temperature for conventional steel)[35] and further to 1050–1250°C.[36] At these temperatures, however, the traditional precipitates (MnS and AlN) cannot be finely dispersed in the material during secondary recrystallisation; thus, different precipitates and processes have been developed to obtain proper inhibitors for the secondary recrystallisation. Copper-bearing precipitates, e.g., $(Cu, Mn)_{1.8}S$, (Cu, Mn)S, CuMnS, and Cu_2S, have been identified as an alternative to the traditional MnS and AlN.[33] The optimal particle size is 10–100 nm and the solid solution temperature for Cu_2S is around 1200°C, which is lower than those of MnS (1280°C) and AlN (between 1200 and 1280°C).[36] The precipitating temperatures for the MnS, AlN, and Cu_2S particles are 1200, 1150, and 1100°C, respectively.[35,71] As a result, the slab reheating temperature can be reduced to 1050–1250°C if Cu_2S is used as the inhibitor.[35] To minimise the precipitation of MnS or AlN, the S or N content is restricted to very low levels in the steel.[35]

Using BN as the main inhibitor[36] can decrease the reheating temperature to 1050–1250°C. The preferred amount of B is 0.001–0.012% and the initial nitrogen content is very low (below 0.008%) so that the precipitation of other nitrides can be neglected. Nitrogen is added (nitriding) during the combined decarbonisation-nitrogenisation annealing process at 850–950°C. BN, instead of AlN, is preferably formed in this process due to the high diffusion speed of B in the steel. The finely and uniformly dispersed BN particles (particle size is about a few tens of nm) across the thickness enable a proper inhibiting force and a stable secondary recrystallisation to form the desired final texture. NbC, NbN, and Nb(C,N) have also been used as inhibitors in GOES,[33,72,73] which not only lower the reheating temperature (the dissolution temperatures of NbC and NbN are in the range of 1210–1240°C)[33,74], but also produce a stronger Goss texture and decreases core loss as compared to GOES with MnS and AlN as inhibitors. However, excessive Nb had a negative effect since Nb(C, N) cannot completely dissolve even at 1250°C,[75] which impacts the magnetic properties by forming less Goss and pinning magnetic domain walls.

In addition to the main inhibitors used in GOES processing, auxiliary inhibitors containing Cr, Nb, Sn, Ni, and Bi have also been used in the processing of GOES at low reheating temperatures.[33,76] Adding Cr has been reported to form (Cr,Si)N after nitriding, which refines and homogenises the primary recrystallisation microstructure and reduces the grain size of the secondary recrystallisation microstructure, thus reducing the iron loss.[33] Nb and Sn have also been simultaneously added to strengthen the inhibiting force and lower the reheating temperature.[33] It has been reported that Bi can accelerate the precipitation of fine MnS and AlN[38] and enhance the inhibiting ability of the inhibitors. Trace Bi (0.0005–0.05%) in GOES can produce ultra high magnetic flux density (B_8 up to 1.94 T).[33,77] A summary of the common inhibitors used in GOES production and their solution and precipitation temperatures during steel processing is listed in Table 2. It is seen that, depending on the inhibitors, different slab reheating and precipitation temperatures should be selected to obtain the desired inhibiting function.

Table 2. Typical inhibitors used in GOES and their solution and precipitation temperatures.

Inhibitor	Solution Temperature/ Processing Step	Precipitation Temperature/ Processing Step	References
MnS	>1250–1280°C/ Slab reheating	<1200°C/Hot rolling	[35]
AlN	>1200–1280°C/ Slab reheating	<1150°C/Hot rolling or intermediate annealing	[35,63,75]
Cu_2S	>1200°C/Slab reheating	<1110°C/Hot rolling	[35]
BN	>1050–1250°C/ Slab reheating	<950°C/ Nitrogenisation	[36]
Nb(C,N)	>1250°C/Slab reheating	<1210°C/Hot rolling	[75]

Hot rolling

Hot rolling plays an indispensable role in the development of the final Goss texture as it forms the initial Goss grains in the near surface region,[78] which come to dominate the final texture after hot band annealing, cold rolling, primary recrystallisation, and secondary recrystallisation ('texture inheritance').[6,31] Recrystallisation, phase transformation, and precipitation are important metallurgical processes to be controlled during hot rolling to achieve the desired microstructure and texture. Initial conditions and operational parameters such as the microstructure before hot rolling, hot rolling temperature, ratio of reduction, holding after hot rolling, etc., can all affect the hot rolling microstructure and texture.

If the initial grain size after slab reheating is excessively large, incomplete secondary recrystallisation may occur since the large grains may remain unrecrystallised (elongated) even after cold rolling, primary, and secondary recrystallisation, causing non-Goss grains in the final product.[79] Hot pre-rolling and lowering the slab reheating temperature can reduce the grain size before hot rolling, thus eliminating incomplete secondary recrystallisation, since grain boundaries are substantial nucleation sites for primary recrystallisation and reducing the initial grain size increases the nucleation sites and thus promoting recrystallisation.

Increasing the hot rolling temperature or increasing the thickness reduction ratio can promote recrystallisation (Figure 4(a)).[80] However, at high temperatures, the

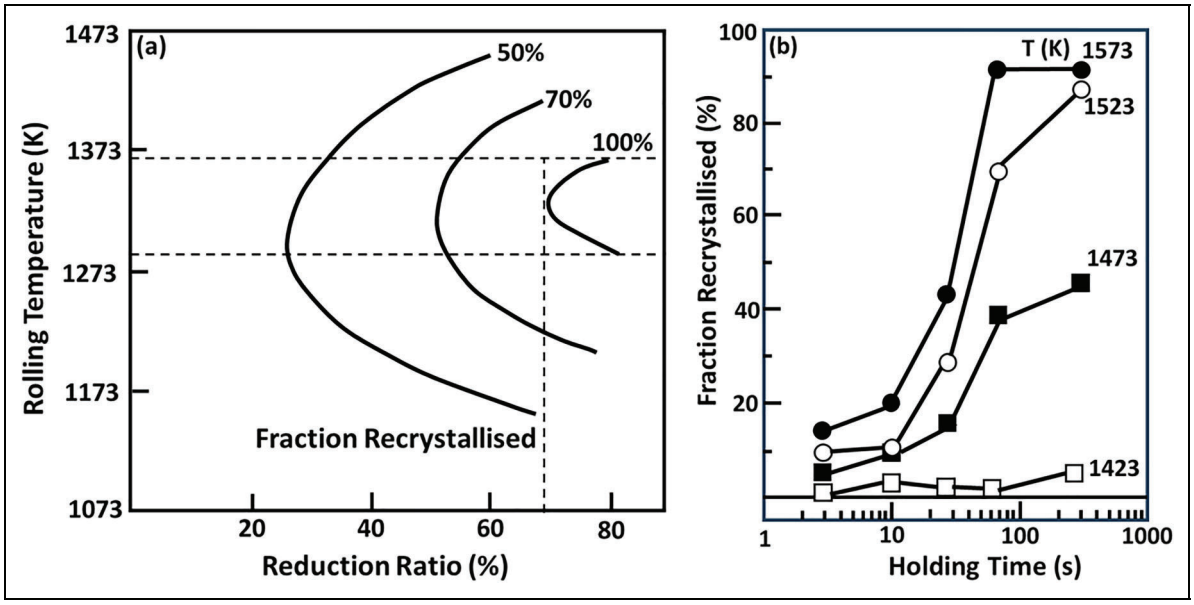

Figure 4. Recrystallisation behaviour of GOES during hot rolling[80]: (a) effect of hot rolling temperature and reduction ratio on recrystallisation, (b) effect of holding temperature and time on recrystallisation.[81]

recovered α-phase (due to the high stacking fault energy) also tends to form precipitation of the inhibitors at the subgrain boundaries, which will grow and decrease the pinning ability. Thus, it is preferable that the grains are recrystallised at high temperatures to prevent the precipitation and coarsening of the inhibitors while the recrystallised grains are rolled at a relatively low temperature so that the fine inhibitors can uniformly precipitate within the deformed structures. Muraki et al.[81] proposed a very-high-temperature and short-time slab reheating approach to limit grain growth (to obtain fine slab grain size) and reach complete inhibitor dissolution before hot rolling. It was shown that holding the steel at high temperatures (above 1473 K) after hot rolling for a sufficient time can also result in complete recrystallisation (Figure 4(b)). It was suggested that hot rolling should not be conducted at an intermediate temperature range 1150–1325 K to avoid the formation of coarse inhibitors.

An important feature of the microstructure of GOES after hot rolling is the inhomogeneity in grain size, precipitate distribution (size and morphology), and texture.[82] The partial austenite (which contains a solid solution of the precipitation-forming elements) to ferrite phase transformation during hot rolling and annealing leads to a fine grain structure and finely dispersed precipitates in the transformed ferrite, while the original ferrite grows to large grains with coarse precipitates. This inhomogeneous microstructure favours the formation of the Goss nuclei and its selective growth during secondary recrystallisation. The texture across the thickness also shows inhomogeneity (gradient), with Goss ({110}<001>) in the subsurface and intermediate layers and rotated cube ({001}<110>) in the centre. After cold rolling and primary recrystallisation, a preferred {111}<112> texture is generated which is the favourable matrix for abnormal growth of the Goss grains, while the fine precipitates inhibit the normal growth of the matrix.[5]

Hot band annealing

Hot band annealing (HBA) before cold rolling is a required processing step to produce high permeability GOES.[47,83] Although annealing after hot rolling does not significantly change the texture or the microstructure after cold rolling and primary recrystallisation, HBA is an important conditioning heat treatment process to control the inhibitors as well as microstructure/texture during secondary recrystallisation. The quick cooling (quenching into boiling water) after soaking is critical to achieving perfect secondary recrystallisation since it promotes the selective coarsening of the Goss grains and preserves the potential nuclei.[5,84]

It has been shown[85] that, without hot band annealing, the precipitates are finer during primary recrystallisation and thus with higher inhibiting force, which strongly inhibit secondary recrystallisation, leading to much weaker Goss texture and worse magnetic properties. Recent work by Giri et al.[83] showed that hot band annealing enhanced the presence of Goss during primary recrystallisation and caused a weaker texture and a coarser grain size. On the other hand, although hot band annealing does not bring clear advantage in the overall grain boundaries that favour the AGG of Goss, it does lead to much higher fractions of favourable boundaries with respect to immediate neighbours, which favours the growth of Goss grains in later stages and results in closer to Goss textures as well as better magnetic properties, i.e., lower core loss and higher permeability.

Cold rolling

Heavy cold rolling is required to produce thin GOES sheets to reduce eddy current loss, which inevitably alters the texture formed after hot rolling and hot band annealing,

especially the Goss texture, which is believed to serve as the potential nuclei for the formation of the Goss grains during secondary recrystallisation. The main texture components after cold rolling are the α-fibre (<110>//RD) and γ-fibre (<111>//ND), similar to typical BCC rolling texture, with only a small fraction (about 1%) of Goss-oriented areas remaining in the microstructure[6] since the Goss texture formed in hot rolling is not stable and rotates to {111}<112> during cold rolling,[86] as was shown in many single crystal studies (Figure 5).[5,86,87] It is believed that (based on relaxed constraints Taylor model)[88] the shear strains parallel to the rolling direction caused the formation of the {111}<112> through the rotation of the Goss around <110> (TD), with the operation of the {112}<111> slip systems which have the largest resolved shear stress.[5] After cold rolling, the Goss texture formed during hot rolling will be weakened and the Goss grains are restricted to regions close to the {111}<112> grains, most of them within the shear bands.[6,89,90]

Carbon has been shown[91] to affect the rotation of the Goss orientation during cold rolling. With ultra-low carbon (0.001%), the Goss rotates to {111}<112> after 66% reduction (Figure 5(a)), while if the carbon content is higher (0.02%), the Goss rotates to both {111}<112> and {100}<011> (Figure 5(b)), the latter being formed due to deformation twinning (Figure 5(c)). The presence of carbon (carbide precipitates) suppresses the slip deformation and promotes deformation twinning, which leads to the {100}<011> orientation.

Cold rolling not only alters the texture of the steel, but also refines the AlN particles precipitated during hot band annealing. It has been shown[92] that the AlN particle size decreases with the increase of the cold rolling reduction rate, which is caused by splitting of coarse AlN particles into smaller parts by shear deformation (slip). Thus, even if large precipitates are formed during hot band annealing, it is possible to refine it by cold rolling and restore their pinning force.

Cold rolling can be applied in two schemes: i) two-stage cold rolling with intermediate annealing, which was used in the production of regular grade GOES with MnS as the inhibitor, i.e., the original Goss method,[4] ii) single-stage cold rolling without intermediate annealing, which was used to produce high-permeability grade GOES with AlN

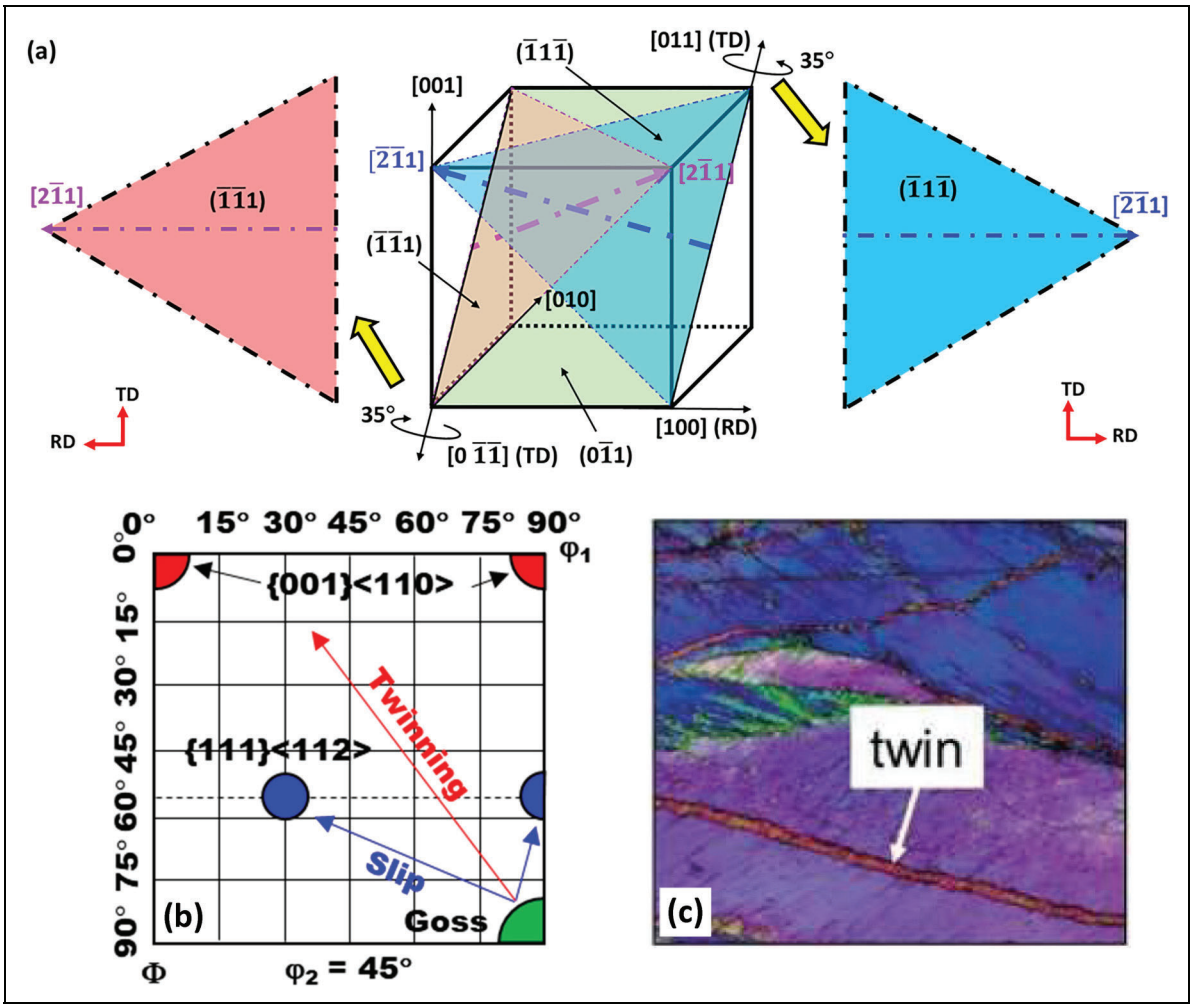

Figure 5. The rotation of Goss during cold rolling: (a) formation of the {111}<211> orientations by slip (35° rotation around the TD or <011>), (b) the rotation of Goss during cold rolling as shown on the $\varphi_2 = 45°$ section of the Euler space (Bunge notation), (c) deformation twinning during cold rolling of Goss oriented crystal.[91]

and MnS as the inhibitors, i.e., the Nippon Steel method.[84] Although in both methods, the Goss oriented grains selected for secondary recrystallisation are believed to originate from the hot rolling process, the two schemes of cold rolling do generate different textures. The texture after cold rolling through both schemes contains typical BCC rolling textures such as α-fibre and γ-fibre. However, the intensity and distribution of the two fibres produced by the two schemes are different. The intermediate annealing in the two-stage cold rolling process generally reduces the overall intensity of the texture, i.e., the maximum intensities of the α- and γ-fibres at both the surface and midplane are generally lower than those after single-stage cold rolling. The largest difference appears in the midplane: the maximum intensity of the α-fibre (at rotated cube) after single-stage cold rolling is several times of that after two-stage cold rolling.[84] In both cases, AGG of the Goss component can occur and the major difference is the deviation from the theoretical Goss: while the two-stage cold rolling leads to a larger deviation of about 7° (regular grade), the one-stage cold rolling results in a smaller deviation of 3° (high-permeability grade).

Primary recrystallisation

Primary recrystallisation in GOES production normally occurs during the decarbonisation/nitriding annealing process. A critical objective of this process is to create a microstructure that favours the selective growth of Goss grains during secondary recrystallisation, thus forming a perfect and sharp Goss texture in the final microstructure. Many studies have been dedicated to this process[46,93–98] and it is now generally accepted that the following should be achieved during primary recrystallisation[5–7]:

1. Recrystallisation is complete, but normal grain growth is supressed (e.g., inhibited by fine precipitates).
2. The matrix texture is suitable for the fast growth of the Goss nuclei, e.g., a {111}<112> texture is preferred, which has a high mobility Σ9 boundary with respect to Goss.
3. The Goss nuclei are preferably located in the subsurface layer and with large enough size,[5] but initial size advantage is not required, nor the requirement to form Goss colonies.[7]

Typical microstructure and texture of GOES after primary recrystallisation are shown in Figure 6. It has also been generally agreed that: i) Goss is generated during hot rolling due to the friction between the steel and rolls, ii) cold rolling rotates Goss to {111}<112>, and iii) Goss reappears during primary recrystallisation. However, why and how Goss reappears during primary recrystallisation is still under debate. Many researchers[5,6,86,89,90] attribute the Goss nuclei to the shear bands (bands of heterogeneous deformation) formed during cold rolling, mainly in grains with high Taylor factors, e.g., <111>//ND grains. It is shown by X-ray diffraction that grains with the Goss orientation store the highest strain energy in the deformed matrix, thus the rate of nucleation by subgrain growth, recovery and recrystallisation of the Goss is the fastest.[5] However, Dorner et al.[6] reported that it is the Goss grains outside of the shear bands (between microbands) that are likely the nuclei for primary recrystallisation, while the Goss grains inside the shear bands mostly disappear.

After primary recrystallisation, Goss is a minor component if the steel has been cold rolled in one stage (high-permeability grade), while it is one of the major components if it has been cold rolled in two stages (regular grade).[6] This is because the thickness reduction during cold rolling affects the Goss texture during primary recrystallisation. If the reduction is moderate (about 70%), e.g., in two-stage cold rolling, a strong Goss texture may develop after primary recrystallisation since the matrix texture, {111}<112>, is only stable at moderately high reductions.[5] In GOES produced in a one-stage cold rolling process, the reduction is around 90%, which results in the weakening of the Goss texture after primary recrystallisation, due to the rotation of the deformation texture away from the {111}<112> orientation.

The grain size before cold rolling also affects the Goss texture after primary recrystallisation. Coarse grains before cold rolling lead to the appearance of Goss in the grain interior as it is easy to develop deformation inhomogeneity and deformation bands/shear bands in large grains, which promotes the formation of Goss grains within the interior of grains during primary recrystallisation.

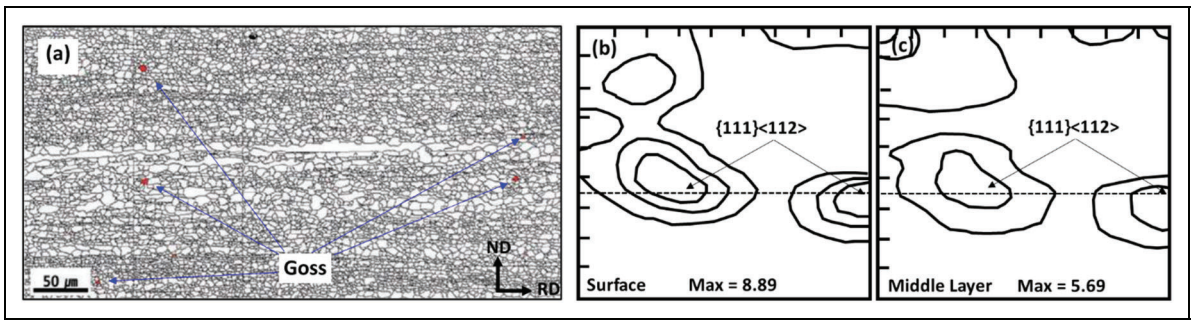

Figure 6. Typical microstructure and texture of GOES after primary recrystallisation: (a) microstructure with distributed Goss grains (±5°),[95] (b) texture at the surface layer,[99] (c) texture at the middle layer (ODF at $\varphi_2 = 45°$ section of the Euler space, Bunge notation).[99]

Heating rate has been reported to influence the primary recrystallisation texture[95,99] since the incubation time for nucleation depends on the orientation of the nuclei; thus, different heating rates may intensify different textures. Rapid heating can suppress the nucleation of other grains while favouring the nucleation of the grains with the highest stored energy, e.g., {011}<100>, as these grains need the shortest incubation time to recrystallise.[5] Finely dispersed precipitates not only retard the overall nucleation rate, but also selectively retard specific nucleation sites, e.g., the precipitation of AlN during heating has been reported to effectively enhance the <111>//ND texture while suppressing the {011}<100> texture.

Secondary recrystallisation

The most critical processing step in GOES production is the high-temperature batch annealing (secondary recrystallisation) which leads to the AGG of Goss and forming an extremely strong Goss texture. Many investigations have been dedicated to the understanding of the selective growth mechanisms of the Goss texture. The startling phenomenon in which a small number of Goss grains selectively grow to form very large grains by consuming other recrystallised grains has been a topic of many investigations and it is currently still a subject of intensive study. It is generally agreed that the critical requirement for the AGG of Goss is a recrystallised matrix with small but uniform grain size together with finely dispersed inhibitors. It is known that controlling the precipitation of inhibitors is the most critical industrial practice to successfully produce GOES.

The Goss nuclei that are selected during secondary recrystallisation are believed to be inherited from hot rolling.[7,30,31,82,86] As mentioned before, Goss at the subsurface layer (10–25% depth) was produced by the shear deformation induced by the friction between the steel and the rolls, which was then subjected to hot band annealing, cold rolling (maybe with intermediate annealing) and primary recrystallisation, and finally survived in secondary recrystallisation. How this specific orientation is retained after all the processing steps and why it can become the crystal to abnormally grow during secondary recrystallisation are still under debate.

A few theories have been proposed to explain the selective growth of the Goss grains during secondary recrystallisation, and comprehensive reviews on these theories have been given by Hayakawa[7] and Yilmaz et al.[100] The three most-cited models are:

- Coincidence Site Lattice (CSL) boundary model.
- High Energy (HE) boundary model.
- Solid-state Wetting (SSW) model.

The CSL model was based on the observation that highly ordered low Σ CSL boundaries accommodate fewer segregated solutes as compared to random high-angle boundaries, and thus move faster than random boundaries due to the lower Zener force exerted by the inhibitors on grain boundaries. The Goss orientation shows a 35°<110> rotation from the {111}<112> orientation (the major texture after primary recrystallisation), which is close to the Σ9 (38.9°<110>) boundary.[101] It has been shown that the Goss grains are surrounded by the highest fraction of CSL boundaries (among all {011}-grains),[102] and the intensities of the Σ9 and Σ5 were stronger than the other Σ's.[103] It has been demonstrated that the Σ9 boundaries play a critical role in the secondary recrystallisation of the Goss grains.[104]

The HE model is based on the assumption that the (tilt) boundaries with misorientation angles between 20° and 45° exhibit the highest grain boundary energy,[7,105–107] and therefore are often associated with a high migration rate due to the special atomic structure of these boundaries as well as a high grain boundary diffusion rate that facilitates the coarsening of inhibitors.[7] Since the Goss grains in silicon steel has a majority (~80%) of the misorientation angles in the range of 20°−45° with respect to the matrix grains,[108] the Goss grain can grow abnormally. Especially, the misorientation (35°<110>) between the Goss and {111}<112> has been related to the maximum energy and boundaries with maximum mobility.[109]

The SSW model[110–112] is based on the assumption that the abnormally growing Goss grains contain an internal structure with a high fraction of low-angle, low-energy subgrain boundaries, which can extrude into the high-angle boundaries at triple junctions and separate normal grains, leading to the growth of the Goss grains. It is required that the sum of the two subgrain boundary energies be smaller than that of the high-angle boundary to enable the growth. The growth direction of the Goss grains is *along* the grain boundaries instead of *perpendicular* to the grain boundaries as in all other models. However, it has been pointed out by others[100] that most of the results on this model are based on modelling, e.g., Mont Carlo[113] or phase field[112]; thus, it lacks experimental verification, or experimental confirmation is limited.

While all these models have attempted to explain the AGG of Goss in GOES production, none of them has been able to give a complete explanation or concrete understanding of the phenomenon. In fact, the theories based on the special grain boundaries (CSL and HE models) have been criticised by other researchers.[114,115] For example, Moraviec[114] has stated that these theories are 'merely scientific speculations and should be treated with skepticism'. It has been shown by Chen et al.[116] that the difference in mobility alone is not sufficient for the abnormal growth of the Goss, especially at the early stage before the size advantage sets in.[114] Moraviec[117] further argued that it was the surface free energy, instead of the grain boundaries, that has driven the AGG of Goss. It was claimed that grains with low surface free energy have a high probability of growth. However, this model also only proposes a theory and needs to be validated by experiments.

A major criticism on the above-mentioned AGG theories is that none of these models can explain the mechanism of the early stage of the growth process, i.e., what mechanism

is responsible for the local growth advantage of a few Goss oriented grains at the onset of AGG? For a given grain boundary between the Goss and another grain, assuming it has an increased migration velocity due to either CSL or HE, the initial growth direction can be either outward or inward, i.e., from the Goss to the other grain, or from the other grain to the Goss. The question is, what is the driving force to cause the Goss to grow into the other grain and not the opposite?

A new theory was recently proposed by Birosca et al.[41] to explain the mechanism of the early-stage abnormal growth of Goss (Figure 7). It is believed that the following three conditions make the AGG of Goss possible:

1. The Si atoms in the α-Fe lattice distort the ideal BCC lattice to favour 1 or 2 of the 6 {011} planes' expansion and superior Δd-spacing during thermal exposure, which is the potential growth direction (with high thermal conductivity) of the Goss in the early stage.
2. The heat flow direction is along the {011} planes, which accelerates the heat flux along the {011} planes to reach the Goss grain boundaries first and dissolve the inhibitors faster than any other orientations, making the mobility of the grain boundaries in this direction higher, thus winning the growth competition.
3. The heating rate of the secondary annealing is slow so that the high expansion rate of the {011} planes is achieved, avoiding the high expansion rate of other planes, thus leading to a sharp Goss texture.

Once the Goss grains win the growth competition at the beginning, the thermal conductivity increases with the grain size, which enables the Goss grains to grow dramatically along the {011} planes where the heat flows rapidly. However, this theory is also questionable. First, it was claimed that the increase of the d-spacing (Δd-spacing) upon thermal exposure is the highest in the d-011 (only 1 or 2 of such planes), which assists the heat flow (high thermal expansion and conductivity). If this is the case, the heat flow should be perpendicular to these {110} planes (along the <011> directions in other {011} planes) (Figure 7(a)), not 'along the {011} plane' as indicated in[41] since there are many directions in this plane. Second, there are other orientations, e.g., brass ({011}<211>), rotated Goss ({011}<011>), etc., that also have the {011} lattice plane parallel to the sheet plane; if the heat flows fast in the {110} planes, why grains with these orientations do not abnormally grow?

Another new theory, called Dislocation-Assisted Particle Dissolution (DAPD), was recently proposed by Yilmaz et al.[100] to explain the AGG of Goss in GOES production, especially in the early stage of AGG (Figure 8). This theory was based on the observation that in abnormally grown Goss grains there are subgrain structures (subgrain boundaries and dislocations) which are believed to be inherited from the Goss after hot rolling and survived from the cold rolling, primary and secondary recrystallisation. The subgrain boundary dislocations absorb a portion of the elements dissolved from the inhibitors at the grain boundaries, which allows more rapid dissolution of the inhibitors around the Goss grain boundaries, reducing the drag of the solutes and particles and increasing the boundary mobility. However, as mentioned by the authors themselves, an unequivocal experimental observation of obvious substructures of Goss grains after primary recrystallisation has yet to be provided. Also, here the question remains why only Goss grains, not any other grains with other crystal orientations, exhibit such subgrain structures (subboundaries and dislocations)? In addition, how such structures could survive the discontinuous solid-state transformation induced by primary recrystallisation?

Hayakawa et al.[7,118] reported that a narrow grain size distribution and a strong texture accumulation can play a more important role than the inhibitors in the selective growth of the Goss grains during secondary recrystallisation. It was claimed that reducing the impurity elements

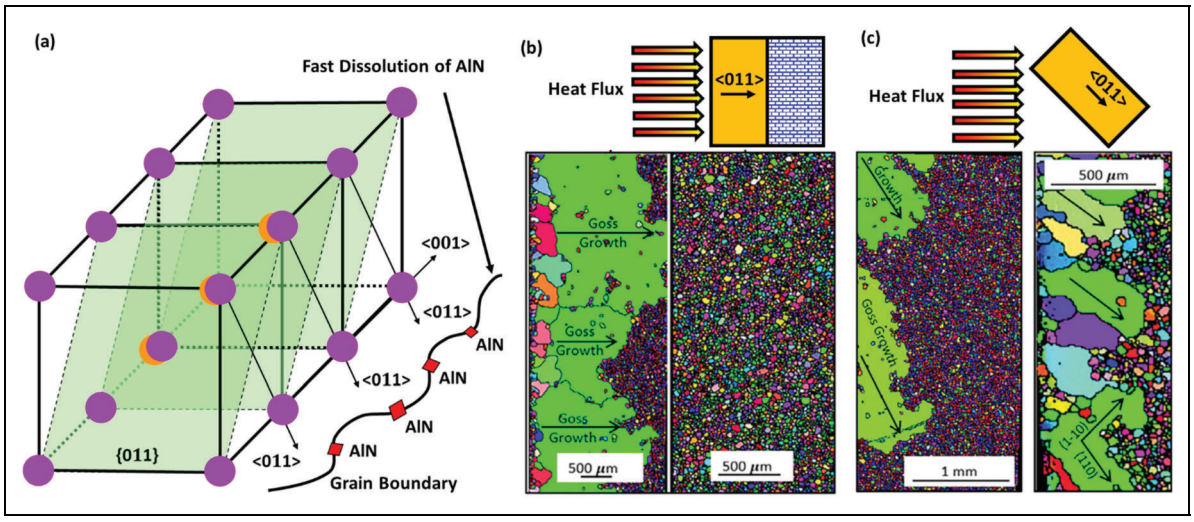

Figure 7. Theory of abnormal growth of Goss based on the heat flux direction[41]: (a) schematic illustration of the direction (<011>) with high heat flux due to high Δd-spacing (expansion), (b) AGG of Goss when heat flux is along the <011> direction, (c) AGG of Goss when heat flux is 45° to the <011> direction.

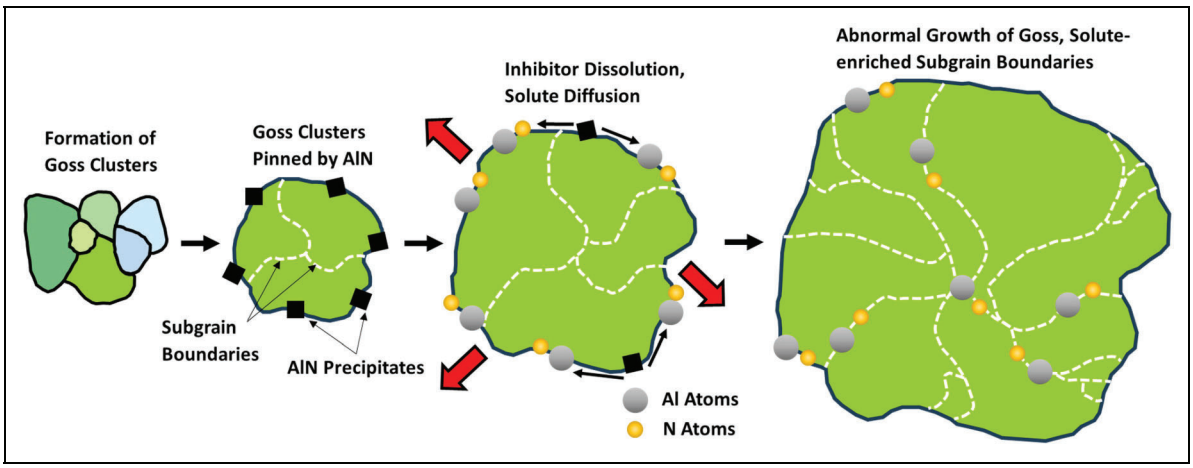

Figure 8. Schematic illustration of the dislocation-assisted particle dissolution theory proposed by Yilmaz et al.[100]

can cause the onset of secondary recrystallisation in steel that does not contain inhibitors. Na et al.[119] claimed that about 90% columnar Goss grains can be formed in silicon steel by concentrated shear strain on the surface, again, without the use of an inhibitor. This was realised by repeated cold rolling and continuous short-time decarbonisation, which produced a two-layer structure: a surface layer containing α-ferrite and an interior layer consisting of pearlite-like structure plus α-ferrite. The difference in strength between the surface and interior layers caused the difference in shear strain between these layers (more strain concentrated on the surface layer), which induced the growth of the Goss. However, these interesting and new methods for GOES development have not been studied by others and the theory regarding the Goss growth has not been investigated.

Summary of the evolution of microstructure and texture in GOES production

Based on the above discussion, the evolution of microstructure and texture (the inheritance of Goss) during the processing of GOES can be summarised as follows (Figure 9):

1. Continuous casting produces a three-layer microstructure with a <001>//ND texture in the columnar grains.
2. Slab reheating dissolves the inhibitors precipitated after solidification and homogenises the microstructure.
3. Hot rolling forms Goss grains in the subsurface layer and an α-fibre texture in the centre layer; inhibitors may precipitate during and after hot rolling.
4. Hot band annealing produces a recrystallised structure with similar textures to those after hot rolling.
5. Cold rolling (with or without intermediate annealing) deforms the recrystallised grains and generates a {111}<112> texture in the matrix and Goss grains near the surface.
6. Primary recrystallisation produces a fine microstructure with a {111}<112> texture in the matrix and large Goss grains near the surface.
7. Secondary recrystallisation promotes the AGG of Goss and prevents the growth of other grains, leading to a strong Goss texture in the final sheet.

Coating and domain refining

Coating is an integral part of the GOES production process and plays an important role in reducing the eddy current loss. In addition, removing the surface oxides and applying coating onto GOES sheets not only protect the steel from corrosion, but also improve the magnetic properties, i.e., reducing the core loss and magnetostriction by providing insulating resistance and improving the surface roughness (increase in the number of mobile domains).[120,121] The tensile stress imparted from the coating on the steel sheet eliminates the surface closure domains and narrows domain wall spacing, thus decreasing the excess (anomalous) loss,[121] which involves microscopic eddy currents induced by moving domain walls. It is a common practice to add MgO separator during or after the decarbonisation process to facilitate the subsequent high temperature annealing by forming a glass film (Mg_2SiO_4) which prevents the sticking of the steel sheets and absorbs harmful impurities from the steel. The separator coating (Mg_2SiO_4 glass film) may be removed after secondary recrystallisation and a layer of metallic plating, e.g., Zn, Sn, Cu or Ni, may be applied.[120] Finally, a phosphate coating (a mixture of colloidal silica and aluminium orthophosphate) is applied and baked (350–450 °C) onto the GOES sheets[121] to form the final insulating coating.

The core loss of the GOES sheets can be further reduced by refining the magnetic domains, normally through the introduction of mechanical or thermal strains (residual stresses) in the GOES sheets.[122,123] While the production of high permeability GOES by reducing the deviation angle from 7° to 3° considerably improves the magnetic induction, the grain size is also increased from about 0.3 mm to 10 mm,[121] which deteriorates the core loss. Since it is difficult to reduce the grain size while achieving the sharp Goss texture using metallurgical means, non-metallurgical techniques were developed, e.g., making

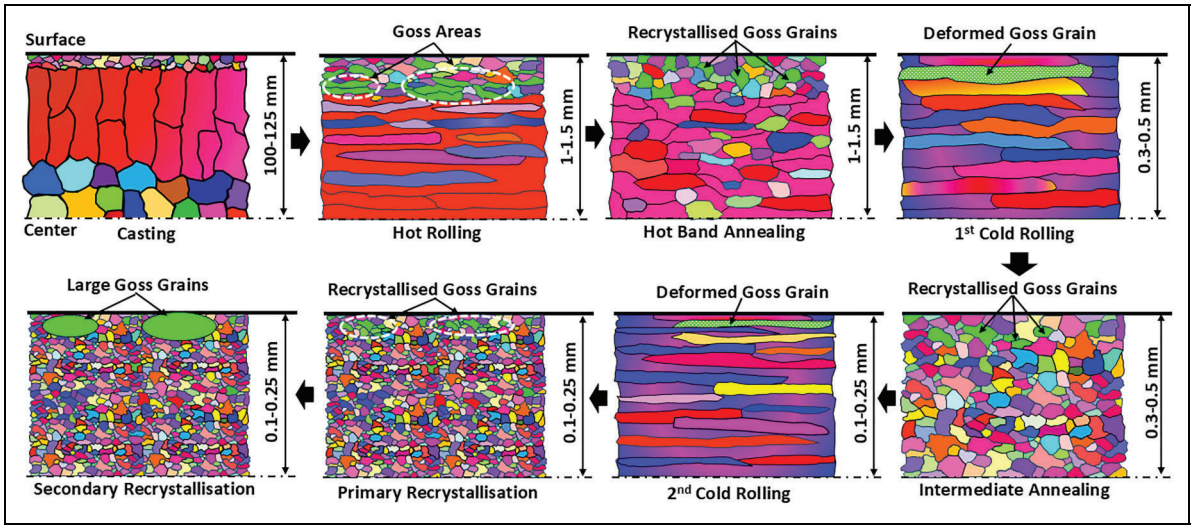

Figure 9. The inheritance of the Goss grains through the processing steps employed during GOES production (the traditional Goss method).

scratches or grooves on the sheet surface using knife, razor, or metal brush,[122] or using laser to scribe on the surface.[123] The purpose is to reduce the anomalous loss through the decrease of magnetic domain size. These methods are relatively simple to apply and can considerably improve the magnetic properties of the GOES sheets.

Future research and development

With continued research and development in the past decades, the magnetic quality of GOES has been significantly improved.[27,124] However, since the 1970's, the improvement of magnetic flux density in GOES has been relatively small,[125–129] as the magnetic induction (B_8 = 2.0 T) is already very close to the saturation flux density of 2.03 T (single {011}<100> crystal).[130] While there is still some room to further reduce the core loss by reducing the sheet thickness and optimising the microstructure, the potential to improve the magnetic flux density (B_8) by texture optimisation is very limited as the deviation angle from the ideal Goss in high permeability GOES has already been reduced to about 3°, which is very close to the theoretical single crystal orientation. Thus, the focus of future research on GOES production should be placed on reducing the costs (e.g., using CSP, TRC, low-temperature slab reheating, etc.) and alleviating the environmental impact (e.g., using electric arc furnace instead of blast furnace for steelmaking) while achieving excellent magnetic properties. Processing routes without using inhibitors may also be interesting to explore as they may significantly simplify the processing procedure and reduce costs.

Although most GOES sheets are used at the power frequency of 50/60 Hz, there is a niche market for high frequency applications where ultra-thin (0.2–0.05 mm) or ultra high silicon (6.5% Si) GOES sheets have apparent advantages, i.e., much lower core losses than the conventional GOES sheets, zero magnetostriction, etc. Developing technologies to economically produce such GOES products is a potential gamechanger in the future, though it remains uncertain if economically viable processing routes can be developed for such ultra-high silicon grades. Increasing the silicon content of relatively low silicon (< 3.2%) steel after it is cold rolled to produce 6.5% Si GOES using more cost effective and environment friendly methods (other than chemical vapour deposition) may also be a route to pursue.

From a scientific point of view, the theory regarding the AGG of Goss is still not completely established, especially the mechanism that governs the preferential growth of Goss during the early stage of secondary recrystallisation. Efforts should be made to understand what exactly causes the rapid growth of the very few Goss grains out of a matrix consisting of many other grains of similar sizes with various orientations or even other Goss grains that do not grow. On the other hand, how is the Goss 'inherited' from the hot rolling process and survives/reappears after hot band annealing, cold rolling, primary recrystallisation, and finally grows abnormally during secondary recrystallisation is still not well understood, which deserves further investigation.

Overview of NOES processing

Different from GOES where forming a sharp and single Goss texture with the <100> in the RD is the final goal, NOES not only requires the <100> directions to be *uniformly distributed* in the sheet plane, but also needs an optimal grain size to minimise the core loss.[131,132] The typical processing procedure for NOES production is schematically illustrated in Figure 10. Again, continuous casting is normally employed to produce NOES, which is followed by hot rolling, cold rolling, and annealing. High-temperature slab reheating and secondary recrystallisation are not needed. For semi-processed NOES, a temper rolling process (also known as skin pass rolling) is

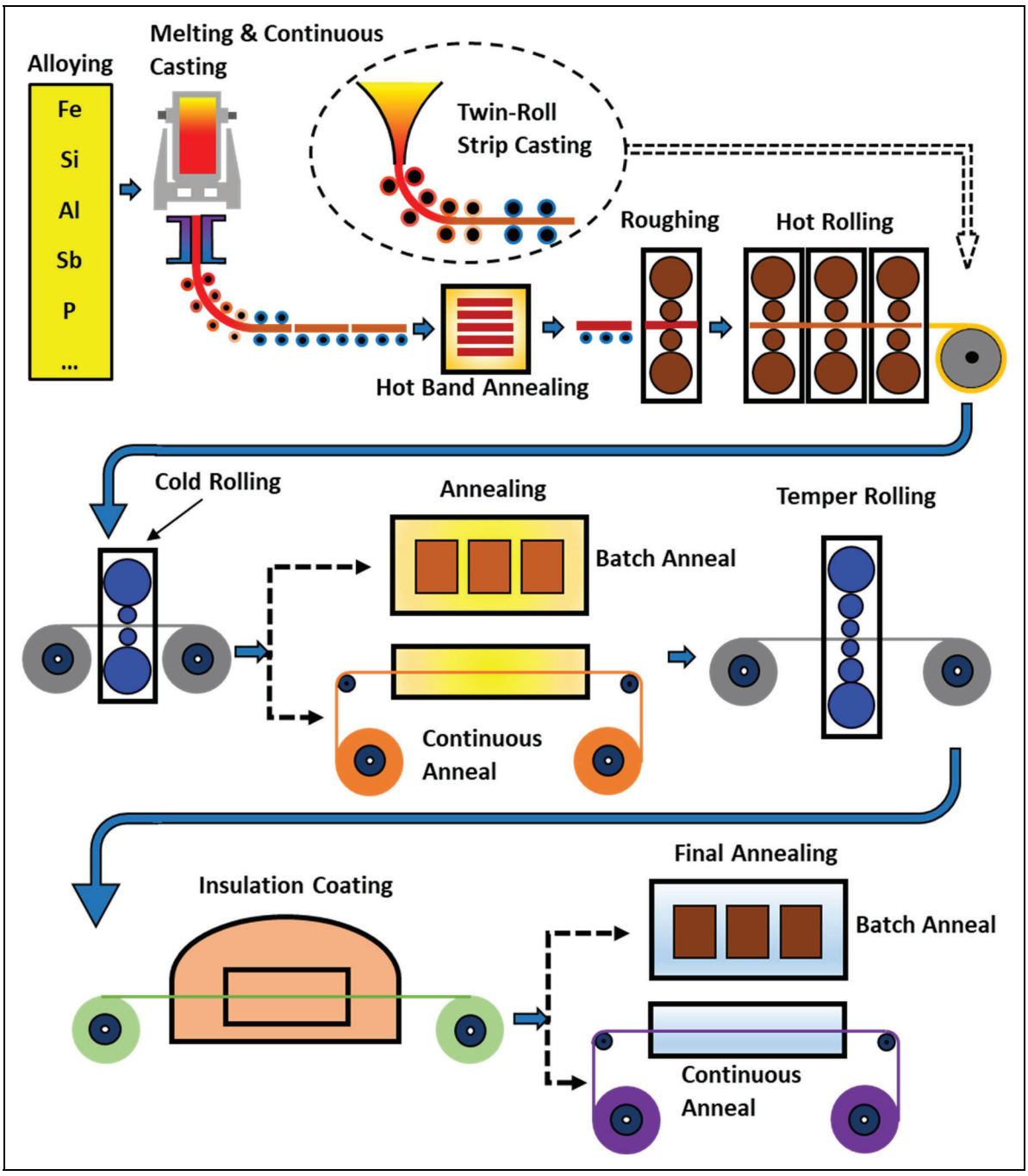

Figure 10. Schematic illustration of the NOES production process.

applied to flatten the steel sheets and ensure smooth surfaces,[133] which is followed by final annealing.

As mentioned before, the ideal final texture for NOES is the <001>//ND fibre texture (also known as θ- or λ- fibre). The evolution of texture in NOES essentially follows similar mechanisms to those of low-carbon steel, which have been extensively investigated.[134–136] However, after conventional rolling and annealing, the final NOES sheets normally show strong <111>//ND and <110>//RD fibres, which are not the desired final texture. How to obtain a uniformly distributed <001>//ND texture in the final sheet together with an optimal grain size is the focus of NOES research. Before discussing the NOES processing steps, the correlation between the magnetic properties and the microstructure/texture of NOES is briefly examined.

Correlation between the magnetic properties and microstructure/texture

The relationship between the core loss of NOES and the grain size (50 Hz) is shown in Figure 11. The eddy current loss and excess loss increase with the grain size (D), while the hysteresis loss decreases with the grain size. More precisely, it was demonstrated[137,138] that the hysteresis loss is proportional to $1/\sqrt{D}$ (where D is the

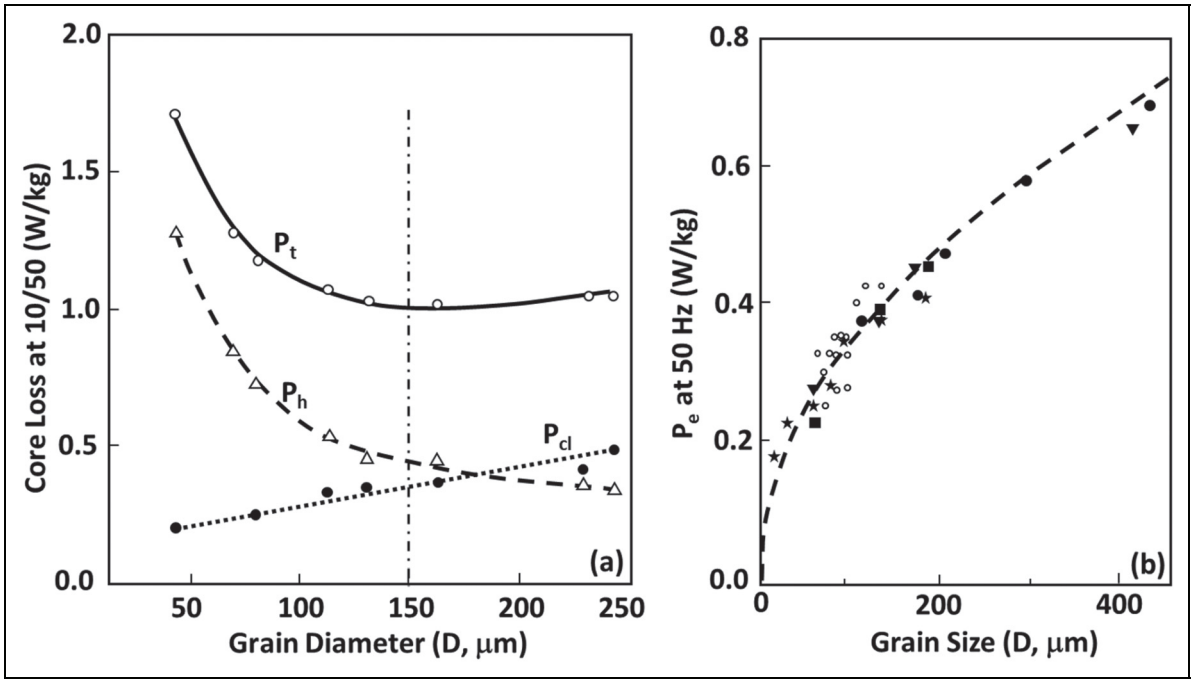

Figure 11. The relationship between the core loss and grain size: (a) hysteresis loss (P_h), eddy current loss (P_{cl}) and total loss (P_t) vs. grain diameter,[138] (b) excess loss (P_e) vs. grain size.[137]

grain size), the excess loss is proportional to $\sqrt{D}$, and the eddy current loss is proportional to D. As a result, the total loss is minimum only when the grain size is optimum, e.g., ~150 μm, as shown in Figure 11a.[138] Thus, in NOES production, it is necessary to produce an optimum grain size during final annealing to minimise the core loss. On the other hand, the core loss is also proportional to the anisotropy parameter, $A(\vec{h})$, as shown in Figure 12(a). A texture that leads to a smaller $A(\vec{h})$ will give rise to a smaller core loss. However, the effect of texture on core loss also depends on the grain size.[17] When the grain size is small (<100 μm), the optimisation of texture may result in a considerable decrease of the core loss; when the grain size is large (>200 μm), the core loss is less sensitive to texture.

The relationship between the magnetic flux density at 5000 A/m (B_{50}) and the anisotropy parameter is shown in Figure 12(b). The magnetic flux density linearly decreases with $A(\vec{h})$[139,140]:

$$B_{50} = C_1 - C_2\, A(\vec{h}) \tag{8}$$

where C_1 and C_2 are material constants depending on the alloying elements and grain size. Optimising the texture to reduce the $A(\vec{h})$ will increase the magnetic flux density. It should be noted that, the B_{50} value is essentially only dependent on the crystallographic texture and not sensitive to the thickness, grain size, and inclusions.[141] Nevertheless, Lee et al.[17] reported that, grain size also slightly affects the magnetic flux density: large grains somewhat reduce the magnetic flux density due to the increase of eddy current with the grain size.

It is thus seen that, during the processing of NOES, controlling the grain size is critical to achieving a minimum core loss, while producing a texture that minimises the anisotropy parameter ($A(\vec{h})$) will increase the magnetic flux density as well as decrease the core loss. The production of NOES is thus aimed at achieving an optimal grain size while obtaining a desired texture that minimises the anisotropy parameter. However, since all the thermomechanical processing steps employed in steel production will change the microstructure and crystallographic texture simultaneously, achieving both the desired grain size and texture is very challenging. Recent progress in optimising the microstructure and texture of NOES is reviewed in the following sections.

Effect of alloying elements on microstructure, texture, and magnetic properties

Silicon. Silicon is also the major alloying element in NOES to effectively reduce eddy current loss.[142,143] Silicon increases the electrical resistivity, decreases the ductility, and reduces the maximum flux density.[3,144] The saturation induction, anisotropy constant, and magnetostriction decrease with the silicon content,[144,145] while the yield strength and tensile strength increase with silicon. A minimum total loss was observed at near 6.5% silicon, but the poor mechanical properties of this material at room temperature have essentially prevented the processing of this alloy through conventional routes. The development of a chemical vapour deposition (CVD) method to increase the silicon content of relatively low silicon steel sheets through siliconizing[146,147] has enabled the commercial production of this steel, but the workability of the final sheet is still low, and the associated cost is high, which limited its wide application. Research on the 6.5% Si NOES has

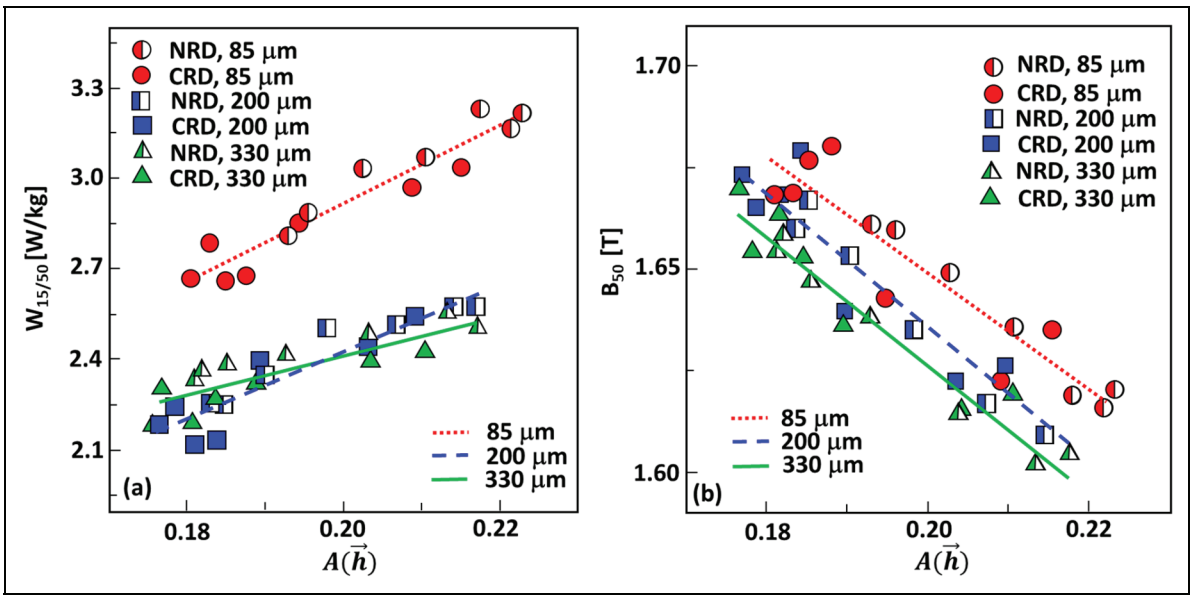

Figure 12. The relationship between the magnetic properties and the grain size and anisotropy parameter of NOES: (a) core loss at 1.5 T/50 Hz vs. the anisotropy parameter, (b) magnetic flux density B_{50} vs. the anisotropy parameter. The data are grouped according to the grain size. NRD: normal rolled, CRD: cross rolled.[17]

been increasing recently, and a comprehensive review on the 6.5% Si electrical steel has been given by Ouyang et al.[34]

Aluminium. Aluminium is often added to NOES to increase the resistivity as well, as it can partially replace silicon while maintaining similar magnetic properties. With additions in the range of 0.1 to 0.6%, the material with a certain amount of Si + Al is generally more ductile than those containing a similar amount of silicon alone.[3] Increasing the Al content increases the phase transformation temperatures during cooling of low silicon NOES containing 0.61% Si.[148] Aluminium has also been used as a dipping element to increase the resistivity of silicon steels, either as pure Al melt or as Al-Si melt, due to their low melting temperatures.

Manganese. Mn has been frequently added to electrical steels to increase the ductility of the material and facilitate the manufacturing.[3] Mn has essentially no effect on the crystallographic texture or the magnetic properties.[3] Adding Mn in NOES has shown contradictory results: Cardoso et al.[149] reported the improvement of the <001>// ND texture in a 3.0% Si NOES by adding 0.54% Mn, and Homma et al.[150] reported similar effect by adding 1.3% Mn in a 0.5% Si NOES. Kubato[151] indicated that adding up to 2.0% Mn to 3.0% Si steel increases the core losses and decreases the magnetic induction. When there is Mn in the steel, the S and O levels should be kept to very low so that Mn is in solid solution instead of manganese sulphide or oxide precipitations. Schulte et al.[152] examined the effect of up to 1.38% of Mn on 2.66% Si steel. It was found that Mn slightly improves the texture and reduces the core losses when the frequency is greater than 100 Hz. However, the saturation magnetic induction and B_{25} are reduced by Mn.

Phosphorus. The effect of P addition on electrical steels is somewhat contradictory in the literature. The works of Hou et al.[153] and Park et al.[154] showed an increase of both electrical resistivity and core loss due to the grain refinement induced by the addition of P. Tanaka and Yashiki[155,156] reported that the addition of 0.1% P in a 2.0% Si electrical steel only slightly reduces the magnetic induction when the thickness of the steel is reduced, while for the steel with 0.01% P, the magnetic induction drops significantly with the reduction of thickness. Lee and De Cooman[157] reported that the addition of P increases the electrical resistivity, which reduces the eddy current loss. However, the grain size is increased (although the recrystallisation was delayed) by the increase of the P content and the texture was improved as well, which reduced the hysteresis loss. Lee et al.[158] studied the effect of P on a 3.0% Si steel, and it was shown that the addition of 0.2% P in the steel can optimise the texture by promoting the cube {001}<100> texture while supressing the {111} <112> texture. The magnetic induction was increased while the core loss was decreased by the addition of P.

Tin and antimony. Sn is generally regarded as a harmful element for steel and is therefore not often considered as an alloying element.[159] Sn is a surface-active element which segregates at surface and grain boundaries during recrystallisation. The decrease of surface energy depends on the grain orientation, which leads to selective growth of grains with certain orientations, e.g., <100>//RD (cube and Goss).[160] The segregation of Sn at the subgrain boundaries of the as deformed/recovering microstructure was suggested to have a pinning effect during subgrain coarsening

and thus retarding the onset of recrystallisation in {111} oriented grains.[161] The works of Chang and Huang,[162] Dong et al.,[163] and Hou et al.[164] showed improved texture and thus low core loss and high magnetic flux density. Due to the positive effect of Sn on the texture and magnetic properties, a few patents were applied on the manufacturing of Sn-added non-oriented electrical steel.[165,166]

Antimony is another surface-active element usually added to NOES to improve the texture.[167,168] The addition of a small amount of Sb (up to 0.2%) causes the retardation of the {111} nucleation at the cold rolled grain boundaries if the steel was annealed after hot rolling.[167] Sb also promotes the growth of the {220} and {200} grains at the expense of the {222} and {211} grains.[169] Together with the increased grain size, this leads to reduced core loss as well as increased magnetic permeability. Jenko et al.[170,171] studied the effect of Sb addition on the texture of 1.8% and 2.0% Si steels and it was found that Sb segregation at the surface selectively decreases the surface energy of {001} grains and promotes the growth of these grains. However, excessive level of segregation coverage will cause the decrease of surface energy of all grain orientations and lose the selective growth of preferential orientations. It was also found that the addition of 0.04 to 0.05% Sb[172,173] can promote the {001} texture while diminishing the {111} texture, thus reducing the core losses. Several more recent studies also confirmed the influence of Sb on the development of the desired texture in NOES.[174,175]

Cr, Cu, V, Ti, Nb, Mo, and Mg. Generally, these elements are not desired in NOES, but they may appear as trace elements from the scrap steel used in the production of NOES. Most of these elements (except Cu and Mg) tend to form precipitates with N and C (nitrides and carbides) in the steel, which suppress grain growth and hinder magnetic domain wall motion, resulting in the deterioration of magnetic properties.[176] Thus, these elements are usually kept as low as possible, e.g., below 0.005~0.002%. It was reported[177] that adding up to 0.3% Cu in 6.5% Si steel was able to improve the plasticity of the steel due to the dissolution of Cu in solid solution which reduces the long-range ordering. The core loss of the 6.5% Si steel with up to 0.5% Cu was reported to be lower than that without Cu, which was caused by the larger grain size after recrystallisation resulted from the addition of Cu.[178]

C, N, S, O and B. Due to the tendency to form precipitations with other trace elements in the steel (thus affecting the magnetic properties), these elements are generally kept as low as possible in NOES. Both C and N are the elements causing magnetic aging in electrical steels.[3] Sulfur tends to form precipitates with Mn, Cu, etc., also causing the deterioration of magnetic properties.[179] As a result, these elements were usually removed by heat treating the material in hydrogen at very high temperatures (1300°C).[180] It has also been shown that the development of crystal orientations in electrical steels is sensitive to impurities, e.g., fine aluminium oxide may inhibit proper growth of favourably oriented grains.[181] Carbon has been reported to have unique effects on the changes of slip activation and twinning deformation[182] as well as on the phases of electrical steels.[3,183] The changes of slip activation and twinning deformation promote the formation of the rotated cube texture ({001}<110>). The addition of carbon extends the austenite + ferrite region in Fe-Si. Therefore, by adding carbon in the electrical steel, the material may experience austenite ↔ ferrite transformations during hot deformation/annealing even if the silicon content is high (> 2.0%), which provides an alternative route to control the texture.[184–186] Again, the C has to be removed or reduced to below ~0.003% in the final sheets to avoid magnetic aging.

The effect of various elements on the microstructure, texture, and magnetic properties of NOES is summarised in Table 3.

Effect of processing steps on microstructure, texture, and magnetic properties

Casting. Continuous casting is also the common casting technology currently used for NOES production. Like in GOES, the casting structure normally consists of equiaxed, columnar, and equiaxed grains, from the surface to the center.[187,188] While the equiaxed grains usually do not show preferred orientations, the columnar crystals normally exhibit relatively strong texture. For cubic metals or alloys, the long axis of the columnar grain is usually aligned in the <100> direction, which grows along the thermal gradient, i.e., perpendicular to the mould wall.[188] As a result, a <001>//ND texture can be obtained after solidification.[141] Although similar issues such as shrinkage and segregation also exist, reports regarding the continuous casting process are rarely seen in the literature, since only major steel companies own such facilities, and the data are normally kept as technical secret.[50]

Considerable recent research on NOES has been dedicated to the TRC process.[60,189,190] Büchner & Schmitz[191] investigated the possibility to produce Fe-6.0% Si strips using TRC and found that a complete columnar structure could form if non-moving rolls were used. Park et al.[192,193] reported the microstructure and texture of 4.3% and 4.5% Si steels processed by TRC. Although the microstructure also consists of chill, dendrite, and equiaxed zones like in mould casting, the dendrite region is not well developed as in direct chill casting. Apparent differences in the deformation of the different layers from the surface were also observed. As a result, the textures along the plate thickness direction can be clearly distinguished as: {100} texture at the surface due to solidification (without deformation), Goss, copper, and brass in subsurface due to shear, and combined solidification and plane strain compression textures such as {100}, α-fibre and γ-fibre in the centre (Figure 13).

It is also demonstrated that both the superheat[193,194] and cooling rate[195] have significant effects on the microstructure and texture of the casting. A low superheat with a high heat transfer coefficient leads to a large undercooling

Table 3. Summary of the effect of alloying elements on NOES.

Element	wt%	Effect
Si	0–6.5	• Increases electrical resistivity, reduces eddy current loss, and decreases saturation magnetic induction. • Stabilises ferrite phase and reduces austenite region. • Reduces magnetic anisotropy and magnetostriction. • Reduces density and ductility and increases yield and tensile strengths. • Essentially does not affect texture.
Al	0–0.6	• Increases electrical resistivity and reduces core loss. • Increases ductility and reduces grain size. • Decreases the saturation magnetic induction and maximum permeability of silicon-free electrical steels (Fe-Al). • Essentially does not affect texture.
Mn	0–2.0	• Increases ductility and slightly increases austenite region. • Promotes grain growth and reduces core loss. • Contradictory in the effect of Mn on texture and core loss in NOES.
P	0–0.16	• Increases electrical resistivity, hardens the steel by solid solution, and reduces grain size. • Contradictory results in the effect of P on texture, core loss, and magnetic induction.
Sn, Sb	0–0.21	• Both are surface-active elements and improve texture. • Both reduce core loss and increase magnetic flux density or magnetic permeability.
Cr, Cu, V, Ti, Nb, Mo, Mg	<0.005	• Mostly tend to form precipitations and hinder domain wall motion. • 0.3% Cu increases the workability and decreases core losses at frequencies higher than 5 kHz. • 0.5% Cu increases plasticity and reduces core loss in 6.5% Si NOES.
C, N, S, O, B	<0.003	• Mostly tend to form precipitations with other residual elements and deteriorate mechanical and magnetic properties. • May prohibit the growth of favourable orientations. • C extends austenite + ferrite region and retains austenite phase when Si content is high.

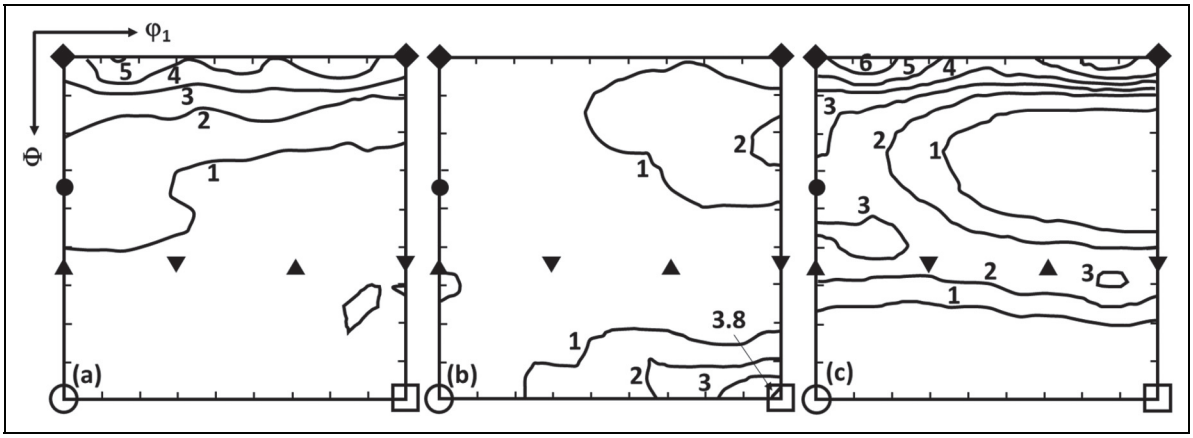

Figure 13. Textures of a 4.5% Si steel after twin-roll casting[193]: (a) surface layer, (b) subsurface layer, (c) centre layer.

and heterogenous nucleation, which gives rise to equiaxed grains throughout the thickness. Increasing the superheat reduces the heat transfer coefficient and enables the selective columnar growth along the <100> direction. A higher superheat promotes the {001} texture (mainly by forming the columnar structure), while a lower superheat tends to form a more random texture (mainly equiaxed microstructure). In most cases, the cast structure and texture are not able to be retained to the final microstructure after hot rolling, cold rolling, and final annealing. However, Cheng et al.[193] reported that the columnar <001> texture formed in the cast structure could be retained by controlling the hot rolling reduction and temperature, intermediate cold rolling reduction, and final annealing temperature, in which it is believed that an exact initial <001> with strong cube orientation is required to retain the <001> texture. Nevertheless, no other evidence on the retention of the <001> casting texture has been reported in the literature.

Hot rolling. Like in GOES production, hot rolling is also a necessary procedure to produce NOES. A few parameters can be varied during the hot rolling process to control the microstructure and texture, e.g., the reheating temperature and soaking time, the starting and finishing rolling temperatures, the number of rolling passes, the inter-pass time, the total amount of reduction, the coiling temperature and time, etc. During hot rolling and the subsequent coiling,

important metallurgical phenomena occur, e.g., work hardening, recovery, recrystallisation, precipitation, phase transformation, etc., which will affect the deformation behaviour, microstructure, and texture of the steel during the subsequent cold rolling, as well as the final microstructure and texture after annealing.

Typical cross-section microstructure and texture of hot-rolled NOES (3.2% Si) are shown in Figure 14.[196] Across the thickness, the microstructure exhibits apparent heterogeneity (Figure 14(a)): small equiaxed (recrystallised) grains near the surface, a mixture of deformed and recrystallised grains in the subsurface region (transition area) and deformed (elongated) grains in the centre. The formation of such a heterogeneous microstructure is due to the stress/strain and thermal gradients along the thickness direction. The texture of the surface region (Figure 14(b)) is similar to that of the shear deformation texture in BCC metals, i.e., mainly copper ({112}<111>), brass ({110}<112>) and Goss ({110}<100>). This is because the nuclei of the recrystallised grains originate from small regions already existed in the deformed state,[197] and they have the same orientations as the deformed material. Since no significant grain growth has occurred, the recrystallised texture is close to the shear deformation texture.

In the sub-surface region, the shear deformation is smaller than that in the surface. The main softening mechanism is recovery (although recrystallisation is also occasionally noticed). The microstructure is mainly composed of elongated grains with some recrystallised crystals. The texture (Figure 14(c)) is similar to the BCC shear deformation texture (copper, brass and Goss). A weak {001}<120> texture is also noticed. In the centre region, the deformation mode is plane-strain compression, and the shear deformation is negligible. The softening mechanism in this region is recovery. As a result, the grains are elongated and the texture (Figure 14(d)) is typical of BCC metals after rolling, i.e., mainly consisting of α- and γ-fibres. A strong <001>//ND fibre is also noted. The

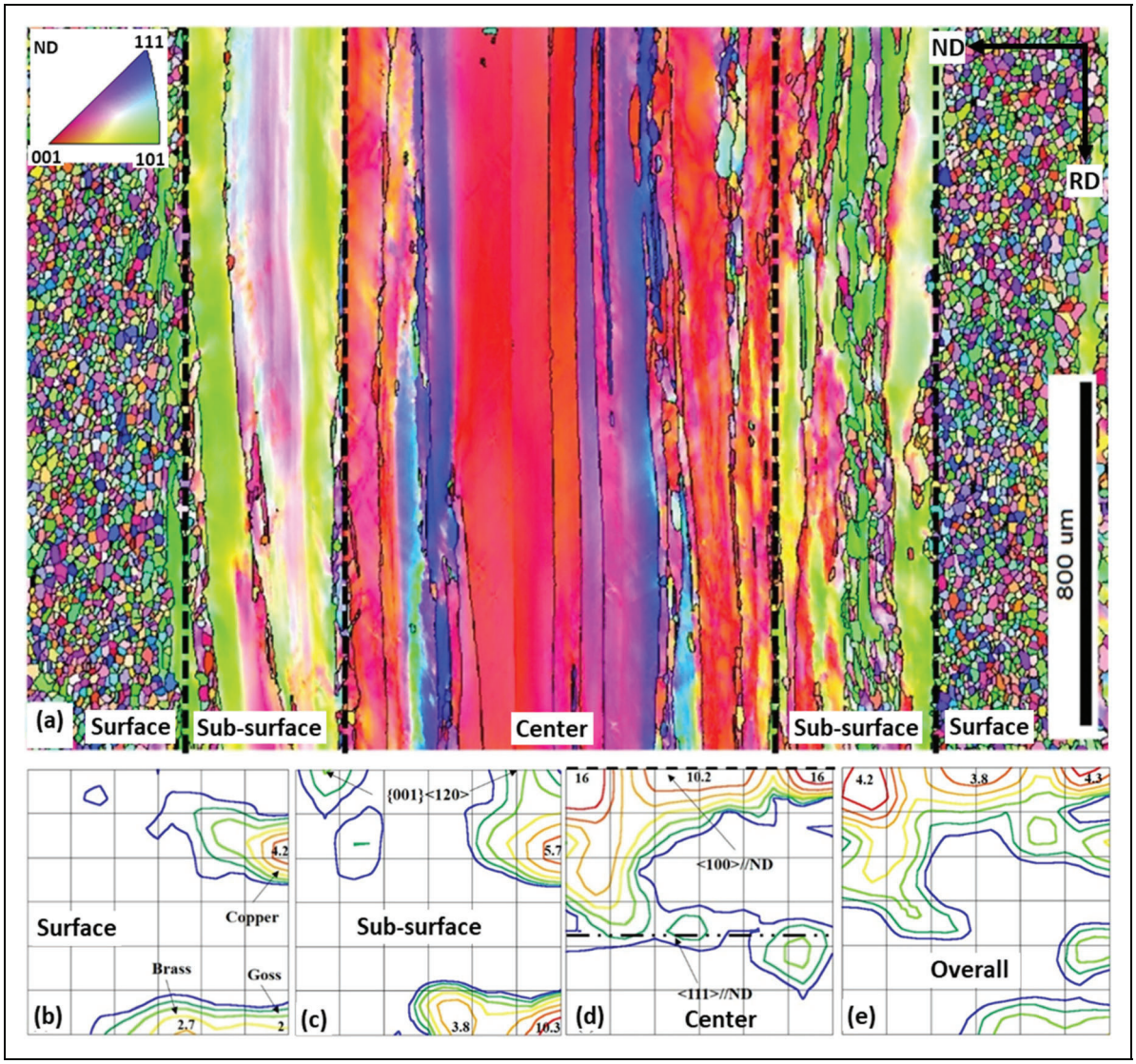

Figure 14. Cross-thickness microstructure and texture of hot rolled 3.2% Si steel[196]: (a) IPF map, (b) texture of surface, (c) texture of sub-surface, (d) texture of centre, (e) overall texture.

overall texture is a combination of the textures from the three layers (Figure 14(e)).

Lyudkovsky and Southwick[198] investigated the effect of thermomechanical processing history on the precipitation, microstructure, texture, and magnetic properties of a 2.0% Si electrical steel with different carbon and aluminium contents. For steels with phase transformation (containing 0.01–0.015% C), the reheating at a lower temperature (1150°C) resulted in a smaller ferrite grain size before hot rolling, which led to complete recrystallisation after coiling at a higher temperature (760°C). The smaller ferrite grain size was due to the presence of austenite, which formed at the ferrite grain boundaries during cooling and hot rolling. Since a smaller starting grain size provides more nucleation sites and requires a lower critical deformation for recrystallisation to occur, it is easier to recrystallise after coiling at a higher temperature. For the steel without phase transformation (0.003% C), the reheating temperature did not significantly affect the ferrite grain size before hot rolling (grain size was large). The hot rolling and the following coiling could not result in complete recrystallisation of the microstructure no matter what the reheating or coiling condition was. The difference in microstructure after hot rolling resulted in differences in the final grain size after continuous annealing or decarburisation annealing, and finally differences in the core loss of the steel. It was also shown that when the reheating temperature was lower, and the coiling temperature was higher, the texture was optimal.

Fischer and Schneider[183] studied the effect of deformation process, especially hot rolling, on the texture and magnetic properties of NOES. It was indicated that (Figure 15), for NOES exhibiting an austenite phase (Si + Al content less than ~2.0%), the hot rolling performed in the austenite region, ferrite region, austenite-ferrite two phase region, or two phase plus ferrite region will give rise to significantly different hot rolling microstructures and textures. This is due to the differences in the deformation and recrystallisation behaviours of the two phases as well as the changes in microstructure and texture associated with the phase transformation process. On the other hand, due to the difference in flow stress of the two phases, hot rolling in different regions may lead to significant variations in the roll forces, which poses challenges to the control of hot rolling during mass production. Knowledge on the flow behaviour of different grades of NOES at high temperatures is crucial to the hot rolling process. However, this data is rarely seen in the literature as it needs to be extracted from the data logs of hot rolling mills, which is commonly considered as highly confidential information by most steel companies.

The effect of hot rolling on the microstructure and texture of NOES shows diverse results in the literature. Da Costa Paolinelli et al.[199] investigated the effect of hot rolling finishing temperature (920–1120°C) on the grain size, texture, and magnetic properties of a 2.0% Si NOES after final annealing. It was shown that increasing the hot rolling finishing temperature to above 1040°C enhanced the cube and Goss textures and reduced the {111}<112> fraction of the final annealed sheets (Figure 16(a)), thus improving the magnetic induction (Figure 16(c)). However, the core loss was also increased (Figure 16(c)) due to the decrease of the final annealed grain size caused by the increased hot band grain size (Figure 16(b)), which induced a large amount of shear bands in the cold rolled structure and a large number of nuclei. It was also shown that the variation of hot rolling temperature only resulted in a small variation in the hot rolling textures. Da Cunha and Da Costa Paolinelli[200] investigated the hot rolling of a 1.3% Si steel, and it was shown that a combination of high hot rolling temperature and hot band annealing resulted in lower core losses and higher permeabilities. In the study of

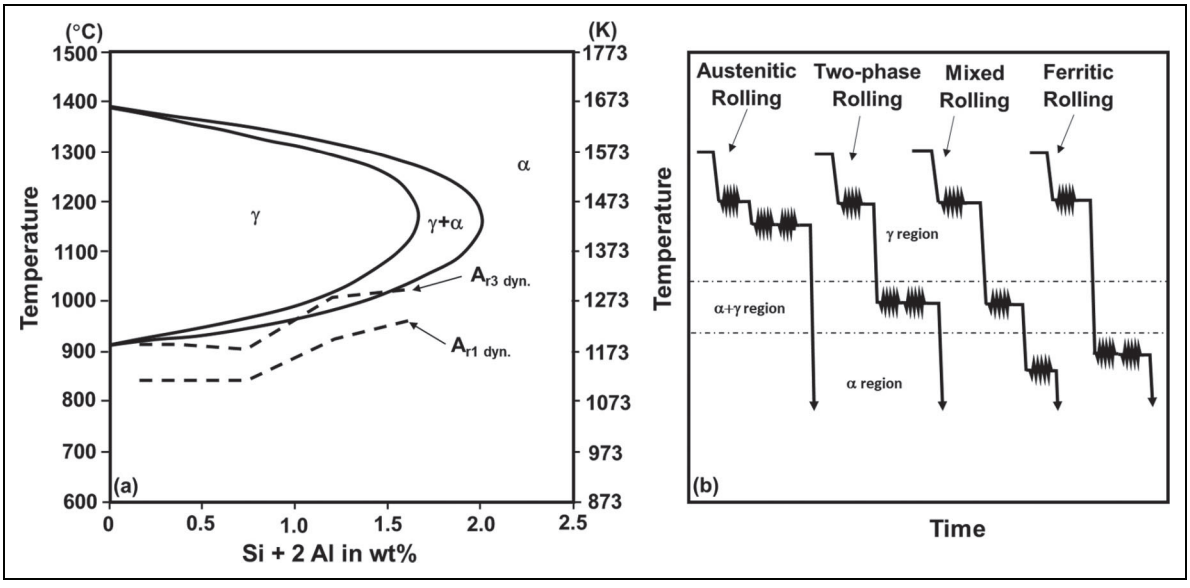

Figure 15. Hot rolling of NOES[183]: (a) Fe-rich portion of Fe-(Si + 2Al) phase diagram superimposed by the dynamic Ar_3 and Ar_1 critical temperatures, (b) various hot rolling routes.

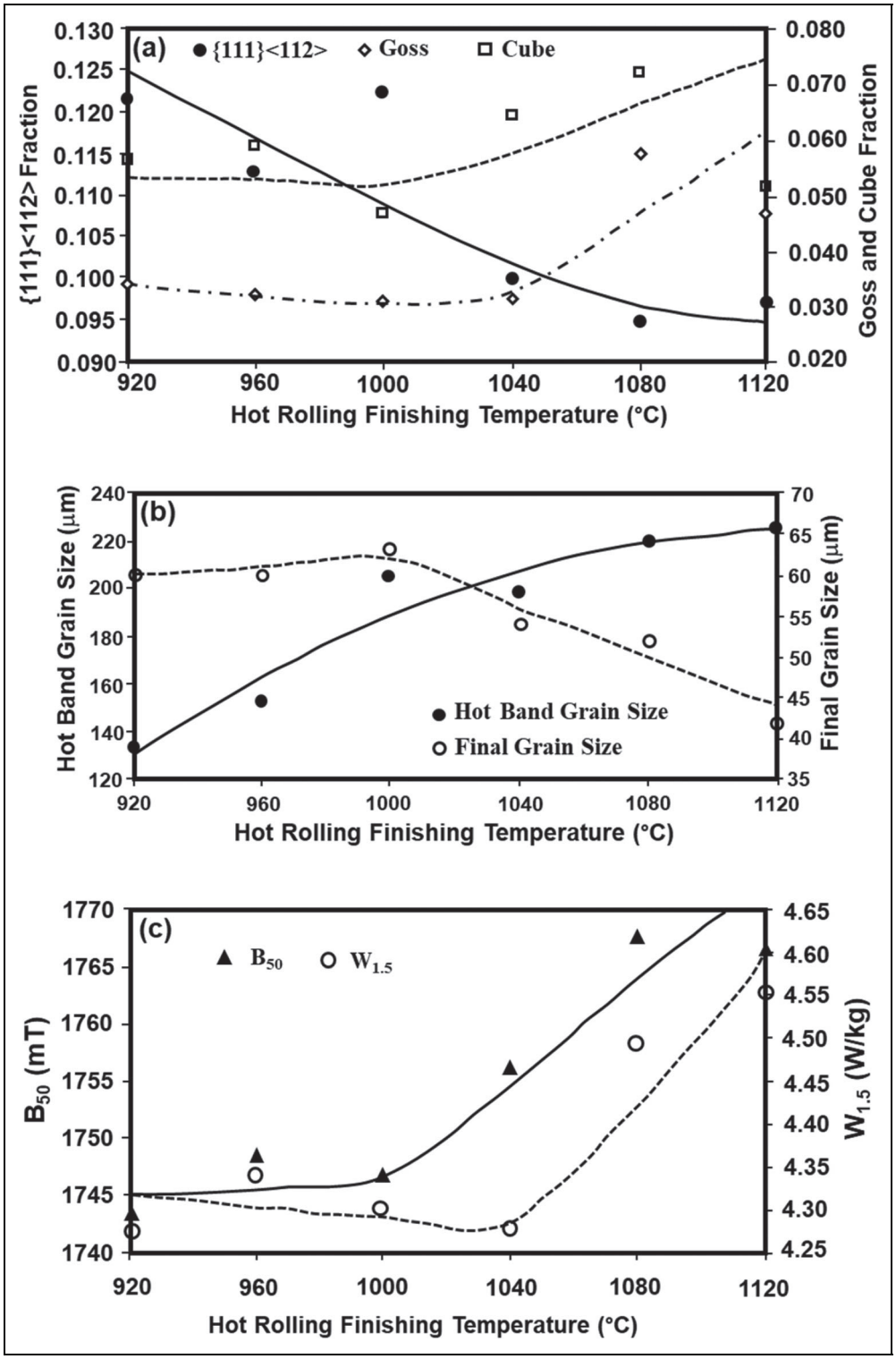

Figure 16. Effect of hot rolling finishing temperature on the final texture, grain size and magnetic properties of a 2.0 wt% Si NOES[199]: (a) volume fractions of texture components, (b) hot band and final grain sizes, (c) magnetic induction (B_{50}, 5000 A/m) and core loss ($W_{1.5}$, 1.5 T/60 Hz).

a 1.0% Si NOES, An et al.[201] showed that combining a low-finishing-rolling temperature with hot band annealing led to appropriate textures and large grain size, thus resulting in high magnetic induction and low core losses.

The effect of hot rolling temperature on the texture and magnetic properties of a 3.0% Si was investigated by De Dafé et al.[202] It was found that shear band formation in the material played an important role in determining the final texture of the steel after cold rolling and final annealing. Verbeken et al.[203] investigated the effect of cooling condition after hot rolling on the texture of a 2.4% Si steel. It was shown that slow cooling from 800 to 200°C

could essentially eliminate the γ-fibre and promote the rotated cube texture. After cold rolling, a strong rotated cube texture was formed. However, after annealing, the texture did not seem to be very different between slow cooling from 800°C to 200°C and rapid cooling from 820°C to 400°C.

Apparently, hot rolling does have important effects on the final microstructure, texture, and magnetic properties. These effects, however, may not be obviously reflected in the final material since the structures and textures after hot rolling are destroyed in the subsequent processing stages, e.g., hot band annealing, cold rolling, intermediate annealing, and final annealing. Furthermore, for low silicon steel or NOES containing a relatively high amount of carbon,[3] phase transformation plays an important role in determining the microstructure and texture of the hot rolled material. Therefore, the hot rolling operational parameters may significantly affect the final material properties. Low silicon steels normally show better texture than those of high silicon steels, which may suggest that phase transformation plays a vital role in determining the final texture. However, in the literature, only limited discussion in this aspect was noticed. Systematic studies on the effect of phase transformation on the microstructure and texture are needed to trace the changes of microstructure and texture from hot rolling to final annealing and verify the influence of various hot rolling parameters on the material properties.

Hot band annealing. Hot band annealing (also known as normalising) is generally *not* a required processing step for NOES since the hot bands can usually be directly cold rolled. However, many studies have shown that hot band annealing can considerably modify the final microstructure and texture after cold rolling and annealing, thus affecting the magnetic properties of NOES. Figure 17 compares the microstructures and textures of a 2.8% Si NOES after hot rolling and after hot band annealing.[196] The layered, heterogenous microstructure after hot rolling (Figure 17(a)) is replaced by a more homogenous, equiaxed structure after hot band annealing (Figure 17(b)).

The textures of the layered structure after hot rolling are altered by hot band annealing,[204] although some of the texture components are inherited (Figs. 17(c) and 17(d)). The brass, Goss, and copper textures in the surface region are essentially retained (copper) or even enhanced (brass and Goss). The inheritance of these texture components from the hot rolled steel is due to the recrystallisation in the surface region that has already occurred during hot rolling, which gives rise to strain-free crystals such as brass, Goss and copper. These grains can preferentially grow into the neighbouring deformed grains that have higher stored energy, thus forming strong recrystallisation textures. New {001}<350> and {110}<110> orientations appear in the surface region after hot band annealing (Figure 17(d)), which are not seen in the hot-rolled material (Figure 17(c)). The centre region shows a significant change of texture after hot band annealing, because the recrystallisation starts from a deformed (but recovered) microstructure after hot rolling. The very strong deformed {001}<110> and {112}<110> components (Figure 17(c)) are replaced by the {001}<120>-{001}<350> and {113}<110> orientations after hot band annealing (Figure 17(d)), while a number of new orientations such as Goss and rotated Goss are also noted. The maximum intensity has been significantly decreased from ~30 to ~6.6. The overall texture across the thickness after hot band annealing (Figure 17(d)) is composed of Goss, brass, copper, {113}<110>, and {001}<120>-{001}<350>, a combination of both the surface and centre regions.

Shimanaka et al.[168] reported that hot band annealing could enhance the {001} texture, while Yashiki and Kaneko[205] showed that a {110} texture was promoted by hot band annealing. In NOES that shows phase transformation,[206] the hot band annealing temperature plays an important role in determining the texture. It was noted that hot band annealing at 800°C led to the highest intensity of the favourable {200} textures and the lowest intensity of the unfavourable {222} textures (Figure 18(a)). Gutiérrez-Castañeda and Salinas-Rodríguez[207] showed similar results in the study of a 0.57% Si (with 0.05% C) steel by varying the hot band annealing temperature from 700 to 1050°C. It was shown that annealing in the intercritical region (800–850°C) led to rapid decarburisation and the development of large columnar ferrite grains, which gave rise to a {001} fibre texture after cold rolling and final annealing at temperatures up to 850°C. Liu et al.[208] studied the effect of hot band annealing on the texture of a 4.2% Si steel and it was shown that hot band annealing promoted the <100>//RD fibre and supressed the γ-fibre. However, the study of Wu et al.[209] showed that hot band annealing (at 920 and 980°C) promoted the formation of the {411}<148> texture as compared to the {111}<112> texture in the steel without hot band annealing.

Hot band annealing temperature also affects the final grain size of the cold-rolled sheets after annealing.[206] With the increase of the hot band annealing temperature, the final grain size increases (Figure 18(b)), mainly due to the coarsening of the MnS inclusions, which decreases the retardation effect on grain growth. It has been shown before that both grain size and texture influence the magnetic properties of the final sheet. From Figure 18(b) it is seen that the lowest core loss was not observed in the sample after hot band annealing at 800°C, which has the highest intensity of {001} and the lowest intensity of {222} (Figure 18(a)). The relatively large core loss at this temperature is mainly due to the small final grain size (not optimal).[17] Similarly, the magnetic flux density at 5000 A/m (B_{50}) does not match the texture, i.e., the maximum B_{50} is not at 800°C where the {100} is the strongest and the {111} is the weakest, but at 900°C (Figure 18(a)). This may also be attributed to the effect of both the texture and grain size on the flux density.[17,206]

In the study of a steel with 2.0% Si, Park and Szpunar[210] investigated the effect of grain size (after hot band annealing) before cold rolling on the texture and magnetic properties. It was demonstrated that a coarse-grained steel led to a

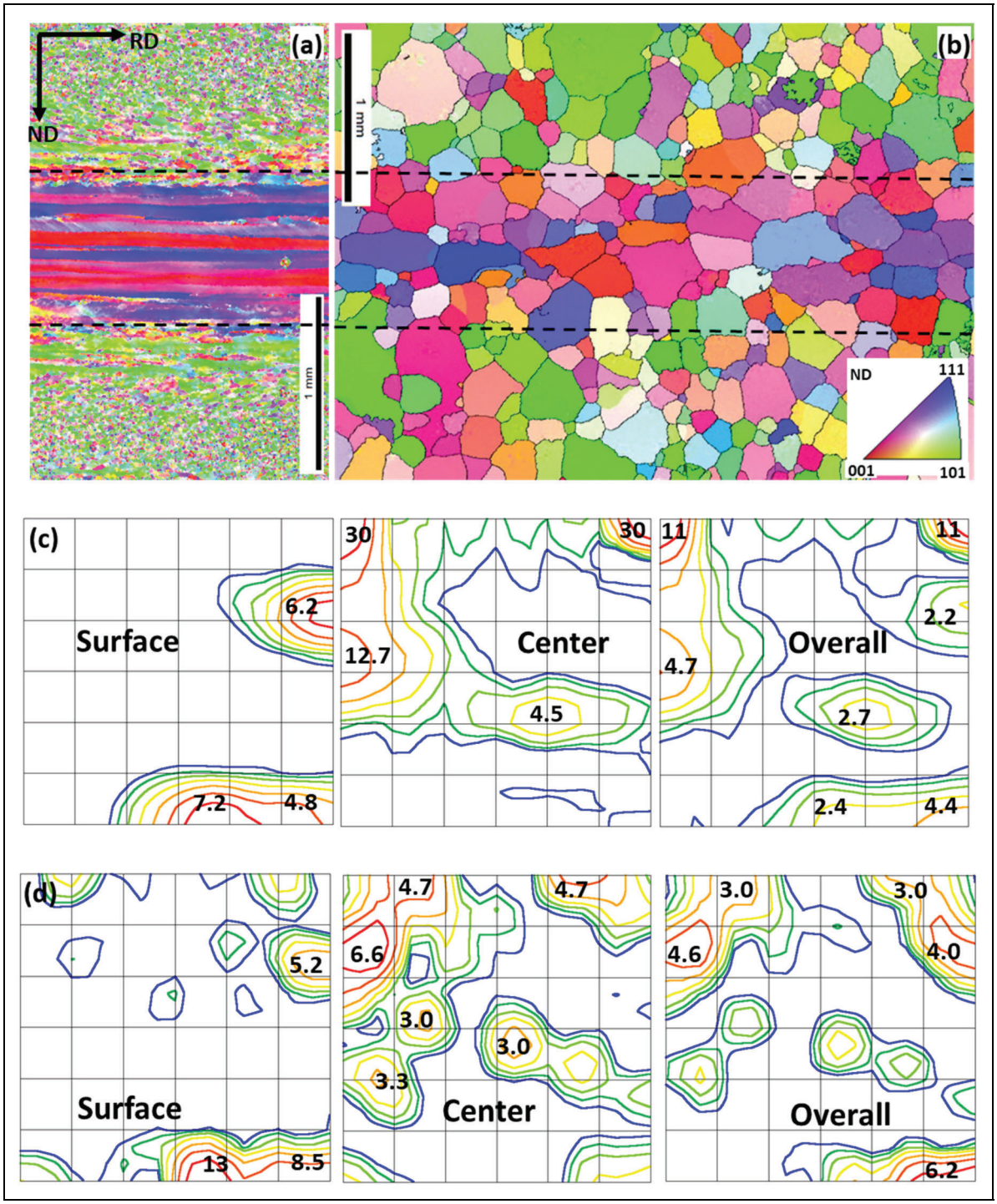

Figure 17. The microstructure and texture of a 2.8% Si NOES[204]: (a) IPF map after hot rolling at 1040 °C, (b) IPF map after hot band annealing at 840 °C for 60 h, (c) texture after hot rolling at 1040 °C, (d) texture after hot band annealing at 840 °C for 60 h.

stronger Goss and a weaker <111>//ND texture than fine-grained steel after cold rolling and final annealing, which gave rise to better magnetic induction but with only slight effect on the core loss. Chang and Huang[211] showed that by hot band annealing, the core loss was reduced while the flux density was increased after final annealing, which was realised through the increase of the final grain size and the optimisation of the texture (higher cube and lower γ-fibre). A few studies (Liu et al.,[212] Xu et al.,[213] Wang et al.[214]) have also been carried out to investigate the effect of hot band annealing on the microstructure, texture, and magnetic properties of twin-roll cast electrical steels. The results are similar to those in the conventionally cast and hot-rolled materials.

It is thus shown that the hot-band grain size significantly affects the microstructure, texture, and magnetic properties of the final product. However, since the core loss of the steel depends on both the grain size and texture, it is difficult to

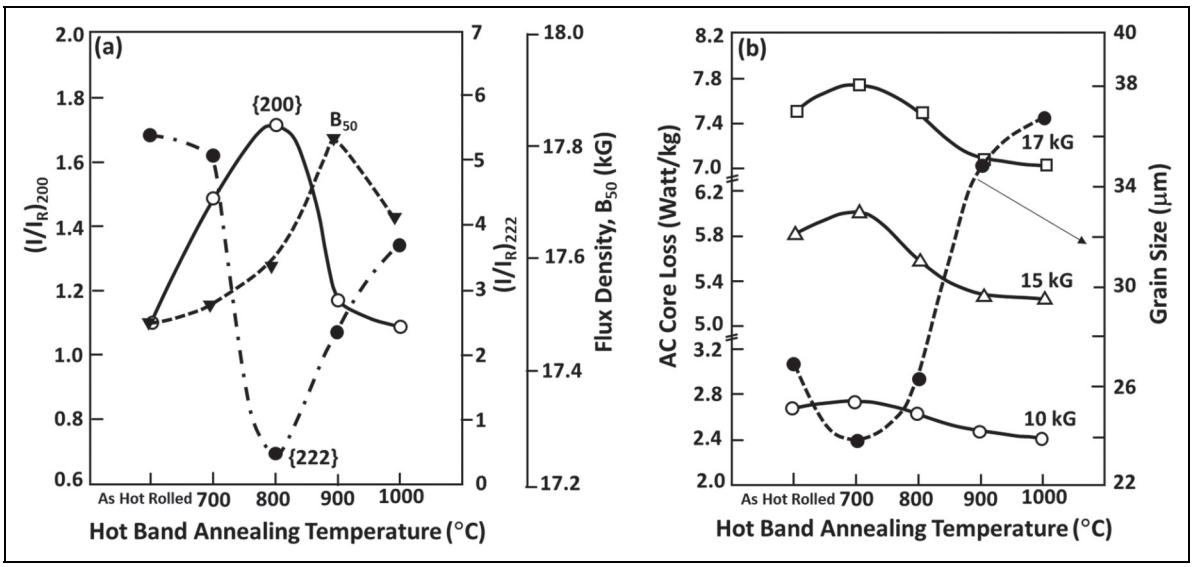

Figure 18. The effect of hot band annealing temperature on texture, microstructure, and magnetic properties of a 0.31% Si NOES[206]: (a) texture intensities and magnetic flux density (B_{50}) vs. hot band annealing temperature, (b) final grain size and core loss vs. hot band annealing temperature.

distinguish the effect of texture from that of the grain size. Lee et al.[215] investigated a 2.0% Si steel by producing hot bands with different grain sizes (150 and 500 μm) but almost the same texture (almost random). After cold rolling, the macrotextures of the two steels were essentially identical, but the microtextures and microstructures were significantly different. The sample with a large initial grain size had an irregular microstructure and a microtexture which promoted the growth of the {001} and {113} grains, beneficial textures for good magnetic properties.

Cold rolling. Cold rolling is an indispensable process to achieve the thin thickness of the final NOES sheets. The controllable parameters during cold rolling include thickness reduction, roll diameter and surface roughness, initial grain size, initial texture, deformation mode, thickness reduction per pass, intermediate annealing between passes, etc. The importance of cold rolling on the magnetic properties of NOES lies in the fact that the microstructure, substructure, texture, and stored energy generated in this process directly determine the microstructure and texture of the steel sheets after final annealing. During cold rolling, a small amount of the plastic work applied to the material is retained in the format of lattice defects, e.g., dislocations.[216] The movement of dislocations accommodates the macroscopic shape change and plastic strain and changes the microstructure and the orientations of the crystals. The stored energy provides the driving force for recovery and recrystallisation during the subsequent annealing.

Figure 19 shows examples of EBSD scans on cold rolled NOES across the thickness.[196,217] It is seen that grains with {001} orientations can usually be readily indexed (since essentially no substructure is created in these grains), while some regions of the {111} grains (with substructures and high density of dislocations) are difficult to index. It is also seen that the cross-section textures of the steels with different silicon contents are quite similar, i.e., consisting of an α-fibre and a γ-fibre. These textures are similar to the typical textures of low carbon steels.[218]

The variation of cold reduction causes differences in the deformed microstructure, substructure, and texture,[219] thus affecting the microstructure and texture after final annealing. Lee and De Cooman[220] investigated the effect of thickness reduction on the texture and magnetic properties of a 3.0% Si NOES. It was shown that with the increase of the cold rolling reduction, the {411}<148> and {111}<112> textures are increased while the {110}<001> is decreased, which decreases the B_{50} magnetic flux density. Kawamata et al.[221] investigated the effect of cold rolling condition on the texture and magnetic properties of a low silicon steel (0.26% Si). The rolling shape factor (RSF), which is the projected contact length divided by the mean thickness of the strip before and after a rolling pass, evaluates the homogeneousness of the strain distribution along the thickness of the strip. It was shown that the smaller the RSF (the smaller the roll diameter or the larger the mean strip thickness), the larger the surface strain, and the more heterogeneous the strain along the thickness, which results in a larger deviation of the surface texture from the central plane-strain texture (normally the α-fibre and γ-fibre). The final result is the formation of a stronger {001}<110> texture after cold rolling and close to cube texture after recrystallisation and grain growth. The improvement of the B_{50} due to a lower RSF is caused by the improvement of the texture.

A special rolling scheme that can significantly change the texture (while not altering the microstructure) is *cross rolling*,[69,222] in which cold rolling is performed along the transverse direction (TD) of the hot rolled plate (90° rotation around the ND). Due to the rotation, the initial texture before cold rolling is rotated, but the microstructure is not changed. As a result, the rotation path of the

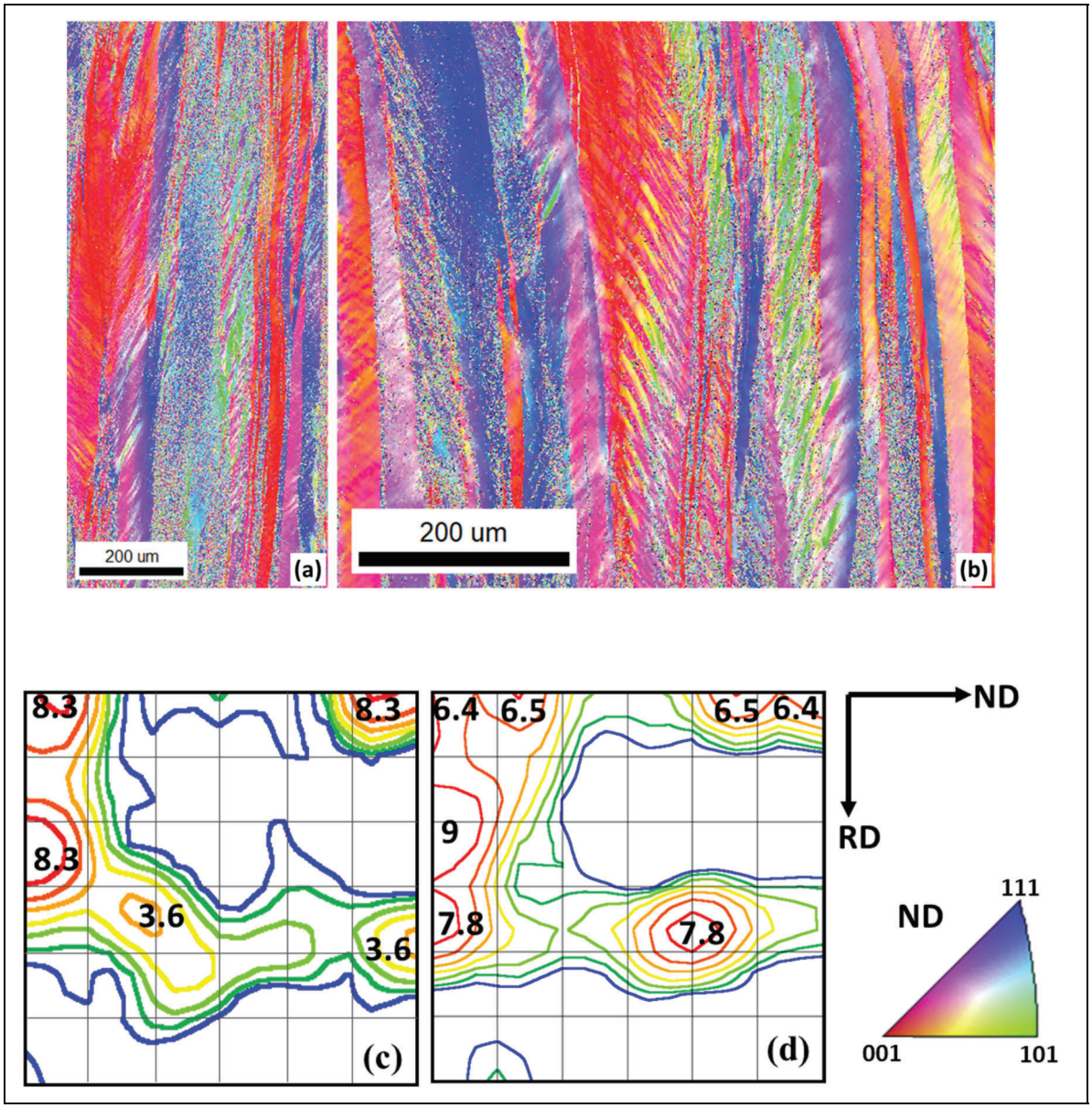

Figure 19. Microtextures of cold-rolled NOES: (a) inverse pole figure map of a 0.88% Si NOES,[217] (b) inverse pole figure map of a 2.8% Si NOES,[204] (c) texture of the 0.88% Si NOES, (d) texture of the 2.8% Si NOES. Both steels were cold rolled to 0.5 mm with ~85% thickness reduction.

orientation flow during plastic deformation is affected.[18] The typical α-fibre texture (<110>//RD) after hot rolling (Figure 20(a)) is rotated to a <110>//TD fibre (Figure 20(b)), which is highly unstable during cold rolling. All the components of this fibre rotate towards the semi-stable orientation {001}<110> (rotated cube), forming an extremely strong (156×) rotated cube texture (Figure 20(c)). The final texture after recrystallisation is a <001>//ND fibre with a very strong (50×) rotated cube component.[18] Similar deformation texture (i.e., extremely strong rotated cube) is also observed in 6.5% Si NOES after warm cross rolling.[223]

He et al.[224] used another special rolling technique (*inclined rolling*) to intentionally change the initial texture before cold rolling by simply rotating the cold rolling direction (CRD) by an angle (≤ 90°) from the hot rolling direction (HRD). The rotation of the initial texture around the ND not only intensified the textures after cold rolling (as compared to that without rotation), but also alters the relative intensities between the {001}<110> and {112}<110> components and between the {111}<110> and {111}<112> orientations. Especially, it is possible to create the rotated Goss texture which is not commonly produced in conventional rolling; the cold rolling of the rotated Goss grains and the formation of shear bands within these grains can significantly change the recrystallisation texture during final annealing (see the Final annealing section).

A few studies have been carried out to investigate the effect of deformation mode during cold rolling on the texture and microstructure of NOES. These included asymmetric rolling, skew rolling, and repetitive bending under

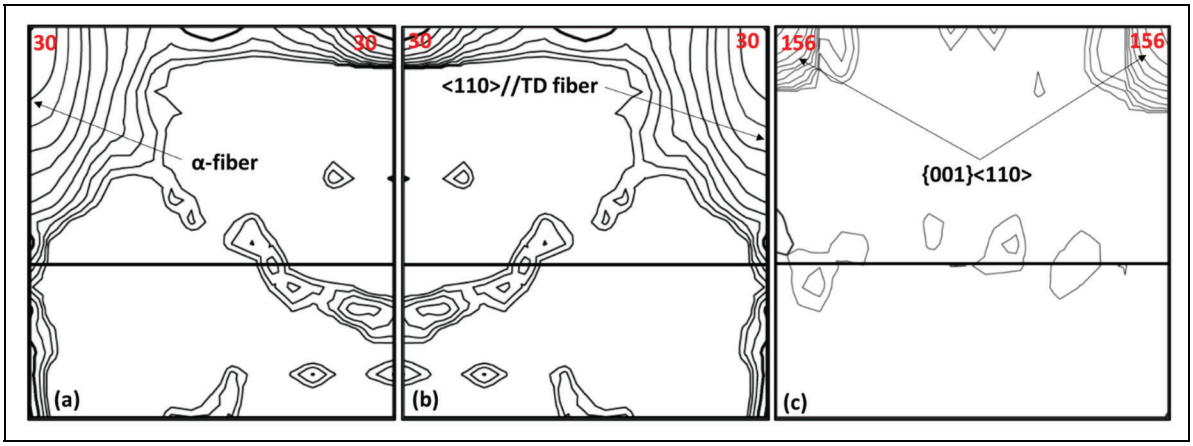

Figure 20. Effect of cross rolling on the texture of NOES[18]: (a) texture after hot rolling, (b) hot band texture after 90° rotation about ND (before cold rolling), (c) texture after cross rolling.

tension. Sha et al.[225] studied the effect of asymmetric cold rolling on the final recrystallisation texture and magnetic properties of a 2.1% Si NOES. It was demonstrated that asymmetric cold rolling could improve the recrystallisation texture by enhancing the <001>//ND fibre and lead to a decrease of the core loss and an increase of the magnetic induction. Fang et al.[226] investigated a 3.3% Si NOES by asymmetric cold rolling, which also illustrated that asymmetric cold rolling could significantly increase the intensities of the {001}<100> and {110}<100> textures after the completion of recrystallisation. Asymmetric hot rolling, however, did not produce the desired texture in the final annealed NOES, although higher <001>//ND and lower <111>//ND textures did form in the asymmetrically hot rolled bands.[227] The different textures produced during asymmetric rolling were attributed to the strong shear between layers of the material across the thickness.

He and Hilinski[228] investigated a special rolling process called *skew rolling*, in which the deformation mode was changed from plane-strain compression to a complicated three-dimensional deformation including a strong shear in the TD (width) together with thickness reduction and elongation. It was shown that this rolling scheme could produce significantly different cold rolling textures from conventional rolling (Figure 21), i.e., drastically increasing the <001>//ND texture while significantly reducing the <111>//ND texture at larger skew angles (30°−45°). The differences in deformation texture after skew rolling were attributed to the different initial textures before cold rolling (rotation around ND) and to the different deformation mode (e.g., with a strong shear strain in TD) in the skew rolling process. Tamimi et al.[229] investigated a special processing technique called *repetitive bending under tension* (R-BUT) on the mechanical properties and texture of a 1.8% Si NOES. It was found that NOES sheets can be deformed far beyond its common elongation limit using R-BUT operation. This may provide a solution to an important industrial challenge when processing NOES with extremely poor formability, e.g., electrical steels containing high silicon.

However, it should be noted that, the abovementioned special rolling or processing techniques are difficult to be implemented in industry for efficient mass production of NOES. Nevertheless, the related studies provided some insight into the understanding of the formation mechanisms of textures in NOES under different conditions. In practice, focus still needs to be placed on the traditional rolling process to improve the magnetic quality of the NOES.

Cheong et al.[133] investigated the effect of temper mill extension and work roll roughness on the texture and magnetic properties of semi-processed NOES. It is shown that higher temper mill tension and smoother work roll roughness produce stronger shear deformation at the surface, which induces a more heterogeneously stored energy profile. Upon final annealing, this may induce significantly different textures, leading to large anisotropy in magnetic properties between the rolling and transverse directions. The inhomogeneously stored energy in the surface also contributes to the difference in work hardening among grains with different orientations, as observed by Shimazu et al.[230] The temper rolling thickness reduction also affects the final microstructure, texture, and magnetic properties of semi-processed electrical steel, since the amount of strain induced in the temper rolling process is critical to determining if nucleation occurs (instead of only grain growth), which will dramatically change the final texture. Barros et al.[231] investigated the effect of temper rolling reduction on the final microstructure and texture of a 1.3% Si steel. It was shown that 1–4% temper rolling reduction produced a very inhomogeneous microstructure consisting of both fine and coarse grains after final annealing, which showed significantly different crystallographic textures. A 6% reduction resulted in the optimal magnetic properties.

It should be stressed that two microstructural characteristics of cold deformation are of paramount importance in determining the final microstructure and texture during recrystallisation, i.e., grain fragmentation (subdivision)[232] and shear banding.[233] Fragmentation of grains into regions of different orientations may provide the initial

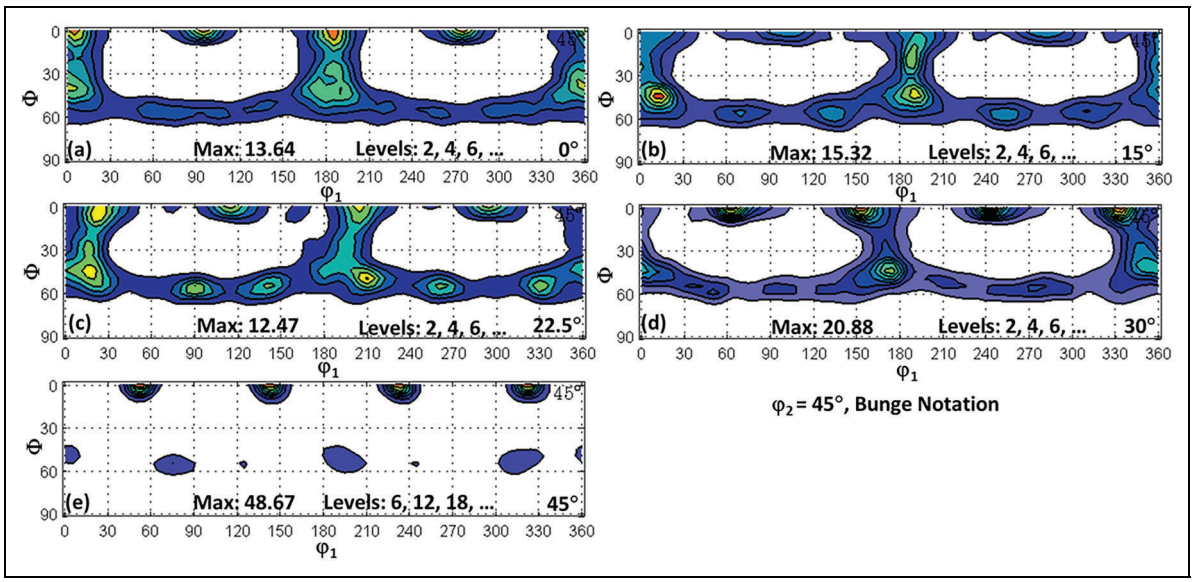

Figure 21. Effect of skew rolling angle on the textures of a 0.88% Si NOES[228]: (a) 0° (conventional rolling), (b) 15°, (c) 22.5°, (d) 30°, (e) 45°. The textures were measured by XRD on the mid-thickness plane. Note that skew rolling does not have an orthorhombic symmetry, so the Euler angle φ_1 is from 0° to 360°.

nuclei during recrystallisation, which determines the orientations of the early recrystallised grains. Shear banding, the creation of microscopic or macroscopic planar regions of severe shear in rolled metals,[233] is the result of heterogeneous plastic deformation at medium to high strains due to plastic instability. The formation of shear bands is closely related to the deformation mode and the crystal orientation, and can be evaluated using the Taylor factor (M), a dimensionless measure of the plastically dissipated power[136]:

$$M = \frac{\sum_{i=1}^{s} \tau_0 |d\gamma_i|}{\sigma_o d\varepsilon_{vM}} \tag{9}$$

where τ_0 is the critical resolved shear stress, $d\gamma_i$ is the instantaneous slip increment on slip system i, s is the number of active slip systems, σ_o is the flow stress and ε_{vM} is the von Mises equivalent strain. Generally, shear bands tend to form in crystals with high Taylor factors.[136,216,234] The formation of shear bands in the deformed microstructure significantly influences the recrystallisation process during annealing, as detailed in the next section.

Final annealing. Final annealing is required in NOES production to release the stresses accumulated during the previous processing steps, and to develop the desired final microstructure and texture to achieve optimal magnetic properties. During final annealing (either batch or continuous), the cold deformed steel is heated to an elevated temperature and held for a specific time to allow the deformed microstructure to completely recrystallise, forming a structure with specific grain size, morphology, and crystallographic texture, which directly affects the magnetic properties. It is of supreme importance to control the final annealing process to obtain the optimal microstructure and texture that deliver the best magnetic properties. The main objective of the final annealing of NOES is to obtain an optimal grain size while achieving the desired <001>//ND texture, which is, however, proved to be very challenging to attain.

Although with extensive research on the recrystallisation phenomena, and with a large amount of literature available, many aspects of the recrystallisation process are still not well understood.[197] As a result, the experimental data and the results reported in the literature regarding the recrystallisation of NOES may not be complete and sometimes even conflicting. It has long been recognised that the recrystallisation textures in various BCC metals at equivalent temperatures and from similar deformation textures are quite similar.[219] For NOES, the common recrystallisation textures (in almost all commercial NOES) are the α-fibre and γ-fibre, which are not the desired <001>//ND fibre texture. A lot of research has been dedicated to the development of the <001>//ND texture, especially the cube component.

In the early works of Assmus et al.,[235] Wiener et al.,[236] and Walter et al.,[237] very thin silicon-iron sheets (~0.1 mm) were produced with a very strong cube texture (90%), normally through secondary recrystallisation. The mechanism for the abnormal cube grain growth was proved to be a surface-energy-driven process (i.e., {001} planes have lower surface energy than other matrix planes),[238,239] very similar to the formation of the Goss texture in GOES. It should be noted that, although the magnetic inductions of these steels were high, the core loss and magnetostriction were also unexpectedly high, which were attributed to the high eddy current loss due to the large grain size (over 2 cm),[130] and to the movements of 90° domain walls created in the transverse direction.[236] On the other hand,

the very high vacuum level or the very stringent atmosphere control required in the annealing process makes mass production of these steel sheets very difficult and costly.

A different method was developed by Taguchi and Sakakura[69] to produce cube texture by cross rolling. Again, this method is very similar to the production of the Goss texture in GOES. AlN precipitates were present to inhibit grain growth in primary recrystallisation, and high temperature secondary recrystallisation was needed to produce the cube texture, but the grain size was large. The cross-rolling technique was then studied by several other researchers to produce the {100} textures (including cube). Vanderschueren et al.[222] investigated the texture evolution of a 0.57% Si steel using cross rolling and produced a strong <001>//ND fibre texture (32 × rotated cube and 8 × cube) after decarbonisation annealing. Hayakawa and Kurosawa[240] studied the mechanisms of selective growth of the cube grains in an Fe-3.3% Si-0.05% C steel after cross rolling. Again, to obtain a strong cube texture, secondary recrystallisation is needed.

Another method to produce NOES sheets with a strong cube texture and a much finer grain size was developed by Tomida et al.[130] In this method, a NOES with 3.0% Si, 1.1% Mn, and 0.05% C was first processed using a two-stage cold rolling strategy (with intermediate annealing), and was then decarburised using a silicon dioxide separator, during which columnar cube grains (more than 90%) grew from the surface to the centre, with final grain size around 0.4 mm. As a result, the core loss was reduced to 1.2 W/kg at 1.5 T and 60 Hz. A similar process without using the two-stage cold rolling was also developed,[241] which resulted in the {001}<120> texture with a grain size of 0.6 mm. In both processes, vacuum decarburisation in the austenite-ferrite two-phase region played an important role in developing the final {001} textures. In addition, prolonged heat treatment at relatively high temperatures and the use of oxide separators were needed to produce the desired microstructure and texture.

To form the <001>//ND texture at relatively low temperatures without secondary recrystallisation, Sung et al.[185] reported a method taking the advantages of austenite-to-ferrite phase transformation in a 0.97% Si steel where the cold rolled steel was annealed at a temperature above the austenite region and cooled relatively slowly. Columnar cube grains were developed starting from the surface, and the mechanism was attributed to the elastic compliance of the {100} faces nucleated at the surface, which minimised the strain energy when growing towards the centre along the thickness direction. The grain size of the cube texture is in the order of the sheet thickness (0.35 mm). With the development of the

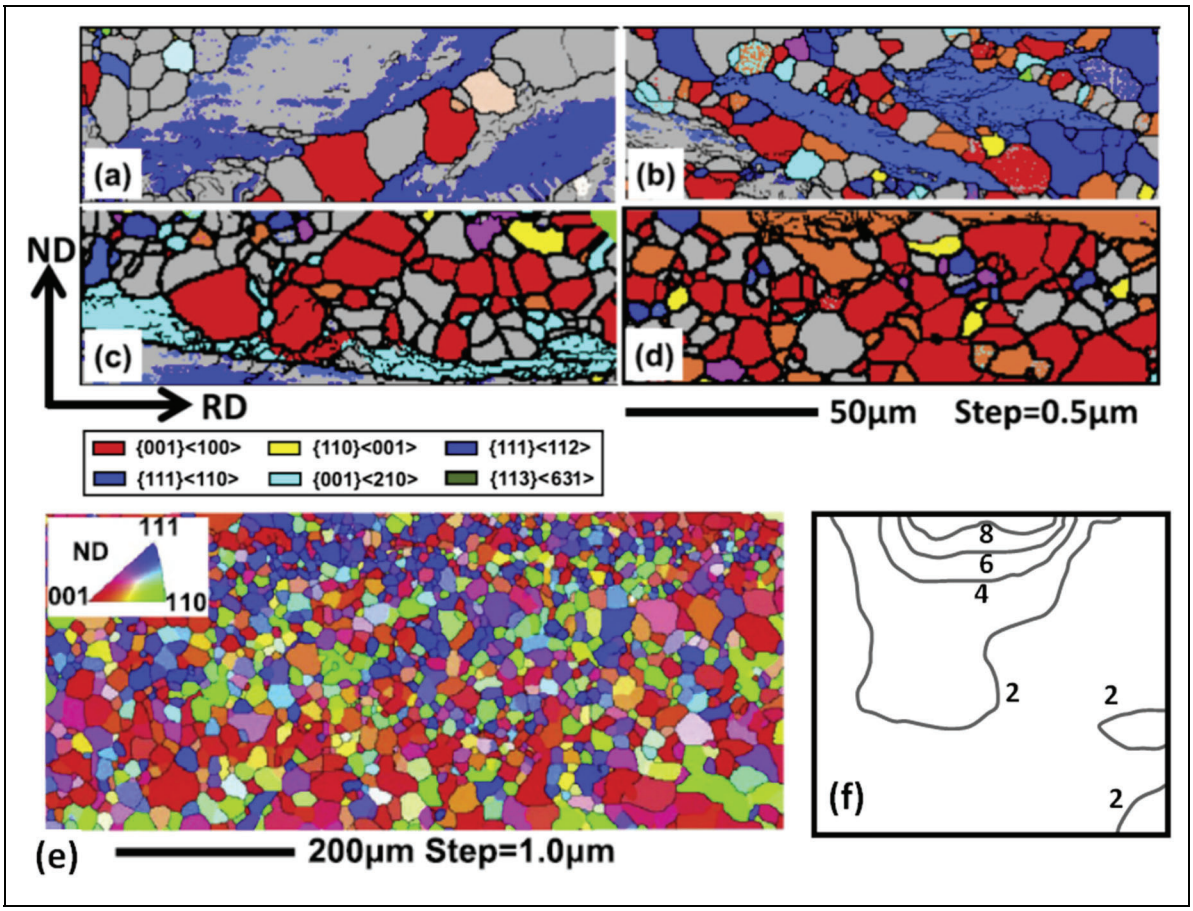

Figure 22. The formation of cube texture in 2.8% Si NOES by twin-roll casting[243]: (a) cube grains at shear bands in {111}<110> deformed matrix, (b) cube grains at shear bands in {111}<112> deformed matrix, (c) cube grains in {001}<210> deformed matrix, (d) cube grains in {113}<631> deformed matrix, (e) inverse pole figure map after final annealing, (f) texture of the final annealed steel.

{001} texture and the relatively small grain size, the core loss was reduced by 25% and the permeability increased by 2–5 times.[242]

Cube texture with fine equiaxed grains (non columnar) was developed by Sha et al.[243] in a 2.8% Si steel through TRC and relatively high temperature annealing (without secondary recrystallisation). It was shown that the cube was nucleated in the cube deformation bands within or near grain boundaries of the deformed {001}<120>-{114}<148>-{113}<136> grains, as well as in the shear bands of {111}<110> grains (Figure 22). It was claimed that the cube recrystallisation texture was due to the frequency advantage of the initial cube grains, i.e., mainly due to an oriented nucleation mechanism. The cube nuclei were mostly from the shear bands of the deformed γ grains and the cube deformation bands. In another study by Jiao et al.[244] (also using TRC, but in a 1.3% Si steel), it was shown that the major nucleation sites of the cube grains were the {114}<481> and {112}<241> deformation bands, including other sites such as the shear bands within the {114} <110>, {112} <110> and {111} <112> matrix. It was pointed out that large blocks of deformed cube could become recrystallised cube grains by extended recovery and the thin strip thickness and the coarse initial microstructure with strong cube texture were the key to producing the cube texture.

Takajo et al.[245] investigated the nucleation and growth of cube grains in a 3.0% Si steel using both *in-situ* and *ex-situ* EBSD techniques. It was shown that the cube nuclei mainly originated from the fragments of deformed {114}<148> grains. The cube nuclei first grew inside the prior grain boundaries at a low temperature, and then grew beyond the boundaries at high temperatures due to size advantage. The relatively high grain boundary mobility of the cube grains with respect to the matrix contributed to the preferred growth of the cube grains. However, the growth of the cube grains did not continue beyond 750°C, due to the possible pinning of dislocations or solute drag at the grain boundaries (Figure 23). When the annealing temperature was 800°C and 850°C, the cube texture could still be retained due to their relatively large size. When the annealing temperature was increased to 950°C, the cube grains were replaced by other grains.

Nguyen-Minh et al.[246] investigated a 1.2% Si steel and observed that cube crystallites could be formed within the shear bands of rotated Goss grains ({110}<110>) after cold rolling (Figure 24(a)), which served as the preferred nuclei during recrystallisation. The rotated Goss texture is not a common rolling texture for NOES, and its appearance may be attributed to the phase transformation of the low silicon steel (which may not occur in high silicon steel), or to the original {110} texture after strip casting.[247] Mehdi et al.[248] used the inclined rolling technique[224] to intentionally create a rotated Goss texture by rotating the hot band around the ND for 55°−60°, and then cold rolled the steel to 50–80% reduction. In this way, it was able to produce a large number of rotated Goss grains, which exhibited numerous shear bands after deformation. It was shown that many cube crystallites were formed in the shear bands of the rotated Goss grains (Figs. 24(b) and 24(c)). It was also illustrated that the stored energy of these cube crystallites was lower than that of their surrounding areas (other regions within the shear bands) (Figure 24(d)). These cube crystallites provided preferred

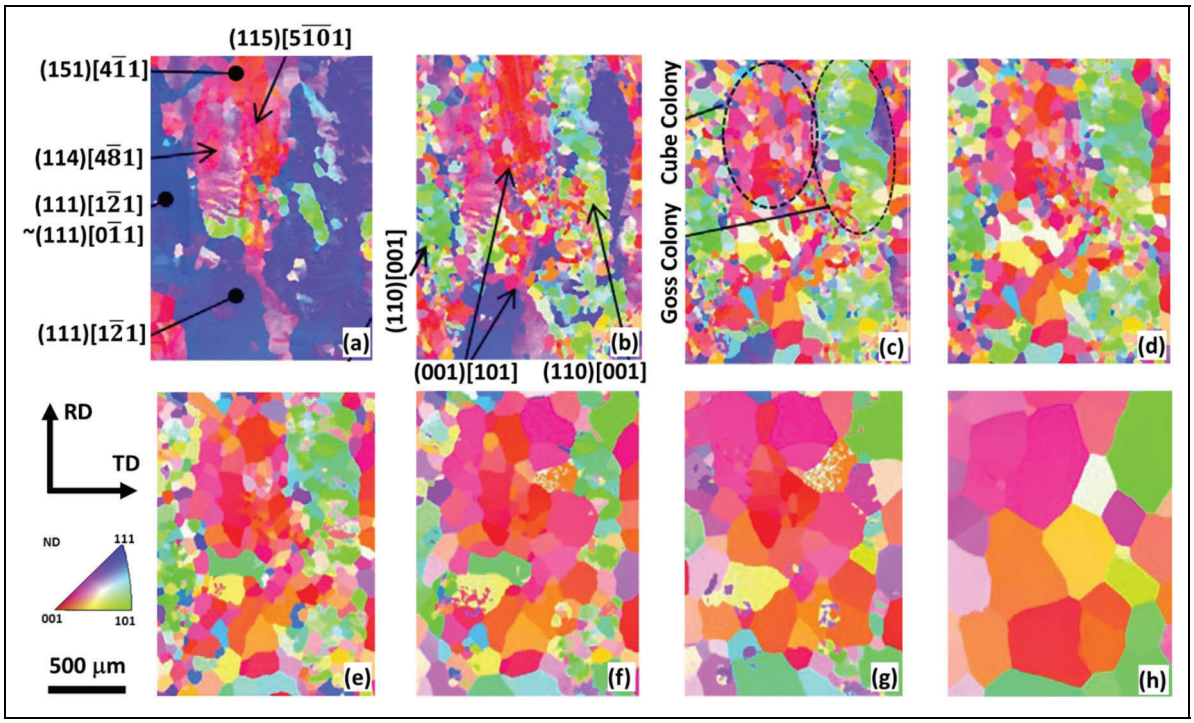

Figure 23. The evolution of microstructure and microtexture during annealing of a 3.0% Si NOES as observed by in-situ EBSD techniques[245]: (a) room temperature, (b) 600°C, (c) 650°C, (d) 700°C, (e) 750°C, (f) 800°C, (g) 850°C, (h) 950°C.

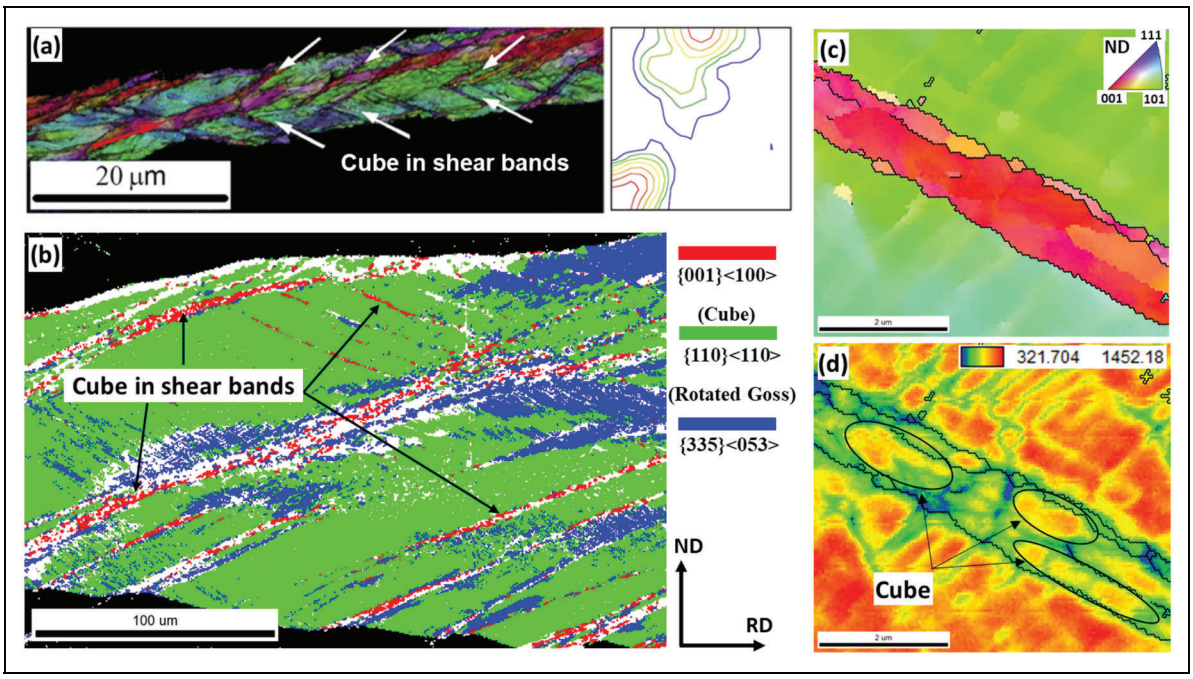

Figure 24. The nucleation of cube grains from shear bands of deformed {110}<110> (rotated Goss) matrix: (a) in a 1.2% Si NOES,[246] (b) in a 2.8% Si NOES,[248] (c) IPF map showing the orientations of the matrix grain and the shear band of a 2.8% Si NOES, (d) image quality (IQ) map showing the difference in IQ within the shear bands. Some cube regions have higher IQ (and thus lower stored energy) than their neighbouring regions, which provides the driving force for growth.[248]

nuclei during recrystallisation, which first grew within the shear bands and finally crossed the boundaries between the shear bands and the matrix, consuming the deformed matrix, thus producing a cube texture.

As can be seen, a very strong cube texture may be developed in NOES through columnar grain growth using several different technical routes. However, these routes mostly require secondary recrystallisation to create the cube texture, which is similar to the formation of the Goss texture in GOES. The major drawback for the cube columnar structure thus formed is that the cube grain size is too large, which causes high core losses. The technical routes that are able to produce a cube texture with a fine grain size usually can only produce the cube texture with reduced intensity as compared to those formed by columnar growth. How to intensify the cube texture in the NOES while maintaining an optimal grain size (~150 μm) using traditional routes is still a challenge. In theory, although it has been shown that the creation of initial cube crystallites in the cold deformed microstructure is important, the reported locations of these cube crystallites are quite different, and it is not clear how exactly these nuclei are formed and how the deformation process can be effectively controlled to form these nuclei. Another issue is that it is still not clear under what conditions can the cube crystals grow to form the final texture when competing with other recrystallised grains during the later grain growth stage.

Thus, it is shown that the ideal final texture for NOES, i.e., a uniformly distributed <001>//ND fibre or a sharp single cube component (like Goss in GOES), has not been produced in commercial NOES products in mass production, although the texture formation mechanisms are similar to those of low carbon steel which have been extensively studied. A technique route that can produce a strong <001>//ND texture together with an optimal grain size in commercial NOES sheets has yet to be developed.

Coating and core manufacturing

Like in GOES, insulating coating is also needed on NOES sheets to reduce the eddy current loss and protect the laminates from corrosion. Since the NOES cores for electric motors and generators are normally manufactured by a punching or stamping process, a coating that can improve the punchability of the steel and extend the life of the punching dies is preferred.[249] Because the NOES laminates are usually welded after stacking, a coating with good weldability is desired. Various welding technologies can be used, e.g., tungsten inert gas (TIG) welding, metal active gas (MAG) welding, laser welding, electron beam welding, plasma arc (PA) welding, etc. The selected welding technology should have minimum impact on the properties of the lamination. The heat resistance of the coating should be high enough to withstand the heat generated in electric motors (normally up to 200°C) while maintaining the electrical insulation. In some cases, the coated NOES sheets may be subjected to stress-relief annealing, which requires the coating be able to withstand temperatures as high as 815°C.[250] Depending on the applications, several different types of coatings are specified in the ASTM Standard A976,[250] which include organic, inorganic, and mixed organic and inorganic coatings.

When manufacturing soft magnetic cores for motors and generators from NOES sheets, the cutting, interlocking, and

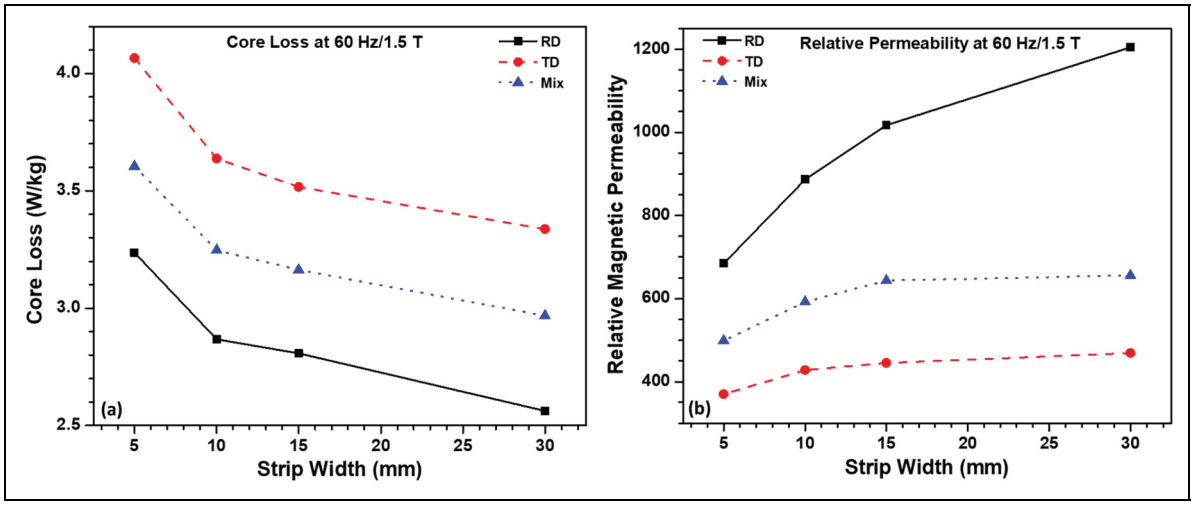

Figure 25. Effect of strip width on the magnetic properties of a 3.3% Si NOES (0.2 mm) as measured by Epstein frame method: (a) core loss, (b) relative magnetic permeability. Strips with width smaller than 30 mm contain 2 (15 mm each), 3 (10 mm each), and 6 (5 mm each) smaller strips and are glued together to make 30 mm strips for standard Epstein frame testing. The increase of the number of cutting edges deteriorates the magnetic properties.

assembling processes may deteriorate the magnetic properties of the NOES sheets. Each of the cutting, stacking, bonding/interconnecting, and shrink fitting processes is known to lead to additional core losses, especially for machines having small sizes.[251] It has been shown that the differences in core loss between the results provided by the steel manufacturers and those measured on the final assembled soft magnetic core can reach more than 40%.[252] Figure 25 shows the effect of strip width on the magnetic properties of NOES sheets as measured by Epstein frame tests. It is seen that, if the width of the strip is reduced to 5 mm (1/6 of the regular 30 mm strip), the core loss is increased by 26% in RD and 22% in TD. The relative permeability is decreased by 43% in RD and 21% in TD. The deterioration of the magnetic properties is mainly caused by the deformation and residual stresses induced in the mechanical cutting (shearing) process, especially near the cutting edge. Laser cutting may eliminate the mechanical stresses but will melt the material at the edge and introduce thermal stresses, which also deteriorate the magnetic properties.[253] Similarly, welding,[254] interlocking[255] and shrinking fitting[256] all deteriorate the magnetic properties of the final core. Thus, a stress-relief annealing step is normally recommended to recover the magnetic properties after the soft magnetic core is assembled.

Future research and development

How to produce NOES with the ideal <001>//ND texture (with all the other textures eliminated, like in GOES) while maintaining an optimal grain size in mass production is still a big challenge and remains as an interesting area for NOES research. There still lacks a cost-effective and efficient processing method to produce a strong <001>//ND texture like the sharp Goss texture in GOES. Since the mechanisms governing the formation of the microstructure and texture of the final steel sheets are still not completely understood, much effort should be made to understand these processes using advanced characterisation techniques, e.g., using *in-situ* EBSD to help understand how the initial nuclei evolve to form the first crystals during early stage of recrystallisation and how crystals with different orientations grow at high temperatures, and using *In-situ* TEM to evaluate the change of dislocation density and the diffusion of elements during the recrystallisation process. Although computer simulation of the recrystallisation process has also been investigated, there still lacks a physical model that can faithfully describe the nucleation and grain growth processes so that the simulations can be used to reliably predict the recrystallisation microstructure and texture.

As has been shown, introducing shear stress during the deformation process can usually reduce the intensity of the <111>//ND texture and promote the <001>//ND texture. However, most of the methods (e.g., asymmetric rolling, skew rolling, etc.) used to introduce the shear stress cannot be effectively used in conventional rolling for mass production. It is well known that changing the surface roughness and/or the lubricating condition of the rolls can change the shear stress on the steel to be rolled. A systematic study on this aspect is needed to understand how the shear stress in the surfaces affects the recrystallisation of the steel during annealing and how to control the recrystallisation from the surface to the centre of the sheet.

Depending on the application, the requirements for magnetic properties of the NOES and thus the costs may be different. For high frequency applications, e.g., traction motors for electric vehicles, increasing the silicon content to 6.5% to reduce the core loss at high frequencies is an emerging area of research. Although a considerable amount of literature in this area can be found, the brittleness of the high silicon steel at room temperature has not been resolved. Mass production of this steel using conventional routes has not been realised. Much effort is still needed in this field and potential research directions may include:

i) designing alloys with suitable chemical compositions to avoid the ordered phases (B_2-FeSi and DO_3-Fe_3Si) or improve the ductility of these phases, ii) finding appropriate processing routes to avoid or reduce the formation of the brittle ordered phases, iii) develop special casting techniques to improve the ductility of the material at both high temperature and room temperature. Once the ductility of the material is improved, the control of the microstructure and texture is essentially the same as other NOES with lower silicon contents.

Increasing the Si content in cold rolled NOES sheets with relatively low Si using novel diffusion technologies (instead of chemical vapour deposition) is another approach that may be pursued. The current chemical vapour deposition technology is too expensive and time consuming to compete with the traditional methods. Amorphous steel (very brittle) and nanocrystalline material (both with lower core loss, higher permeability, and lower saturation magnetisation than electrical steel) may be developed as alternative materials to electrical steel, which also deserves further research. More recently, additive manufacturing (3D printing) has emerged as a new technology to produce electrical machines.[257,258] Although with its advantages such as being able to produce complex geometries and generate the desired <001> texture, it has inherent drawbacks. High eddy current loss (due to the 3D nature) and high density of defects (e.g., porosity) are the main issues of this technology.[259] The magnetic quality of the 3D printed electrical steel is as yet not comparable to the thin sheets (a 2D material) produced by conventional rolling. Other unconventional methods, e.g., peeling and large strain extrusion machining,[260,261] have also been explored, but the application is limited to small machines as it is difficult to produce large sheets with uniform properties using this method.

Finally, it should be noted that, twin-roll strip casting is a cost-effective and energy-efficient metal solidification and forming technology that has great potential to efficiently produce NOES. The studies appearing in the literature[60,262] have shown that excellent magnetic properties of NOES can be achieved using this method. However, mass production of NOES using this technology has not been reported, although this process has been successfully used to produce both low-carbon steel and stainless steel by a few companies. The steel industry should consider this alternative technology to produce NOES with reduced cost, increased efficiency, and improved product quality.

Acknowledgements

Y.H. gratefully acknowledges the financial support of the Office of Energy Research and Development, Natural Resources Canada. Alana Pollock-Greenwood, Ashley Thompson, and Kelly Dickson are thanked for their help on literature search.

Declaration of conflicting interests

The authors declared no potential conflicts of interest with respect to the research, authorship, and/or publication of this article.

Funding

The authors disclosed receipt of the following financial support for the research, authorship, and/or publication of this article: This work was supported by the Office of Energy Research and Development, Natural Resources Canada (grant number CMAT-23-108).

References

1. Panwar N, Kaushik S and Kothari S. Role of renewable energy sources in environmental protection: a review. *Renewable Sustainable Energy Rev* 2011; 15: 1513–1524.
2. Vittori C, Evans G and Fini M. Electrical steel – Another temporary supply chain shortage or a threat to OEMs' electrification plans? IHS Markit, S&P Global Mobility, https://www.spglobal.com/mobility/en/research-analysis/electrical-steel-another-temporary-supply-chain-shortage.html, 2021.
3. Bozorth RM. *Ferromagnetism*. 3rd ed. Toronto: D. Van Nostrand Company, Inc., 1951.
4. Goss NP. Electrical Steel Sheet and Method and Apparatus for Its Manufacturing and Test. USA Patent 1,965,559, 1934.
5. Matsuo M. Texture control in the production of grain oriented silicon steels. *ISIJ Int* 1989; 29: 809–827.
6. Dorner D, Zaefferer S, Lahn L, et al. Overview of microstructure and microtexture development in grain-oriented silicon steel. *J Magn Magn Mater* 2006; 304: 183–186.
7. Hayakawa Y. Mechanism of secondary recrystallization of Goss grains in grain-oriented electrical steel. *Sci Technol Adv Mater* 2017; 18: 480–497.
8. Hummel RE. *Electronic Properties of Materials*. 4th ed. New York: Springer, 2011.
9. Chukwuchekwa N. *Investigation of Magnetic Properties and Barkhausen Noise of Electrical Steel, Wales*. PhD Thesis, Wolfson Centre for Magnetics, Cardiff University, UK, 2011.
10. Spaldin NA. *Magnetic materials: fundamentals and applications*. 1st ed. New York: Cambridge University Press, 2003.
11. Doverbo M. *Correlation between material properties, grinding effects and Barkhausen noise measurements for two crankshaft steels, Goteborg, Sweden*. Master's Thesis, Department of Materials and Manufacturing Technology, Chalmers University of Technology, 2012.
12. Jiles D. *Introduction to Magnetism and Magnetic Materials*. 1st ed. New Delhi: Chapman and Hall, 1991.
13. Cullity B and Graham C. *Introduction to Magnetic Materials*. 2nd ed. Hoboken, New Jersey: John Wiley & Sons, Inc., 2009.
14. Daem A. *Manufacturing Effects on Electromagnetic Properties of Ferromagnetic Cores in Electrical Machines*. PhD Thesis, Department of Electromechanical, Systems and Metal Engineering, Ghent University, Ghent, Belgium, 2021.
15. Barkhausen HG. Gerausche bien ummagnetisieren von eisen. *Physikalishe Zeitschr* 1919; 20: 401–403.
16. Kang H, Lee K, Huh M, et al. Quantification of magnetic flux density in non-oriented electrical steel sheets by analysis of texture components. *J Magn Magn Mater* 2011; 323: 2248–2253.
17. Lee K, Park S, Huh M, et al. Effect of texture and grain size on magnetic flux density and core loss in non-oriented electrical steel containing 3.15% Si. *J Magn Magn Mater* 2014; 354: 324–332.

18. Kestens L and Jacobs S. Texture control during the Manufacturing of nonoriented electrical steels. *Texture Stress Microstruct* 2008; Article ID 173083: 1–9.
19. Bertotti G, Fiorillo F and Soardo GP. The prediction of power losses in soft magnetic materials. *J Phys* 1988; Colloque C8: 1915–1919.
20. Bertotti G. General properties of power losses in soft ferromagnetic materials. *IEEE Trans Magn* 1988; 24: 621–630.
21. Fiorillo F. *Measurement and Characterization of Magnetic Materials*. 1st ed. New York: Elsevier Academic Press, 2004.
22. Steinmetz CP. On the law of hysteresis. *Proc IEEE* 1984; 72: 196–221.
23. Pry RH and Bean CP. Calculation of the energy loss in magnetic sheet materials using a domain model. *J Appl Phys* 1958; 29: 532–533.
24. Bozorth RM. The orientation of crystals in silicon iron. *Trans Am Soc Met* 1935; 23: 1107–1111.
25. Dunn CG. Recrystallization textures. In: Trans. ASM, Symposium on Cold Working of Metals, 1949, pp.113.
26. Kubota T, Fujikura M and Ushigami Y. Recent progress and future trend on grain-oriented silicon steel. *J Magn Magn Mater* 2000; 215-216: 69–73.
27. Gunther K, Abbruzzese G, Fortunati S, et al. Recent technology developments in the production of grain -oriented electrical steel. *Steel Res Int* 2005; 76: 413–421.
28. Xia Z, Kang Y and Wang Q. Developments in the production of grain-oriented electrical steel. *J Magn Magn Mater* 2008; 320: 3229–3233.
29. Takamiya T, Hanazawa K and Suzuki T. Recent development of grain-oriented electrical steel in JFE Steel. JFE Technical Report No. 21., JFE Steel Corporation, Japan, 2016.
30. Mishra S, Farmann C and Lucke K. On the development of the Goss texture in iron-3% silicon. *Acta Metall* 1984; 32: 2185–2201.
31. Botthcher A and Lucke K. Influence of subsurface layers on texture and microstructure development in RGO electrical steel. *Acta Metall. Mater* 1993; 41: 2503–2514.
32. Dorner D, Zaefferer S and Raabe D. Retention of the Goss orientation between microbands during cold rolling of an Fe3%Si single crystal. *Acta Mater* 2007; 55: 2519–2530.
33. Zhu C, Liu Y, Xiao Y, et al. A new review on inclusion and precipitate control in grain-oriented silicon steels. *JOM* 2022; 74: 3141–3161.
34. Ouyang G, Chen X, Liang Y, et al. Review of Fe-6.5wt% Si high silicon steel—A promising soft magnetic material for sub-kHz application. *J Magn Magn Mater* 2019; 481: 234–250.
35. Choi GS, Lee CS, Woo JS, et al. Method for manufacgturing oriented electrical steel sheet by heating slab at low temperature. Republic of Korea Patent 5,653,821, 5 August 1997.
36. Lee CS, Han CH, Woo JS, et al. Method for manufacturing high magnetic flux density grain oriented electrical steel sheet based on low temperature slab heating method. Republic of Korea Patent WO 99/02742, 26 June 1998.
37. Kurosaki Y, Abe N, Tachibana N, et al. Grain-oriented electrical steel sheet and method for producing same. Japan Patent 6,159,309, 12 December 2000.
38. Nanba E, Yanagihara K, Arai S, et al. Ultra-high magnetic flux density grain-oriented electrical steel sheet excellent in iron loss at a high magnetic flux density and film properties and method for producing the same. Japan Patent US 7,399,368 B2, 15 July 2008.
39. Fortunati S, Cicale S and Abbruzzese G. Process for the production of grain oriented electrical steel strips. Italy Patent US 2005/0115643 A1, 2 June 2005.
40. Shingaki Y, Takashima M, Nakanishi T, et al. Grain-oriented electromagnetic steel sheet and process for producing the same. Japan Patent EP 1818420 A1, 28 November 2005.
41. Birosca S, Nadoum A, Hawezy D, et al. Mechanistic approach of Goss abnormal grain growth in electrical steel: theory and argument. *Acta Mater* 2020; 185: 370–381.
42. Kreuzer H, Cicale S and Albini L. A process for the production of a grain-oriented electrical steel. Austria Patent EP 2775007 A1, 10 September 2014.
43. Yasuda M, Ushigami Y, Takahashi M, et al. Grain-oriented electrical steel sheet. Japan Patent EP 3744868 B1, 19 April 2023.
44. Silveiraa CC, Landgraf FJG and Paolinellia SC. Effect of primary grain size and nitrogen content on the magnetic properties. *J Magn Magn Mater* 2020; 503: 166629.
45. Gao Y, Xu G, Guo X, et al. Effect of Cr on secondary recrystallization behaviors in high permeability grain oriented silicon steel manufactured by low-temperature slab reheating. *J Magn Magn Mater* 2019; 476: 428–436.
46. Gao Y, Xu G, Guo X, et al. Primary recrystallization characteristics and magnetic properties improvements of high permeability grain-oriented silicon steel by trace Cr addition. *J Magn Magn Mater* 2020; 507: 166849.
47. Taguchi S and Sakakura A. Process of producing single-oriented silicon steel. Japan Patent 3,159,511, 1 December 1964.
48. Kumano T, Haratani T and Usgigami Y. Influence of primary recrystallization texture through thickness to secondary texture on grain oriented silicon steel. *ISIJ Int* 2003; 43: 400–409.
49. Takamiya T and Furukimi O. Precipitation behavior and inhibition effect of MnS, MnSe and AlN in 3% Si steel. *Tetsu-to-Hagane* 2014; 100: 67–74.
50. Li JB, Deng BR, Yang XZ, et al. Microstructure control of continuous casting slab of grain oriented silicon steel. *Mater Trans* 2022; 63: 112–117.
51. Tzavaras AA and Brody HD. Electromagnetic stirring and continuous casting — achievements, problems, and goals. *JOM* 1984; 36: 31–37.
52. An H, Bao YP, Wang M, et al. Reducing macro segregation of high carbon steel in continuous casting bloom by final electromagnetic stirring and mechanical soft reduction integrated process. *Metall Res Technol* 2017; 114: 405.
53. Li X, Wang X, Bao Y, et al. Effect of electromagnetic stirring on the solidification behavior of high-magnetic-induction grain-oriented silicon steel continuous casting slab. *JOM* 2020; 72: 3628–3633.
54. Li X, Wang M, Bao YP, et al. Solidification structure and segregation of high magnetic induction grain-oriented silicon steel. *Met Mater Int* 2019; 25: 1586–1592.
55. Boettcher A, Lahn L, Inden G, et al. Method for producing a grain-oriented electrical steel strip or sheet intended for electrotechnical applications. Germany Patent US 2014/0230966 A1, 21 August 2014.
56. Bottcher A, Klinkenberg C and Schuster I. Process for producing grain-oriented electrical steel strip and grain-oriented electrical steel strip obtained according to said process. Germany Patent WO 2016/059099 A1, 21 April 2016.
57. Bao SQ, Xu Y, Zhao G, et al. Microstructure, texture and precipitates of grain-oriented silicon steel produced by thin

slab casting and rolling process. *J Iron Steel Res Int* 2017; 24: 91–96.
58. Wang LT, Deng CH, Dong M, et al. Development of continuous casting technology of electrical steel and new products. *J Iron Steel Res Int* 2012; 19: 1–6.
59. Fu B, Xiang L, Qiao JL, et al. Primary recrystallization behaviors of Hi-B steel with lower initial nitrogen produced by the thin slab casting and rolling process. *Metals (Basel)* 2021; 11: 189.
60. Maleki A, Taherizadeh A and Hosseini N. Twin roll casting of steels: an overview. *ISIJ Int* 2017; 57: 1–14.
61. Muller M, Bailly D and Hirt G. Microstructure evolution and magnetic properties of a 4.5 wt% silicon steel produced by twin-roll casting. *Steel Res Int* 2022; 93: 2200554.
62. Matsushita T, Nakayama K, Fukase H, et al. Development and commercialization of twin roll strip caster. *IHI Eng Rev* 2009; 42: 1–6.
63. Wang Y, Zhang YX, Lu X, et al. A novel ultra-low carbon grain oriented silicon steel produced by twin-roll strip casting. *J Magn Magn Mater* 2016; 419: 225–232.
64. Wang Y, Xu Y-B, Zhang Y-X, et al. Effect of annealing after strip casting on texture development in grain oriented silicon steel produced by twin roll casting. *Mater Charact* 2015; 31: 361–370.
65. Liu HT, Yao SJ, Sun Y, et al. Evolution of microstructure, texture and inhibitor along the processing route for grain-oriented electrical steels using strip casting. *Mater Charact* 2015; 106: 273–281.
66. Song HY, Liu HT, Wang YP, et al. Secondary recrystallization behavior in a twin-roll cast grain-oriented electrical steel. *J Magn Magn Mater* 2017; 428: 325–331.
67. Wang YP, Liu HT, Song HY, et al. Ultra-thin grain-oriented silicon steel sheet fabricated by a novel way: twin-roll strip casting and two-stage cold rolling. *J Magn Magn Mater* 2018; 452: 288–295.
68. Xu H, Xu Y, He Y, et al. Influence of hot rolling reduction rate on the microstructure, texture and magnetic properties of a strip-cast Fe-6.5 wt% Si grain-oriented electrical steel. *J Magn Magn Mater* 2020; 494: 165755.
69. Taguchi S and Sakakura A. The effects of AlN on secondary recrystallization textures in cold rolled and annealed (001)[100] single crystals of 3% silicon iron. *Acta Metall* 1966; 14: 405–423.
70. Sakai T, Shiozaki M and Takashina K. A study on AlN in high permeability grain-oriented silicon steel. *J Appl Phys* 1979; 50: 2369–2371.
71. Iwayama K and Haratani T. The dissolution and precipitation behavior of ain and MnS in grain-oriented 3% silicon-steel with high permeability. *J Magn Magn Mater* 1980; 19: 15–17.
72. Hulka K, Vlad C and Doniga A. The role of niobium as microalloying element in electrical sheet. *Steel Res* 2002; 70: 453–460.
73. Hou R, Zhu C, Li G, et al. Effect of Niobium on precipitates and texture evolution of Fe-3% Si grain-oriented electrical steel annealed hot band. *ISIJ Int* 2017; 57: 2245–2254.
74. Li H, Feng Y, Zhang D, et al. Balanced solubility product and enthalpies of formation of Nb compounds in 0.09% oriented silicon steel. *Rare Met* 2013; 32: 318–322.
75. Feng Y, Guo J, Li J, et al. Effect of Nb on solution and precipitation of inhibitors in grain-oriented silicon steel. *J Magn Magn Mater* 2017; 426: 89–94.
76. Gao Y, Xu G, Guo X, et al. Primary recrystallization characteristics and magnetic properties improvement of high permeability grain-oriented silicon steel by trace Cr addition. *J Magn Magn Mater* 2020; 507: 166849.
77. Fang F, Hou D, Zhang Y, et al. Improvement of texture and magnetic properties of strip-cast grain-oriented electrical steel by trace Bi addition. *J Mater Sci* 2021; 56: 11988–12000.
78. Shimizu Y, Ito Y and IiDa Y. Formation of the Goss orientation near the surface of 3 pct silicon steel during hot rolling. *Metall Trans A* 1986; 17: 1323–1334.
79. Littmann M. Development of improved cube-on-edge texture from strand cast 3pct silicon-iron. *Metall Trans A* 1975; 6: 1041–1048.
80. Muraki M, Obara T, Satoh M, et al. Control of recrystallization during high-temperature hot-rolling of grain-oriented silicon steel. *J Mater Eng Perform* 1995; 4: 413–417.
81. Muraki M, Ozaki Y, Obara T, et al. Development of high-temperature hot-rolling process for grain-oriented silicon steel. *J Mater Eng Perform* 1996; 5: 323–327.
82. Matsuo M, Sakai T and Suga Y. Origin and development of through-the-thickness variations of texture in the processing of grain-oriented silicon steel. *Metall Trans A* 1986; 17: 1313–1322.
83. Giri SK, Kumdu S, Prakash A, et al. Defining the role of hot band annealing in high-permeability grain-oriented (GO) electrical steel. *Metall Mater Trans A* 2022; 53: 1873–1888.
84. Mishra S, Darmann C and Lucke K. New information on texture development in regular and high-permeability grain-oriented silicon steels. *Metall Trans* 1986; 17: 1301–1312.
85. Chang SK. Influence of hot band normalizing on recrystallization behaviour in grain oriented silicon steels. *Steel Res Int* 2005; 76: 660–665.
86. Shingaki Y, Takashima M and Hayakawa Y. Influence of initial crystal orientation and carbon content on rolling-induced texture in 3 mass% Si steel. *ISIJ Int* 2022; 62: 2382–2388.
87. Zhang N, Meng L, Zhang B, et al. Experimental investigation and simulation of crystallographic orientations evolution in a cold-rolled ultra-thin grain-oriented silicon steel. *J Magn Magn Mater* 2021; 517: 167385.
88. Lee DN and Jeong HT. The evolution of Goss texture in silicon steel. *Scr Mater* 1998; 38: 1219–1223.
89. Giri SK, Durgaprasad A, Mehtani H, et al. Origin of Goss (110) <001> grains in hot-worked grain-oriented steel. *Metal Mater Trans A* 2020; 51: 5268–5284.
90. Jain V, Modak P, Patra S, et al. Origin of Goss texture in grain oriented electrical steel: role of shear bands. *Materialia* 2022; 22: 101398.
91. Shingaki Y, Takashima M and Hayakawa Y. Influence of initial crystal orientation and carbon content on rolling-induced texture in 3 mass% Si steel. *ISIJ Int* 2022; 62: 2382–2388.
92. Wang X, Zhang W, Hao Y, et al. Refinement of coarse AlN by the shear effect of dislocation slip during cold rolling in low-temperature grain-oriented silicon steel. *Intermetallics* 2021; 132: 107136.
93. Kumano T, Haratani T and Ushigami Y. Influence of primary recrystallization texture through thickness to secondary texture on grain oriented silicon steel. *ISIJ Int* 2003; 43: 400–409.
94. Omura T and Hayakawa Y. Influence of primary-recrystallization texture on selective growth of Goss grains. *Mater Trans* 2013; 54: 14–21.

95. Park NJ, Joo HD and Park JT. Evolution of Goss orienation during thermal heating with different heating rate for primary recrsytallization in grain-oriented electrical steel. *ISIJ Int* 2013; 53: 125–130.
96. Silveria CC, Landgraf FJG and Paolinelli SC. Effect of primary grain size and nitrogen content on the magnetic properties of a grain-oriented electrical steel obtained by Steckel mill. *J Magn Magn Mater* 2020; 503: 166629.
97. Zhang H, Zhang C, Wu Z, et al. Study on primary recrystallization behavior of Fe-3%Si-Cu alloy with copper-rich precipitates as main inhibitor. *J Mateials Res Technol* 2022; 21: 1843–1855.
98. Song HY, Wang YP, Esling C, et al. The role of grain colony on secondary recrystallization in grain-oriented electrical steel: new insights from an original tracking experiment. *Acta Mater* 2021; 206: 116611.
99. Park NJ, Lee EJ, Joo HD, et al. Evolution of Goss orientation during rapid heating for primary recrystallization in grain-oriented electrical steel. *ISIJ Int* 2011; 51: 975–981.
100. Yilmaz C, Poul M, Lahn L, et al. Dislocation-assisted particle dissolution: a new hypothesis for abnormal growth of Goss grains in grain-oriented electrical steels. *Acta Mater* 2023; 258: 119170.
101. Shinozaki MMI, Kan T and Gotoh T. Effect of primary recrystallized texture on the behavior of secondary recrystallization in 3% silicon steel. *Trans Jpn Inst Met* 1978; 19: 85–91.
102. Harase J and Shimizu R. Distribution of {110}<001> oriented grains in the primary recrystallized 3% Si-Fe alloy. *Trans Jpn Inst Met* 1988; 29: 388–398.
103. Shimizu R, Harase J and Dingley DJ. Prediction of secondary recrystallization texture in Fe-3% Si by three-dimensional texture analysis. *Acta Metall Mater* 1990; 38: 973–978.
104. Homma H and Hutchinson B. Orientation dependence of secondary recrystallization in silicon-iron. *Acta Mater* 2003; 51: 3795–3805.
105. Dunn CG and Lionetti F. The effect of orientation difference on grain boundary energies. *Trans Met Soc AIME* 1949; 185: 125–132.
106. Dunn CG, Daniels FW and Bolton MJ. Measurement of relative interface energies in twin related crystals. *Trans Met Soc AIME* 1950; 188: 368–377.
107. Dunn CG, Daniels FW and Bolton MJ. Relative energies of grain boundaries in silicon iron. *Trans Met Soc AIME* 1950; 188: 1245–1248.
108. Hayakawa Y, Muraki M and Szpunar JA. The changes of grain boundary character distribution during the secondary recrystallization of electrical steel. *Acta Mater* 1998; 46: 1063–1073.
109. Gubernatorov VV, Sokolov BK and Sbitnev AK. On texture formation in metals during recrystallization. I. Texture effect on grain growth relative rate. *Phys Met Metall* 1996; 81: 261–267.
110. Park H, Kim DY, Hwang NM, et al. Microstructural evidence of abnormal grain growth by solid-state wetting in Fe-3% Si steel. *J App Phys* 2004; 95: 5515–5521.
111. Ko KJ, Park JT, Kim JK, et al. Morphological evidence that Goss abnormally growing grains grow by triple junction wetting during secondary recrystallization of Fe-3% Si steel. *Scr Mater* 2008; 59: 764–767.
112. Ko KJ, Cha PR, Srolovitz D, et al. Abnormal grain growth induced by sub-boundary-enhanced solid-state wetting: analysis by phase-field model simulation. *Acta Mater* 2009; 57: 833–845.
113. Lee D, Ko KJ, Lee BJ, et al. Monte Carlo simulations of abnormal grain growth by sub-boundary-enhanced solid-state wetting. *Scripta Materalia* 2008; 58: 683–686.
114. Morawiec A. Grain misorientations in theories of abnormal grain growth in silicon steel. *Scr Mater* 2000; 43: 275–278.
115. Pease NC, Jones DW, Wise M,HL, et al. SEM Study of origin of Goss texture in Fe-3.25% Si. *Met Sci* 1981; 15: 203–209.
116. Chen N, Zaefferer S, Lahn L, et al. Effects of topology on abnormal grain growth in silicon steel. *Acta Mater* 2003; 51: 1755–1765.
117. Morawiec A. On abnormal growth of Goss grains in grain-oriented silicon steel. *Scr Mater* 2011; 64: 466–469.
118. Hayakawa Y, Omura T and Imamura T. Onset of secondary recrystallization in high purity 3.3% Si steel. *ISIJ Int* 2014; 54: 2385–2393.
119. Na J, Park S, Ko HS, et al. Novel process for the formation of Goss grains by concentrated shear strain on surface in inhibitor-free silicon steel. *Met Mater Int* 2023; 29: 821–832.
120. Wada T, Nozawa T and Takata T. Method for producing a super low watt loss grain oriented electrical steel sheet. Japan Patent 3932236, 13 January 1976.
121. Goel V. *Novel coating technologies for electrical steels*. Ph.D. Thesis, Cardiff University: UK, 2016.
122. Fiedler A and Pepperhoff W. Method for reducing lossiness of sheet metal. Germany Patent 3,647,575, 7 March 1972.
123. Ichiyama T, Yamaguchi S, Iuchi T, et al. Grain-oriented electromagnetic steel sheet with improved Watt loss. Japan Patent 4,293,350, 6 October 1981.
124. Taguchi S. Review of the recent development of electrical steel in Japan. *Trans ISIJ* 1977; 17: 604–615.
125. Steel N. Grain-oriented electrical steel sheets. https://www.nipponsteel.com/en/product/catalog_download/, Tokyo, Japan, 2023.
126. Takamiya T, Hanazawa K and Suzuki T. Recent development of grain-oriented electrical steel in JFE steel. *JFE Tech Rep* Mar. 2016; 21: 1–6.
127. Ushigami Y, Mizokami M, Fujikura M, et al. Recent development of low-loss grain-oriented silicon steel. *J Magn Magn Mater* 2003; 254-255: 307–314.
128. Nozawa T, Nakyama T, Ushigami Y, et al. Production of single-crystal 3% silicon-iron sheet with orientation near (110)[001]. *J Magn Magn Mater* 1986; 58: 67–77.
129. Lee S and Kim SJ. Statistical analysis of misorientation to Goss orientation of highly grain-oriented silicon steel. *J Magn Magn Mater* 2022; 560: 169563.
130. Tomida T, Uenoya S and Sano N. Fine-grained doubly oriented silicon steel sheets and mechanism of cube texture development. *Mater Trans* 2003; 44: 1106–1115.
131. Senda K, Uesaka M, Yoshizaki S, et al. Electrical steels and their evaluation for automobile motors. *World Electric Veh J* 2019; 10: 1–10.
132. Oda Y, Kohno M and Honda A. Recent development of non-oriented electrical steel sheet for automobile electrical devices. *J Magn Magn Mater* 2008; 320: 2430–2435.
133. Cheong S, Hilinski E and Rollett A. Effect of temper rolling on texture formation in a low loss cold-rolled magnetic lamination steel. *Metall Mater Trans A* 2003; 34: 1311–1319.
134. Ray RK and Jonas JJ. Transformation textures in steels. *Int Mater Rev* 1990; 35: 1–36.
135. Ray RK, Jonas JJ and Hook RE. Cold rolling and annealing textures in low carbon and extra low carbon steels. *Int Mater Rev* 1994; 39: 129–172.

136. Kestens LAI and Pirgazi H. Texture formation in metal alloys with cubic crystal structures. *Mater Sci Technol* 2016; 32: 1303–1315.
137. Bertotti G, Schino GD, Ferro A, et al. On the effect of grain size on magnetic losses of 3% non-oriented SiFe. *J Phys* 1985; 46-C6: 385–388.
138. Shiozaki M and Kurosaki Y. The effects of grain size on the magnetic properties of nonoriented electrical steel sheets. *J Mater Eng* 1989; 11: 37–43.
139. Yonamine T and Landgraf FJG. Correlation between magnetic properties and crystallographic texture of silicon steel. *J Magn Magn Mater* 2004; 272: E565–E566.
140. Houbaert Y, Ros-Yáñez T, Monsalve A, et al. Texture evolution in experimental grades of high-silicon electrical steel. *Phys B* 2006; 384: 310–312.
141. Landgraf F, Yonamine T, Emura M, et al. Modelling the angular dependence of magnetic properties of a fully processed non-oriented electrical steel. *J Magn Magn Mater* 2003; 254-255: 328–330.
142. Barret WF, Brown W and Hadfield RA. Electrical conductivity and magnetic permeability of various alloys of Fe. *Sci Trans Roy Dublin Soc* 1900; 7: 67–126.
143. Moses AJ. Electrical steels: past, present and future developments. *IEE Proc A (Phys Sci Meas Instrum Manage Educ)* 1990; 137: 233–245.
144. Hawezy D. The influence of silicon content on physical properties of non-oriented silicon steel. *Mater Sci Technol* 2017; 33: 1560–1569.
145. Matsumura K and Fukuda B. Recent developments of non-oriented electrical steel sheets. *IEEE Trans Magn* 1984; 20: 1533–1538.
146. Oda Y, Kohno M and H A. Recent development of non-oriented electrical steel sheet for automobile electrical devices. *J Magn Magn Mater* 2008; 320: 2430–2435.
147. Landgraf FJG. Nonoriented electrical steels. *JOM* 2012; 64: 764–771.
148. Equihua F, Salinas A and Nava E. Effect of aluminum content on austenite-ferrite transformation temperature in low carbon (Si-Al) hot rolled GNO electrical steels. *Revista de Metalurgia* 2010; 46: 78–85.
149. Cardosoa RFA, Brandaoa L and Cunhab MA. Influence of grain size and additions of al and mn on the magnetic properties of non-oriented electrical steels with 3 wt. (%) Si. *Mater Res* 2008; 11: 51–55.
150. Honma K, Nozawa T, Kobayashi H, et al. Development of non-oriented and grain-oriented silicon steel (invited). *IEEE Trans Magn* 1985; 21: 1903–1908.
151. Kubota T. Recent progress on non-oriented silicon steel. *Steel Res Intenational* 2005; 76: 464–470.
152. Schulte M, Steentjes S, Leuning N, et al. Effect of manganese in high silicon alloyed non-oriented electrical steel sheets. *J Magn Magn Mater* 2019; 477: 372–381.
153. Hou CK, Hu CT and Lee S. The effect of phosphorus on the core loss of lamination steels. *J Magn Magn Mater* 1992; 109: 7–12.
154. Park JT, Woo JS and Chang SK. Effect of phosphorus on the magnetic properties of non-oriented electrical steel containing 0.8wt% silicon. *J Magn Magn Mater* 1998; 182: 381–388.
155. Tanaka I and Yashiki H. Magnetic properties and recrystallization texture of phosphorus-added non-oriented electrical steel sheets. *J Magn Magn Mater* 2006; 304: e611–e613.
156. Tanaka I and Yashiki H. Magnetic properties and recrystallization texture evolutions of phosphorus-bearing non-oriented electrical steel sheets. *ISIJ Int* 2007; 47: 1666–1671.
157. Lee S and De Cooman BC. Effect of phosphorus on the magnetic losses of non-oriented 2% Si steel. *ISIJ Int* 2012; 52: 1162–1170.
158. Lee HY, Hsiao IC and Tsai MC. Texture improvement of 3% Si non-oriented electrical steel. *China Steel Tech Rep* 2015; 28: 1–5.
159. Stephenson E. The effect of tin on the toughness of some common steels. *Metall Trans A* 1980; 11: 517–524.
160. Godec M, Jenko M, Grabke H, et al. Sn segregation and its influence on electrical steel texture development. *ISIJ Int* 1999; 39: 742–746.
161. Mavrikakis N, Saikaly W, Calvillo P, et al. How Sn addition influences texture development in single-phase Fe alloys: correlation between local chemical information, microstructure and recrystallisation. *Mater Charact* 2022; 190: 112072.
162. Chang SK and Huang W. Texture effect on magnetic properties by alloying specific elements in non-grain oriented silicon steels. *ISIJ Int* 2005; 45: 918–922.
163. Dong H, Zhao Y, Yu XJ, et al. Effects of Sn addition on core loss and texture of non-oriented electrical steels. *J Iron Steel Res Int* 2009; 16: 86–89.
164. Hou CK and Lee TH. Effect of tin on the texture of nonoriented electrical steels. In: Rollett A (eds) *Materials processing and texture*. New Jersey: John Wiley & Sons, 2008, pp.173–182.
165. Miyoshi K, Shimoyama Y and Kubota T. Non-oriented electrical steel sheet having a low watt loss and a high magnetic flux density and a process for producing the same. USA Patent 4,666,534, 1985.
166. Leunis E, Putte TVD, Jacobs S, et al. Method of production of tin containing non grain-oriented silicon steel sheet, steel sheet obtained and use thereof. Europe Patent E 3209807A1, 2015.
167. Shimanaka H, Irie T, Matsumura K, et al. A new non-oriented Si-steel with texture of {100}<0vw>. *J Magn Magn Mater* 1980; 19: 63–64.
168. Shimanaka H, Ito Y, Matsumara K, et al. Recent development of non-oriented electrical steel sheets. *J Magn Magn Mater* 1982; 26: 57–64.
169. Lyudkovsky G and Rastogi PK. Effect of antimony on recrystallization behavior and magnetic properties of a nonoriented silicon steel. *Metall Mater Trans A* 1984; 15: 257–260.
170. Jenko M, Vodopivec F, Grabke H, et al. Orientation dependent surface segregation of antimony on non-oriented electrical steel sheet. *Steel Res* 1994; 65: 500–504.
171. Jenko M, Vodopivec F, Grabke HJ, et al. Influence of antimony on the texture and properties of 2% Si, 0.3% Al steel for non-oriented sheet. *J Phys IV* 1995; 5: 225–231.
172. Vodopivec F, Marinšek F, Grešovnik F, et al. Effect of antimony of energy losses in non-oriented 1.8 Si, 0.3 Al electrical sheets. *J Magn Magn Mater* 1991; 97: 281–285.
173. Solyom A, Zentko V, Fric P, et al. Effect of antimony on magnetic properties in non-oriented 2.4 wt% Si electrical sheets. *IEEE Trans Magn* 1994; 30: 931–933.
174. Li N, Xiang L and Zhao P. Effect of antimony on the structure, texture and magnetic properties of high efficiency non-oriented electrical steel. *Adv Mat Res* 2013; 602-604: 435–440.
175. Babapour A, Hosseinipour S, Jamaati R, et al. Effect of antimony addition and asymmetric cold rolling on the

texture and magnetic properties of a 1.2% Si steel. *J Magn Magn Mater* 2022; 554: 169258.
176. Kim JH, Jun GH and Park SH. Non-oriented electrical steel sheet and method for preparing same. Europe Patent EP 3 733 916 A1, 2018.
177. Cheng ZY, Liu J, Xiang JJZD, et al. Effects of Cu addition on plasticity of Fe-6.5 Si (wt.%) alloy at temperatures below 550° C. *Intermetallics* 2020; 120: 106747.
178. Cheng LJZ, Xiang Z, Jia J, et al. Effect of Cu addition on microstructure, texture and magnetic properties of 6.5 wt% Si electrical steel. *J Magn Magn Mater* 2021; 519: 167471.
179. Oda Y, Tanaka Y, Yamagami N, et al. Ultra-low Sulfur non-oriented electrical steel sheets for highly efficient motors: NKB-CORE. *NKK Tech Rev* 2002; 87: 12–18.
180. Cioffi PP. Magnetic material. USA Patent 2110569, 1938.
181. Morill W. Imroved silicon iron for electrical equipment. *Met Prog* 1948; 54: 675–678.
182. Takenaka M, Fujita N, Hayakawa Y, et al. Unique effect of carbon addition on development of deformation texture through changes in slip activation and twin deformation in heavily cold-rolled Fe-3% Si alloys. *Acta Mater* 2018; 157: 196–208.
183. Fischer O and Schneider J. Influence of deformation process on the improvement of non-oriented electrical steel. *J Magn Magn Mater* 2003; 254: 302–306.
184. Tomida T. A new process to develop (100) texture in silicon steel sheets. *J Mater Eng Perform* 1996; 5: 316–322.
185. Sung JK, Lee DN, Wang DH, et al. Efficient generation of cube-on-face crystallographic texture in iron and its alloys. *ISIJ Int* 2011; 51: 284–290.
186. Ahn YK, Kwon SB, Jeong YK, et al. Fabrication of cube-on-face textured Fe-1wt% Si and Fe-2wt% Si-1wt% Ni electrical steel using surface nucleation during $\gamma \rightarrow \alpha$ phase transformation. *Mater Charact* 2020; 170: 110724.
187. Chalmers B. *Principles of Solidification*. 1st ed. New York: John Wiley & Sons, 1964.
188. Hu H. Texture of metals. *Texture* 1974; 1: 233–258.
189. Bessemer H. Improvement in the Manufacture of Iron and Steel. US Patent 49053, 1865.
190. Zapuskalov N. Comparison of continuous strip casting with conventional technology. *ISIJ Int* 2003; 43: 1115–1127.
191. Büchner AR and Schmitz JW. Thin-strip casting of steel with a twin-roll caster – discussion of product defects of $\asymp$ 1 mm-Fe6%Si-strips. *Steel Res* 1992; 63: 7–11.
192. Park JY, Oh KH and Ra HY. Microstructure and crystallographic texture of strip-cast 4.3 wt% Si steel sheet. *Scr Mater* 1999; 40: 881–885.
193. Park JY, Oh K and Ra H. The effects of superheating on texture and microstructure of Fe–4.5 wt% Si steel strip by twin-roll strip casting. *ISIJ Int* 2001; 41: 70–75.
194. Liu H, Liu Z, Li C, et al. Solidification structure and crystallographic texture of strip casting 3 wt.% Si non-oriented silicon steel. *Mater Charact* 2011; 62: 463–468.
195. Xu PG, Yin FX and Nagai K. Solidification cooling rate and as-cast textures of low-carbon steel strips. *Mater Sci Eng A* 2006; 441: 157–166.
196. Mehdi M. *Texture Evolution of Non-oriented Electrical Steels during Thermomechanical Processing*. PhD Thesis, University of Windsor, Windsor, Ontario, Canada, 2019.
197. Humphreys FJ and Hatherly M. *Recrystallization and Related Annealing Phenomena*. 2nd ed. New York: Elsevier Ltd., 2004.
198. Lyudkovsky G and Southwick P. The effect of thermomechanical history upon the microstructure and magnetic properties of nonoriented silicon steels. *Metall Trans A* 1986; 17: 1267–1275.
199. Da Costa Paolinelli S, Cunha D and Cota A. The influence of hot rolling finishing temperature on the structure and magnetic properties of 2.0% Si non-oriented silicon steel. *Mater Sci Forum* 2007; 558: 787–792.
200. Da Cunha MA and Da Costa Paolinelli S. Effect of hot rolling temperature on the structure and magnetic properties of high permeability non-oriented silicon steel. *Steel Res Int* 2005; 76: 421–425.
201. An L, Wang Y, Wang G, et al. Fabrication of high-performance low silicon non-oriented electrical steels by a new method: low-finishing-temperature hot rolling combined with batch annealing. *J Magn Magn Mater* 2022; 546: 168907.
202. d SSF, De Dafe CPS and Cota AB. Influence of thermomechanical processing on shear bands formation and magnetic properties of a 3% Si non-oriented electrical steel. *J Magn Magn Mater* 2011; 323: 3234–3238.
203. Verbeken K, Schneider J, Verstraete J, et al. Effect of hot and cold rolling on grain size and texture in Fe-2.4 wt% Si strips. *IEEE Trans Magn* 2008; 44: 3820–3823.
204. Mehdi M, He Y, Hilinski E, et al. Texture evolution of a 2.8 Wt Pct Si non-oriented electrical steel and the elimination of the $\langle$ 111$\rangle$ //ND texture. *Metallurgical and Materials Transactions A* 2019; 50: 3343–3357.
205. Yashiki H and Kaneko T. Effect of hot-band annealing on anisotropy of magnetic properties in low-Si semi-processed electrical steels. *J Magn Magn Mater* 1992; 112: 200–202.
206. Hou C. Effect of hot band annealing temperature on the magnetic properties of low-carbon electrical steels. *ISIJ Int* 1996; 36: 563–571.
207. Gutiérrez-Castañeda E and Salinas-Rodríguez A. Effect of annealing prior to cold rolling on magnetic and mechanical properties of low carbon non-oriented electrical steels. *J Magn Magn Mater* 2011; 323: 2524–2530.
208. Liu J, Sha Y, Yao Y, et al. Effects of normalizing annealing on the recrystallization texture of 4.2 wt.% Si non-oriented electrical steel thin sheets. *Adv Mat Res* 2012; 535: 615–619.
209. Wu X, Yang P, Gu X, et al. The influence of normalization temperatures on different texture components and magnetic properties of nonoriented electrical steels. *Steel Res Int* 2021; 92: 2000361.
210. Park J and Szpunar J. Effect of initial grain size on texture evolution and magnetic properties in nonoriented electrical steels. *J Magn Magn Mater* 2009; 321: 1928–1932.
211. Chang S and Huang W. Effect of normalizing of hot band on magnetic properties and texture in high silicon non-oriented electrical steels. *Steel Res Int* 2007; 78: 340–347.
212. Liu H, Li H, Schneider J, et al. Effects of coiling temperature after hot rolling on microstructure, texture, and magnetic properties of non-oriented electrical steel in strip casting processing route. *Steel Res Int* 2016; 87: 1256–1263.
213. Xu Y, Jiao H, Zhang Y, et al. Effect of pre-annealing prior to cold rolling on the precipitation, microstructure and magnetic properties of strip-cast non-oriented electrical steels. *J Mater Sci Technol* 2017; 33: 1465–1474.
214. Wang YQ, Zhang XM, Zu GQ, et al. Effect of hot band annealing on microstructure, texture and magnetic properties of non-oriented electrical steel processed by twin-roll strip casting. *J Magn Magn Mater* 2018; 460: 41–53.
215. Lee K, Huh M, Lee H, et al. Effect of hot band grain size on development of textures and magnetic properties in 2.0% Si

non-oriented electrical steel sheet. *J Magn Magn Mater* 2015; 396: 53–64.
216. Kestens L and Jonas JJ. Transformation textures associated with steel processing. In: Semiatin SL (eds) *ASM Handbook, volume 14 A, metalworking: bulk forming*. Materials Park: ASM International, 2005, pp.685–700.
217. Sanjari M, He Y, Hilinski E, et al. Texture evolution during skew cold rolling and annealing of a non-oriented electrical steel containing 0.9 wt% silicon. *J Mater Sci* 2017; 52: 3281–3300.
218. He Y and Hilinski E. Texture and magnetic properties of non-oriented electrical steels processed by an unconventional cold rolling scheme. *J Magn Magn Mater* 2016; 405: 337–352.
219. Dillamore I and Roberts W. Preferred orientation in wrought and annealed metals. *Metall Rev* 1965; 10: 271–380.
220. Seil L and Burno C. Cold rolling reduction dependence of the recrystallization texture of 3% Si non-oriented electrical steel. *J Phys: Conf Ser* 2019; 1270: 012005.
221. Kawamata R, Kubota T and Yamada K. The effect of cold rolling parameters on the recrystallization texture of non-oriented electrical steel. *J Mater Eng Perform* 1997; 6: 701–709.
222. Vanderschueren D, Kestens L, Van Houtte P, et al. The effect of cross rolling on texture and magnetic properties of non oriented electrical steels. *Textures Microstruct* 1991; 14: 921–926.
223. Xu H, Xu Y, He Y, et al. Two-stage warm cross rolling and its effect on the microstructure, texture and magnetic properties of an Fe-6.5 wt% Si non-oriented electrical steel. *J Mater Sci* 2020; 55: 12525–12543.
224. He Y, Hilinski E and Li J. Texture evolution of a non-oriented electrical steel cold rolled at directions different from the hot rolling direction. *Metal Mater Trans A* 2015; 46: 5350–5365.
225. Sha Y, Zhang F, Zhou S, et al. Improvement of recrystallization texture and magnetic property in non-oriented silicon steel by asymmetric rolling. *J Magn Magn Mater* 2008; 320: 393–396.
226. Fang Z, Guo Y, Fu B, et al. Effect of shear bands induced by asymmetric rolling on microstructure and texture evolution of non-oriented 3.3% Si teel. *Materials (Basel)* 2020; 13: 4696.
227. Chen S, Butler J and Melzer S. Effect of asymmetric hot rolling on texture, microstructure and magnetic properties in a non-grain oriented electrical steel. *J Magn Magn Mater* 2014; 368: 342–352.
228. He Y and Hilinski EJ. Skew rolling and its effect on the deformation textures of non-oriented electrical steels. *J Mater Process Technol* 2017; 242: 182–195.
229. Tamimi S, He Y, Sanjari M, et al. Mechanical properties and crystallographic texture of non-oriented electrical steel processed by repetitive bending under tension. *Mater Sci Eng A* 2022; 835: 142665.
230. Shimazu T, Shiozaki M and Kawasaki K. Effect of temper rolling on texture formation of semi-processed non-oriented steel. *J Magn Magn Mater* 1994; 133: 147–149.
231. Barros J, Targhetta A, León O, et al. Effect of temper rolling on the texture formation and magnetic properties of non-oriented semi-processed electrical steel. *J Magn Magn Mater* 2007; 316: e865–e867.
232. Tóth LS, Estrin Y, Lapovok R, et al. A model of grain fragmentation based on lattice curvature. *Acta Mater* 2010; 58: 1782–1794.
233. Dillamore I, Roberts J and Bush A. Occurrence of shear bands in heavily rolled cubic metals. *Met Sci* 1979; 13: 73–77.
234. Barnett MR. Role of in-grain shear bands in the nucleation of <111>//ND recrystallization textures in warm rolled steel. *ISIJ Int* 1998; 38: 78–85.
235. Assmus F, Detert K and Ibe G. Über eisen-silizium mit würfeltextur. *Z. Metallkd* 1957; 48: 344–349.
236. Wiener G, Foster K and Shull D. Domain configuration and losses in cube-textured silicon iron. *J Appl Phys* 1967; 38: 1102–1103.
237. Walter J, Hibbard W, Fiedler H, et al. Magnetic properties of cube textured silicon-iron magnetic sheet. *J Appl Phys* 1958; 29: 363–365.
238. Walter JL. A mechanism for secondary recrystallization in high-purity silicon iron. *Acta Metall* 1959; 7: 424–426.
239. Walter J. Control of texture in magnetic material by surface energy. *J Appl Phys* 1965; 36: 1213–1220.
240. Hayakawa Y and Kurosawa M. Orientation relationship between primary and secondary recrystallized texture in electrical steel. *Acta Mater* 2002; 50: 4527–4534.
241. Tomida T. Decarburization of 3% Si-1.1% Mn-0.05% C steel sheets by silicon dioxide and development of 100<012> texture. *Mater Trans* 2003; 44: 1096–1105.
242. Sung JK and Koo YM. Magnetic properties of Fe and Fe-Si alloys with {100}< 0vw> texture. *J Appl Phys* 2013; 113: 17A338.
243. Sha Y, Sun C, Zhang F, et al. Strong cube recrystallization texture in silicon steel by twin-roll casting process. *Acta Mater* 2014; 76: 106–117.
244. Jiao H, Xu Y, Zhao L, et al. Texture evolution in twin-roll strip cast non-oriented electrical steel with strong Cube and Goss texture. *Acta Mater* 2020; 199: 311–325.
245. Takajo S, Merriman C, Vogel S, et al. In-situ EBSD study on the cube texture evolution in 3 wt% si steel complemented by ex-situ EBSD experiment—from nucleation to grain growth. *Acta Mater* 2019; 166: 100–112.
246. Nguyen-Minh T, Sidor J, Petrov R, et al. Occurrence of shear bands in rotated Goss ({110}<110>) orientations of metals with bcc crystal structure. *Scr Mater* 2012; 67: 935–938.
247. Xu Y, Zhang Y, Wang Y, et al. Evolution of cube texture in strip-cast non-oriented silicon steels. *Scr Mater* 2014; 87: 17–20.
248. Mehdi M, He Y, Hilinski E, et al. The evolution of cube ({001}<100>) texture in non-oriented electrical steel. *Acta Mater* 2020; 185: 540–554.
249. Lindenmo M, Coombs A and Snell D. Advantages, properties and types of coatings on non-oriented electrical steels. *J Magn Magn Mater* 2000; 215–216: 79–82.
250. A. International. *ASTM A976: Standard Classification of Insulating Coatings for Electrical Steels by Composition, Relative Insulating Ability and Application*. West Conshohocken, PA, USA: ASTM International, 2018.
251. Al-Timimy A, Vakil G, Degano M, et al. Considerations on the effects that core material machining has on an electrical machine's performance. *IEEE Trans Energy Convesion* 2018; 33: 1154–1163.
252. Sundaria R, Lehikoinen A, Arkkio A, et al. Effects of manufacturing processes on core losses of electrical machines. *IEEE Trans Energy Convers* 2021; 36: 197–206.
253. Bourchas K, Stening A, Soulard J, et al. Quantifying effects of cutting and welding on magnetic properties of electrical steels. *IEEE Trans Ind Appl* 2017; 53: 4269–4278.

254. Wang H, Zhang Y and Li S. Laser welding of laminated electrical steels. *J Mater Process Technol* 2016; 230: 99–108.
255. Senda K, Toda H and Kawano M. Influence of interlocking on core magnetic properties. *IEEJ J Ind Appl* 2015; 4: 496–502.
256. Miyagi D, Maeda N, Ozeki Y, et al. Estimation of iron loss in motor core with shrink fitting using fem analysis. *IEEE Trans Magn* 2009; 45: 1704–1707.
257. Mix T, Gröninger M, Jin Z, et al. Additive manufacturing of low loss electrical steel sheets for high efficiency electrical devices. *IEEE Trans Transp Electrification* 2023; 9: 5226–5231.
258. Wrobel R and Mecrow B. A comprehensive review of additive manufacturing in construction of electrical machines. *IEEE Trans Energy Convers* 2020; 35: 1054–1064.
259. Giannotta N, Sala G, Bianchini C, et al. A review of additive manufacturing of soft magnetic materials in electrical machines. *Machines* 2023; 11: 702–725.
260. Kustas A, Chandrasekar S and Trumble KP. Magnetic properties characterization of shear-textured 4 wt% Si electrical steel sheets. *J Mater Res* 2016; 31: 3930–3938.
261. Kustas AB, Johnsonb DR, Trumbleb KP, et al. Enhancing workability in sheet production of high silicon content electrical steel through large shear deformation. *J Mater Process Technol* 2018; 257: 155–162.
262. Jiao H, Xu Y, Xiong W, et al. High-permeability and thin-gauge non-oriented electrical steel through twin-roll strip casting. *Mater Des* 2017; 136: 23–33.